FAILURE ANALYSIS OF HIP PROSTHESIS

A Thesis Submitted in

Partial Fulfillment of the Requirements

for the Degree of

DOCTOR OF PHILOSOPHY

By

M. SIVASANKAR

DEPARTMENT OF MECHANICAL ENGINEERING

INDIAN INSTITUTE OF TECHNOLOGY GUWAHATI

GUWAHATI-781 039, INDIA

November 2007

FAILURE ANALYSIS OF HIP PROSTHESIS

A Thesis Submitted in

Partial Fulfillment of the Requirements

for the Degree of

DOCTOR OF PHILOSOPHY

By

M. SIVASANKAR

(Registration Number: 01610302)

DEPARTMENT OF MECHANICAL ENGINEERING

INDIAN INSTITUTE OF TECHNOLOGY GUWAHATI

GUWAHATI-781 039, INDIA

November 2007

Dedicated to my Parents

Mr.S.Murugaiyan, Mrs.Vedha Murugaiyan

and to my Grand Parents Mr.S.P.Chidambaram, (Late) Mrs. Unnamalai Chidambaram, (Late) Mr.K.Subbulingam, (Late) Mrs. Sivagami Subbulingam

MECHANICAL ENGINEERING DEPARTMENT
INDIAN INSTITUTE OF TECHNOLOGY GUWAHATI
GUWAHATI 781 039

CERTIFICATE

It is certified that the work contained in the Thesis entitled **"Failure Analysis of Hip Prosthesis"** submitted by **Mr. M. Sivasankar** to the Indian Institute of Technology Guwahati for the award of the degree of Doctor of Philosophy has been carried out under our supervision in the Department of Mechanical Engineering, Indian Institute of Technology Guwahati. This work has not been submitted elsewhere for the award of any other degree or diploma.

Santosha Kumar Dwivedy
Associate Professor
Department of Mechanical Engineering
Indian Institute of Technology Guwahati
India.

Debabrata Chakraborty
Associate Professor
Department of Mechanical Engineering
Indian Institute of Technology Guwahati
India.

ACKNOWLEDGEMENTS

First of all, I would like to say my heart felt thanks to my thesis supervisors Dr. Santosha Kumar Dwivedy and Dr. Debabrata Chakraborty for their support through out my five years and eight months tenure in this campus.

I thank Head of the Department, Prof. Uday Sankar Dixit, who has helped me in my critical situations including the financial crisis times. Thanks are extended to my doctoral committee members Prof. Anoop Kumar Dass, Dr. Sashindra Kumar Kakoty, Dr. Damodar Maity for their endless helps in my research tenure. My thanks are also due to all other faculty members and staff of Mechanical Engineering Department, Indian Institute of Technology Guwahati for their help and cooperation during my stay here.

I should say thanks to my friends and colleagues too, for sharing their valuable time especially, Mr.Amal Kalita, Mr.T.Benarjee, Mr.Barun Pratiher, Mr.Ravikiran, Mr.Prateek Prasad, and all people who helped me a lot in this work to complete it successfully. Then, thanks to Mr.Shaikh Karimulla, my best friend who received me in this IIT Guwahati and helped me a lot. Dr. P. Rajesh Kanna, Dr. Manoranjan Kar, Mr. Abhigyan Prasad, Mr.G.Senthil Raja, Dr.William Johnbosco, Mr.Antony, Mr.K.Rajesh, Mr.S.Manikandan, Mr. N.Suresh Kumar, Mr.Sivagurumurthy, Mr. N.Subramanian, Dr. P.Muthukumaran, Mr.D.Arumuga Perumal, Mr.E.Vishnu Vardhana Rao, Dr. Manabendra Pathak, Dr. Karuna Kalita, Dr.P.Vinod, Ms. Jyotirmoyee, Ms. Radha, Ms. Sridevi, to all these people, I extend my sincere thanks.

I would like to express my sincere thanks to my parents, my sister Ms.M.Kanchana, my brother Dr. M.Sridhar, and my grand parents for their kind blessings in time to complete my Ph.D.

Thanks to WIPRO TECHNOLOGIES, Bangalore, for given me an opportunity to work with them. Thanks to one and all who helped me in completing my thesis.

Nandrigal, Vanakkangal. Jai Hind!

M.Sivasankar.

Abstract

The present thesis deals with the study of failure analysis of total hip prosthesis. A complete 3D finite element model has been developed for assessing the failure of hip prosthesis. Fatigue life of the prosthesis has been determined using 3D finite element analysis along with residual strength degradation model. A methodology for determination of fatigue constants in residual strength degradation model has been proposed for fatigue life calculation of hip prosthesis. Finite element contact stress analysis in conjunction with Archard's law has been used to assess the wear rate of the acetabular cup. Empirical relations have also been proposed for calculation of wear rate of acetabular cup as a function of head radius, roughness for different daily activities of patients. Different prosthesis materials have been studied to have a comparative assessment of the fatigue lives of the prosthesis and the wear rate of the acetabular cup.

Based on the results obtained from the present analysis, some important conclusions have been drawn. It has been observed that prosthesis made of Ti6Al4V have more fatigue life compared to Co Cr alloy for the cases studied here. Results of stress analysis show that conical stem shapes are better compared to stepped stems. From the analysis of stem shapes, it has been observed that type of activities such as slow walking, fast walking, normal walking, climbing stairs has significant importance in deciding the life of prosthesis and which among the activities is most critical depends upon the condition of the patient. The activities of standing 2-1-2 have been observed to be a critical activity for most of the patients. Wear rate of the acetabular cup increases as the head radius and surface roughness increase for a particular patient. The wear rate of the acetabular cup calculated using the developed empirical relations closely agree with the available clinical results. The results of this study will find applications in development of total hip replacement surgery.

Contents

List of Figures

List of Tables

CHAPTER 1
INTRODUCTION

1.1 Introduction

Hip joint is an important joint in human body and it is one of the largest weight bearing joints in it. It consists of two parts namely, a ball (femoral head) at the top of the thighbone (femur) and the ball fits into a rounded socket (acetabulum) in the pelvis as shown in Fig 1.1.

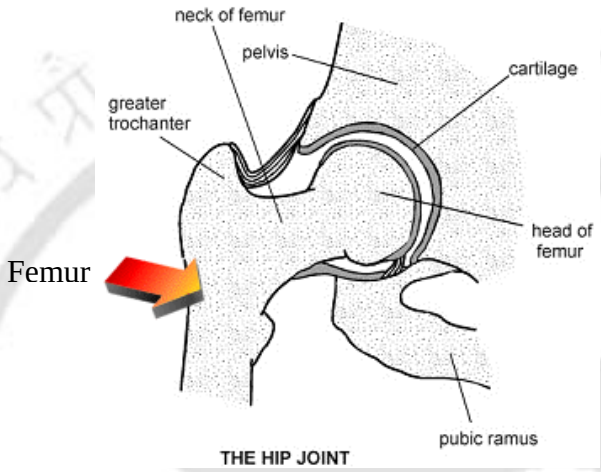

Fig1.1: Anatomy of hip joint (http://www.hipsandknees.com/hip/)

A band of tissues called ligaments connect the ball to the socket and provide stability to the joint. The hip joint may get damaged due to diseases like rheumatoid arthritis, osteoarthritis, fractures, and dislocations and sometimes due to accidents too. This may cause the fracture of hip and may lead to the permanent handicap to the person. Two common types of fractures that occur in hip joints are femoral neck fracture and intertrochanteric fracture (Fig 1.2 and Fig 1.3), which are described in the following section.

Femoral neck fracture occurs just below the thighbone's head, in the neck of the thighbone. Pins (surgical screws) are used if the person is younger and more active, and if the broken bone is not removed much out of place. If the person is older and less active, a high strength metal device that fits into hip socket, replacing the head of the femur (hemiarthroplasty) is needed. The most commonly used classification system for femoral

neck fracture is the Garden system (Fig 1.2), which is based on the amount of displacement of the fracture.

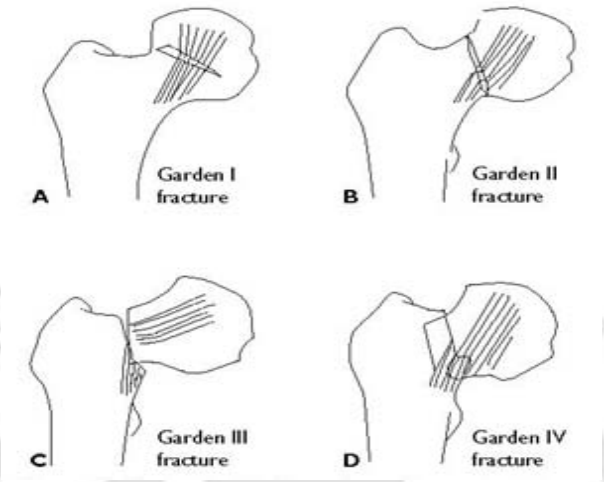

Fig 1.2: Garden classification system of femoral neck fractures
(A) Garden I fracture, (B) Garden II fracture, (C) Garden III fracture, (D) Garden IV fracture.(http://www.orthoassociates.com/hipfx.htm)

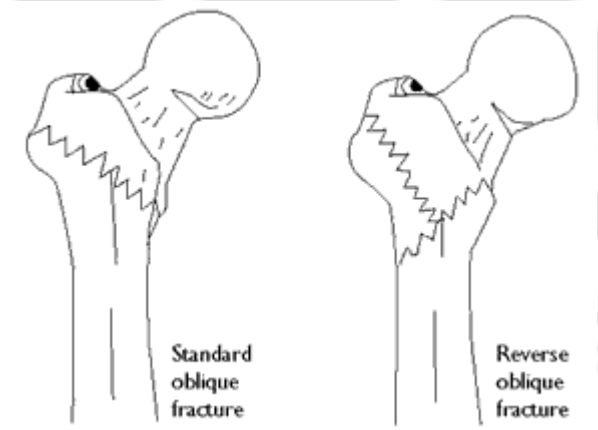

Fig 1.3: Simplified Evans' classification of intertrochanteric fractures: standard oblique fracture (stable) and reverse oblique fracture (unstable)
(http://www.orthoassociates.com/hipfx.htm)

Garden I fractures are minimally displaced and incomplete and are usually impacted with the femoral head tilting in the posterolateral direction. Garden II fractures are complete

but nondisplaced. Garden III fractures are complete and partially displaced, and Garden IV fractures are completely displaced.

Figure 1.3 shows the intertrochanteric fracture, which occurs in the area just below the neck, where the thighbone broadens. A metallic device (compression screw and side plate) holds the broken bone in place while it lets the head of the femur move normally in the hip socket.

1.2 Total Hip Replacement

The artificial hip joint replaces an amputated hip joint. A device that replaces an amputated joint or removed part of the body is called prosthesis. So it is appropriate to call an artificial hip joint as total hip replacement (THR). Total hip replacement is a surgical procedure where the diseased cartilage and the bone of the hip joint are surgically replaced with artificial materials. THR is done to patients suffering from hip diseases in order to relieve pain and restore joint function so that the patient can perform normal daily activities.

There has been a lot of development in THR since its inception. THR involves surgical removal of diseased ball and socket and replacing them with a metallic ball and stem inserted into the femur bone and an artificial plastic cup socket. The metallic artificial ball and stem are referred to as prosthesis. Important issues, which decide the success of THR are

- Correct operative technique for fixation
- Choice of suitable bio compatible materials and
- Satisfactory design ensuring safety

1.2.1 Correct operative technique for fixation

Basically the prosthesis fixations are classified into two types,

i) Cemented fixation

ii) Cementless fixation

1.2.1.1 Cemented Fixation

The femur and acetabulum cup are fixed to the skeleton with a self- curing polymer compound called bone cement or acrylic cement like Polymethylmethacrylate (PMMA). The bone cement fills completely the space between skeleton and prosthesis. The cup has a form of a hemisphere with slots on it that fits in the bed made in the pelvic bone. The bone cement hardens within 10 minutes. The cemented hip prosthesis is shown in Fig 1.4. The advantages of cemented hip prosthesis are as follows.

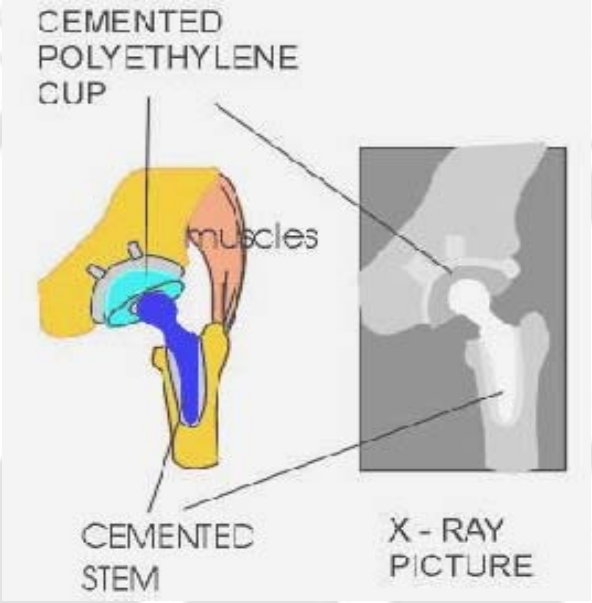

Fig 1.4: Cemented hip prosthesis

(http://www.totaljoints.info/cemented_and_cementless_thr.htm)

1. The cemented total hip replacement tolerates small deviations from the precise operation technique. The bed cut for the prosthesis in the skeleton need not to be exact because the bone cement filter will leave out all incongruities.
2. The patients can put weight on their new total hips immediately after the operation.
3. The cement layer also acts as an intermediate bumper between the very stiff metal of the total hip prosthesis and the weak skeleton. This bumper levels the peak forces acting on the skeleton around the total hip during gait.

Cemented fixation also has the following limitations:

1. The bone cement ages, cracks and after sometime the bond between the prosthesis and the skeleton may be lost.
2. Pressing the doughy bone cement into the raw bone marrow cavity during the operation may cause circulatory disturbances.
3. Repetitive and cyclic mechanical stress often causes the cement to fragment. Debris from the fragmenting cement can cause osteolysis.

1.2.1.2 Cementless Fixation

The components of the total hip prosthesis is pushed directly in the space made by reaming in the skeleton and held there by the elastic force generated in the bone tissue. The surface of the shaft component must be made rough, to avoid sliding against marrow cavity, and to achieve stable fixation. A typical cementless hip prosthesis is shown in Fig1.5.

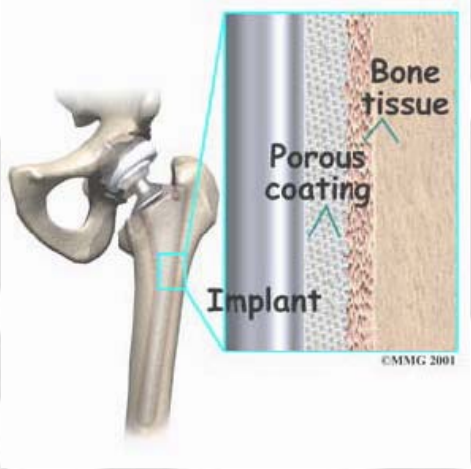

Fig 1.5: Cementless hip prosthesis
(http://www.totaljoints.info/cemented_and_cementless_thr.htm)

Cementless fixation has the following advantages.

1. The surgeon avoids all problems with cementing the total hip during the operation like mixing the bone cement, waiting for hardening of the doughy bone cement, changes of the position of prosthetic components while the bone cement is still in doughy state, risk of blood pressure fall and heart failure during cementing of the prosthesis.

2. The patient avoids the risk that the bone cement layer will crack and successively disintegrate after the operation.

Limitations of cementless fixations are as follows.

1. The risk that chunks of the bone marrow substance will be pushed into the circulation during the forceful hammering of the cementless total hip into place.

2. Risk of a fracture of the skeleton during operation, when the surgeon blows the total hip too vigorously into an undersized bony bed.

3. The post-operative need for restricted weight bearing for 6- 12 weeks.

1.2.2 Choice of Bio-Compatible Materials

A material is said to be biocompatible if it is well tolerated by bone and other tissues. The most frequently used biocompatible materials are

- Stainless steel
- Cobalt-Chromium alloys
- Titanium alloys
- Ultra high molecular weight polyethylene (UHMWPE)

The comparison of the material properties of different biocompatible materials is given in Table 1.1. A comparison of characteristics such as stiffness, strength, corrosion resistance, and biocompatibility of Co Cr alloy, Ti6Al4V and UHMWPE materials are also given in Table 1.2.

Table 1.1 Comparison of characteristics of bio compatible materials.[39,106]

Properties	CoCr alloy	Ti6Al4V	Cortical Bone	UHMWPE
Tensile Yield Strength (MPa)	655	800	90-131	19
Ultimate Tensile Strength (MPa)	750	900-1200	90	40
Modulus of elasticity (GPa)	225	110	12.4	0.725
Shear Modulus (GPa)	-	42	4.5-6.2	-
Hardness	400 Brinell	-	-	61 Shore D
Density (gm/cc)	8.3	4.5	1.7	0.95
Poisson's Ratio	-	0.33	0.22	-

Table 1.2: Qualitative Comparison of the characteristics of different biocompatible materials (**www.matweb.com**T).

Characteristic	CoCr alloy	Ti Alloy	UHMWPE
Stiffness	Medium	Low	Low
Strength	Medium	High	Low
Corrosion Resistance	Medium	High	High
Bio-compatibility	Medium	High	High

The stem portions of most hip implants are made of titanium or cobalt/chromium-based alloys; they come in different shapes and degrees of roughness. Cobalt/chromium-based alloys or ceramic materials (aluminum oxide or zirconium oxide) are used in making the ball portions, which are polished smooth to allow easy rotation within the prosthetic socket. The acetabular socket can be made of metal, UHMWPE, or a combination of polyethylene backed by metal. All together, these components weigh between 14 to 18 ounces (i.e., 397 to 510 gms), depending on the size needed. Figures 1.6, 1.7 and 1.8 are showing the stress strain curves of CoCr alloy, Ti6Al4V and UHMWPE materials respectively.

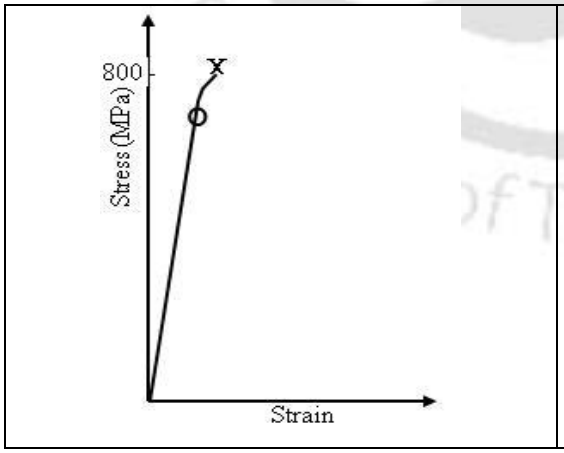

Fig 1.6: Stress strain curve of CoCr alloy
(http://www-personal.umich.edu/~sbayne/dental-materials)

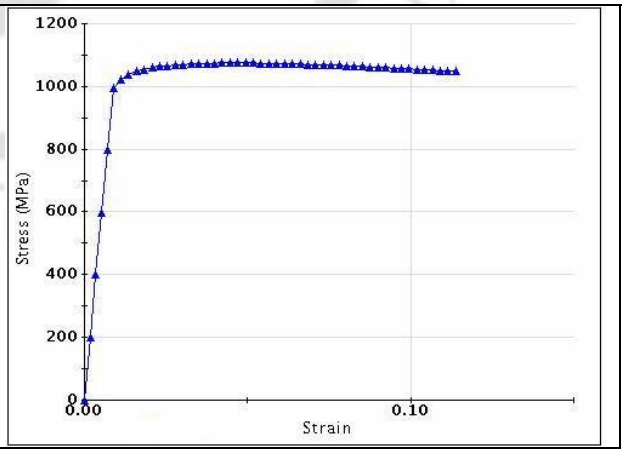

Fig 1.7: Stress strain curve of Ti6Al4V
(http://www.thermotech.co.uk/details.html)

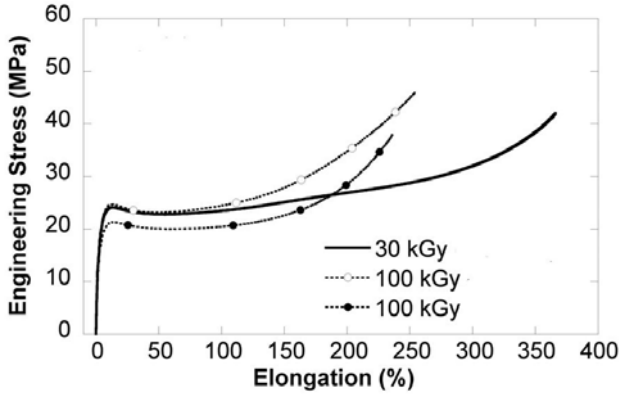

Fig 1.8: Stress strain curve of UHMWPE (http://www.uhmwpe.unito.it/web3/Kurtz.pdf)

All the materials used in a total hip replacement have four characteristics in common:

- They are biocompatible; that is, they can function in the body without creating either a local or a systemic rejection response.
- They are resistant to corrosion, degradation and wear, so they will retain their strength and shape for a long time. Resistance to wear is particularly significant in maintaining proper joint function and preventing the further destruction of bone due to particulate debris generated as the implant parts move against each other.
- They have mechanical properties that duplicate the structures they are intended to replace; for example, they are strong enough to take weight-bearing loads, flexible enough to bear stress without breaking and able to move smoothly against each other as required.
- They meet the highest standards of fabrication and quality control at a reasonable cost.

1.2.3 Satisfactory Design of Prosthesis

The size, shape and material of prosthesis in THR should be such that the prosthesis does not fail during service. One of the most common causes of failure of hip prosthesis is asceptic loosening. Asceptic loosening is the gross motion of the prosthesis within the bone and this may lead to associated pain and restriction in the range of joint motion. So it is important to have proper analysis and design to ensure safety of the THR.

Stress shielding is a mechanical phenomenon, occurring in composites of stiff and flexible materials, and prominent in the femoral total hip arthroplasty configuration. A

femur, in its natural state, carries its external loads all by itself. When provided with an intramedullary stem, it shares load with the implant. Where the same load was first carried by one structure, the bone, it is now carried by both stem and the bone. Force transferred to bone depends on the stiffness ratio of the bone to the implant. The transfer of load must take place through shear stress at the bone implant interface. This shear stress repeats many cycles per day and that determines the longevity of the bone implant interface. This phenomenon is called stress shielding.

Analysis of hip prosthesis involves determination of stress induced in the prosthesis as well as at the interface of the bone and stem under daily normal activities like slow walking, fast walking, climbing stairs etc. Essentially, all these activities give rise to low cycle fatigue loading on the prosthesis. Therefore, detailed failure analyses need to be performed in order to assess the failure and fatigue life of the prosthesis. Another important aspect of THR is the wear of the acetabular cup because of constant rubbing between the cup and the spherical head. Since the wear rate depends upon the contact stress developed between the mating parts, a detailed contact stress analysis has to be performed to evaluate the contact stress and hence the wear rate of acetabular cup.

1.3 Motivation of the Present Work

Total hip replacement (THR) is an important and commonly used procedure employed to patients with diseased hip, which may occur due to variety of reasons. While careful surgical procedure is very important for successful total hip replacement, it is equally important to analyze the life and safety of such a THR. Important aspects deciding the life and safety of a THR are choice of appropriate biocompatible materials for the prosthesis and the choice of appropriate dimensions and shape of the prosthesis. The size and shape determine the magnitude of stresses induced which might lead to the failure of hip joint and the choice of material is important to provide adequate resistance against such failure as well as to reduce wear of the prosthesis. Therefore, the present work aims at analysis of hip prosthesis in terms of evaluating the fatigue life and wear rate of the prosthesis. It has also been aimed to assess the comparative performances of different biocompatible materials and different possible models of hip prosthesis in guarding against the failure under different daily activities. A detailed literature review has been

done to take stock of the state of art of research in this area and based on the literature review, specific objectives of the present work have been laid down.

1.4. Organisation of the Report

The report has been divided in to seven chapters. Chapter 1 introduces the hip prosthesis, the importance of design and analysis of hip prosthesis and the motivation of the present work. In chapter 2, a detailed discussion on the literature review has been presented and the specific objectives of the present work have been listed. Finite element modeling of hip prosthesis has been discussed in Chapter 3. In chapter 4, fatigue analysis of hip prosthesis has been done based on equivalent static loading. Chapter 5 deals with the dynamic finite element analysis of hip prosthesis with actual time dependent loading corresponding to different activities. In chapter 6, the contact stress analyses and wear rate estimation of acetabular cup have been presented. Chapter 7 concludes the present work with important observations.

CHAPTER 2

LITERATURE REVIEW

2.1. Introduction

In this chapter, an exhaustive literature review on the works reported in the area of hip prosthesis has been presented. Literatures available in the area of hip prosthesis are broadly classified into the following categories.

- Estimation of forces on hip joint.
- Design of hip prosthesis
- Material used for hip prosthesis
- Experimental analysis
- Finite element analysis of hip prosthesis
- Fatigue analysis of hip prosthesis
- Contact and wear analysis of hip prosthesis

2.2 Estimation of forces on hip joint

For design and analysis of hip prosthesis accurate estimation of the forces acting on the prosthesis is essential. There are several experimental studies available in this direction and a few important literatures are discussed in this section.

Bergmann *et al.* [1-6] performed a number of experiments on different type of patients using instrumented hip implants and forces were recorded corresponding to different activities. From their results they reported that stresses induced in implants and bone were influenced by both magnitude and direction of force as well as by the kind of activities. The forces were found to be as high as 870% of body weight (BW) in some activities.

Stansfield and Nicol [8] studied the contact forces for two patients with hip prostheses. In their work, forces at hip joints were calculated using a three-dimensional model of the leg in walking at slow, normal and fast speeds (0.97 to 2.01m/s). Direct comparisons were made between the measured hip joint contact forces and the calculated forces. Hurwitz *et al*. [9] developed an analytical model to estimate the natural biological variations in muscle forces and their effect on the hip forces subjected to physiological constraints based on the joint kinematics and kinetics.

2.2.1 Design of Hip Prosthesis

Vora *et al.* [10] made an investigation on early failure of 22 proximally cemented, distally uncemented total hip arthroplasty with a minimum follow-up time of 24 months and observed that the early failure rates of these prosthesises were unacceptably high for a contemporary hip design. Scifert *et al.* [11] designed a convex curved acetabular lip to reduce the propensity for dislocation. For studying the dislocation phenomenon, a 3D non-linear finite element (FE) model was developed using ABAQUS® software and it was shown that the new design achieved 28% more resisting moment build-up during dislocation. Gross *et al.* [12] had done a finite element analysis of hollow stemmed hip prosthesis to reduce the stress shielding in the femur.

Phillips [13] used a 2D FE model of the acetabulum consisting of four layers viz., plastic, cement, graft and bone using plane strain elements. The inside diameter of the acetabular cup was taken as 50mm. The plastic, cement and bone were considered as linear elastic materials and the graft layer was considered as elasto-plastic material. The maximum force applied to the model was 1000% BW, which was more than that measured by Bergmann *et al*. [1-3] and the body weight was assumed as 1000 N. Implant separation from bone tissue is a serious drawback and the reason for it is the unnatural stress distribution around the implant. Stresses and motions in bone and implant depend mainly on loading conditions and implant design. Kowalczyk [14] used optimization of cementless femoral hip to improve the reliability of joint prosthesis. Chang *et al.* [15-16] carried out design of robust total joint replacements under the influence of environmental variables viz., joint force angle, cancellous bone elastic modulus and implant-bone interface friction. Senapati and Pal [17] carried out FE analysis on a simplified three-dimensional (Axi-symmetric) model and showed that for a stiffer prosthesis material (CoCrMo alloy), the peak interface stress occurred on the distal end of the stem whereas for a flexible implant like UHMWPE-Al_2O_3 the peak interface stress occurred at the proximal end. They concluded that a more flexible stem or less stiff materials caused more proximal load transfer.

Katoozian *et al.* [18], Katoozian [19], Katoozian and Davy [20] and Nicolella *et al.* [21] developed a numerical optimization technique to design a fibre-reinforced composite implant to minimize the potential for bone remodeling and stress shielding. In their

investigations, two different design objectives (failure-based and stress shielding-based) were used to design a carbon fibre-reinforced composite implant. Weisse *et al.* [22] did an optimization of a proof test procedure of ceramic hip joint ball heads for rejecting defective samples in the production line before implanting into human body. Prendergast [23] reviewed the FE modeling in three major areas such as analysis of a skeleton, analysis and design of orthopaedic devices and analysis of tissue growth.

Simoes *et al.* [24] and Simoes and Marques [25] designed and fabricated prototype of a controlled-stiffness composite femoral prosthesis composed of a cobalt-chrome core surrounded by a flexible composite outer layer. Predicted performance of the new design was compared with that of conventional single-modulus prosthesis. Li *et al.* [26-27] and Zhou *et al.* [28] developed a numerical method to predict the progressive failure of a thick laminated composite femoral component for total hip arthroplasty. In their work, the major failure of non-cemented metallic femoral components was observed to be the component loosening and the reason for this was attributed to stress shielding. Mavcic *et al.* [29] analyzed the forces acting on the hip and the peak stress in the hip joint and other relevant radiographic and biomechanical parameters using a mathematical model of an adult human hip in the static one-legged stance position of the body. Heida *et al.* [30] described about a new method for shape optimization of a hip prosthesis to maximize the fatigue life of the cement. Werner *et al.* [31] described about a methodology for the design and manufacture of implants in cases when the medical indications favor the application of an anatomic custom design implant. They provided a new possibility allowing surgeons to make the final decision as to the selection of prosthesis from the standard set based on geometric modeling preceded by a computerized tomography (CT) based process of identification.

Howell *et al.* [32] carried out a study on the appearance and mechanism of femoral stem in 172 retrieved femoral components, of which 74 stems had been stable in vivo. Macroscopic, microscopic, and nano-level scales of examination were used and it was reported that the loss of stem surface in response to micro-motion (wear) was found to affect 93% of stems. Pawlikowski *et al.* [33] described a design procedure for hip joint prosthesis, which was performed for a particular patient suffering from severe trauma of a hip joint. They created a set of three prostheses and then carried out some

numerical calculations with the use of ADINA software. The results of the numerical analyses allowed them to decide which one of the three designed prostheses was the most capable for the patient. Tanner *et al.* [34] described a method of testing hip prostheses in which the prosthesis was implanted in a proximal section of femur and loaded to model the forces applied through the acetabulum via the greater trochanter. Shirandami and Esat [35] proposed a new design for a hip prosthesis using polyethylene –hydroxyapatite, a composite material with layered stiffness and good bone compatibility. In order to overcome the low stiffness of the matrix, carbon fiber reinforcement was suggested. They carried out a 2D FE analysis and compared the results with those for titanium alloy prosthesis.

2.3 Materials selection for hip prosthesis

Selvaduray [36] discussed in details the factors to be considered in the material selection for hip implants. Scotchford *et al.* [37] analyzed the use of a low elastic modulus composite of polyetherketone and carbon fibre for the femoral stem component of a THR system. Hallab *et al.* [38] analyzed on differences in the fretting corrosion of metal-metal and ceramic-metal modular junctions of total hip replacements. They used an in vitro comparison of ceramic (zirconia, ZrO_2) and metal (Co-alloy) femoral head fretting upon Co-alloy stem components. In their study of a single total hip replacement stem and head design, it was reported that zirconia heads mated with Co-alloy stems produced less fretting than Co-alloy heads mated with Co-alloy stems.

Katti [39] studied the biomaterials properties of different materials used in total hip replacement. The merits and demerits of the metals, polymers, ceramics and composites were evaluated in the context of mechanical properties most suitable for total joint replacement such as a hip replacement. Schmalzried and Callaghan [40] reviewed the concepts of wear in total hip and knee replacements where 256 published articles were referred. In their work, the concepts in improving the durability of hip and knee replacements with a reduction in the total production and release of small particles into the biological environment were analyzed. Miller *et al.* [41] took an orthotropic material model to predict the proximal femur trabecular structure.

Helsen and Breme [42] described about the metals, which were used as biomaterials in different biomechanical activities like hip prostheses, knee prostheses, cardio vascular

stents etc. Kurtz *et al.* [43] did a comparative study of the yielding, plastic flow, and fracture behavior of two implantable grades of UHMWPE (GUR 1120 vs 4150 HP). Sloten *et al.* [44] illustrated two case studies for the design and material selection in the development of orthopaedic implants.

2.4 Experimental analysis

Many researchers experimentally worked on hip prosthesis to determine the loads, stresses, wear and fatigue life for different prosthesis materials. A brief description on this has been presented in this section.

As stated in section 2.1, Bergmann *et al.* [1-7] carried out many experiments to determine the loads on the prosthesis for different activities. Waide *et al.* [45] analyzed the modeling of the fibrous layer in cemented hip replacements with experimental and finite element methods to investigate the load transfer characteristics of two types of cemented hip replacements (Lubinus SPII and Muller-curved) with a fibrous tissue layer. Zimmerman *et al.* [46] compared the outcomes of 271 cases of hip osteoarthritis receiving primary total hip replacement and indicated that while the totally non-cemented prosthesises were more costly, there were no statistically significant differences in clinical or functional outcomes between the non-cemented and the hybrid prostheses upto 12 months post surgery. RoyChowdhury *et al.* [47] developed an acetabular cup of high-density polyethylene (HDPE) reinforced with different percentages of kevlar and carbon fibre by compression moulding. They also developed a walk simulator, which was used for testing the tribological performance of those cups. Kirkwood *et al.* [48] carried out the radiographic and non-invasive determination of the hip joint center location.

Lennon *et al.* [49] developed an experimental model of the implanted proximal femur that allowed visualization of damage growth in the cement layer. Sibella *et al.* [50] developed a biomechanical model using inverse dynamics equations for describing the sit-to-stand (STS) movement using kinetic and kinematic experimental data. Styles *et al.* [51] made an attempt to develop accelerated fatigue-testing procedures to enhance the methodology of hip implant lifetime prediction. McCormack *et al.* [52] studied experimentally the damage accumulation in cemented hip prosthesis to develop a methodology to characterize the pattern of crack initiation and damage accumulation in the intramedullary fixated cemented prostheses. McCormack *et al.* [53] made an

exclusive study on fatigue of cemented replacements under torsional loads. From their work, it was found that the majority of the cracks initiated from the PMMA/metal and PMMA/bone interfaces more often than the pores in the PMMA. Nallaa *et al.* [54] studied the in vitro fatigue in human cortical bone. Jin *et al.* [55] reviewed about the tribological aspects of hip joints considering the natural hip joints, cartilage substitution, artificial replacements to cartilage tissue engineering, which covered the full spectrum from natural hip joints to total hip replacements, as well as tissue engineered articular cartilage.

Mathias and Tabeshfar [56] developed acetabular cup prostheses with a ceramic on ceramic bearing surface that could last longer and perform better, thus reducing the necessity for costly and debilitating revisions. Simoes and Marques [57] designed and manufactured a composite femoral prosthesis which is a multi-material structure composed of a cobalt-chrome core surrounded by a flexible controlled stiffness composite structure and was first assessed by means of finite element analysis and its predicted performance compared with conventional bonded and press-fit Co-Cr and titanium prostheses.

2.4.1. Experimental stress analysis

Heller *et al.* [58] studied the musculoskeletal loading conditions of a hip joint during walking and staircase climbing. Muscle and joint contact forces were calculated using an optimization algorithm. The calculated peak contact forces both over estimated as well as under estimated the measured forces. They differed by a mean of 12% during walking and 14% during stair climbing.

Simoes and Marques [59] determined stiffness properties of two different composites made of braided glass and hybrid carbon glass fiber reinforced epoxy resins, which were used to manufacture two prototypes of a composite femoral prosthesis with controlled stiffness. Olotu *et al.* [60] studied on the use of handheld cement sample as a guide to the setting of in situ cement mantle. Christofolini *et al.* [61] developed a transducer for the measurement of cement – prosthesis interface forces in cemented orthopaedic devices. Christofolini *et al.* [62] again studied on experimentally partially cemented Anca Dual Fit stems and found that they did not fail in stimulated active patients. The partially cemented hip stems have been introduced to offer the advantages

of cemented stems on the short term, and of cementless ones on the long term. Lennon *et al.* [63] developed an experimental model of the implanted proximal femur that allowed visualization of damage growth in the cement layer to study the effect of surface finish on fatigue damage accumulation in a bone cement mantle. It was concluded that, despite the higher cement stresses with debonded stems, polished prostheses did not provoke the damage accumulation failure scenario. Garcia *et al.* [64] studied the adaptive bone remodeling and carried out a qualitative computational study of the long-term bone evolution, especially of the human femur, when different types of implants were employed to stabilize several kinds of fractures.

2.4.2 Experimental fatigue analysis

Yang and Liu [65] and Yang [66] developed residual strength degradation model for determination of fatigue life of graphite/epoxy composite laminates using experimental data for static and fatigue failure of a number of specimens. Tai *et al.* [67] analyzed the fatigue behavior of continuous carbon fiber-reinforced poly ether ether ketone (PEEK) composites under tension-tension (T-T) and tension-compression (T-C) fatigue loadings. Valle *et al.* [68] provided a case study report of 10 patients with cemented forged cobalt chrome stem under fatigue fracture for total hip arthroplasty. Santis *et al.* [69] manufactured and characterized a composite hip prosthesis made from poly ether-amide reinforced with carbon and glass fibers and evaluated the effect of fibre orientation on the mechanical properties of the composite femoral implant and compared with the bone.

2.4.3. Experimental wear analysis

Gispert *et al.* [70] reported a comparative study of joint material behavior in several lubricants by analyzing on the friction and wear mechanisms in hip prosthesis. In their work, the most commonly used joint materials for substitution of hip joints, UHMWPE for the cup, and alumina, stainless steel or CoCrMo alloy for the head, were submitted to pin-on-disk tribological tests. Saiko *et al.* [71] studied the wear of ultra-high molecular weight polyethylene acetabular cups with a new biaxial hip wear simulator using diluted calf serum as a lubricant. The wear mechanisms, including the size and shape of the wear particles, agreed well with those seen in clinical studies. Wall *et al.* [72] found a new technique for high sensitivity “in vitro” wear measurement of UHMWPE hip joint liners using radioactive tracing technology. Wu *et al.* [73] proposed

an algorithm for estimation of wear in artificial hip joint and they had reconstructed a pin-on-disk plate experiment to assess the efficiency and validity of the proposed algorithm. The algorithm was found to be useful and helpful in understanding the wear behavior for alternative or new designs of artificial hip joints and even for other analogous structures. Watters *et al.* [74] devised a non-conforming apparatus to study the wear properties of hip replacement materials (stainless steel femoral head and mainly UHMWPE and reported that PEEK had superior wear properties to UHMWPE. Cho *et al.* [75] studied the wear behavior of an UHMWPE sliding on the discs made of two types of ceramics by a ring-on-disc reciprocal wear test. Their results indicated that the friction coefficient and wear factor were closely controlled by the roughness of the disc. Podra and Anderson [76] made a wear simulation approach with commercial FE software ANSYS. Spherical pin-on-disc unlubricated steel contact was analysed both experimentally and with FEM. Oral *et al.* [77] conducted a study on wear resistance and mechanical properties of high density UHMWPE material doped with vitamin E with the hypothesis was that cross-linked, UHMWPE stabilized with vitamin E (a-tocopherol) would be wear-resistant and fatigue-resistant. The data indicate good in vitro wear properties and improved mechanical and fatigue properties for vitamin E– stabilized, cross-linked UHMWPE. Borlin *et al.* [78] presented and evaluated novel algorithms for radiostereometric measurements of the femoral head and metal-backed hemi-spherical cups of a total hip replacement on phantom images and clinical double examinations of patients. Geringer *et al.* [79] have conducted a fretting test to understand the asceptic loosening and fretting corrosion between the prosthesis and bone cement by conducting a fretting test between a stainless steel and PMMA in Ringer solution. Rodriguez *et al.* [80] did a study of the influence of dimensional and microstructural parameters upon the wear behaviour of metal-metal hip implants of a Co-Cr cast alloy by means of laboratory simulation. Chanda *et al.* [81] studied the wear and friction behaviour of UHMWPE against height purity fine grained alumina, the ideal material combination for total hip joint prosthesis under different contact pressures and sliding velocities using a pin-on-disc type wear and friction monitor. They observed that the wear heights in wet conditions were much lower than those in dry conditions.

2.5 Finite element analysis of hip prosthesis

Finite element analysis has been extensively used to find the maximum stresses in the hip joint and the life period of the prosthesis by static and dynamic loading. The fatigue, wear and contact analysis also have been carried out for finding the life of the prosthesis using different engineering software such as ANSYS, ABAQUS, CATIA, etc. In the following paragraph, a brief literature review is carried out for finite element analysis of hip prosthesis. According to the review of Huiskes and Chao [82], first application of finite element in orthopaedics was carried out by Brekelmans *et al.* [83].

2.5.1 Finite element analysis of femoral stem

Sheikh *et al.* [84] used finite element method for simulation of the hip joint during stumbling in static and dynamic loading and concluded that it was not the peak stress but the proportion of the stressed elements (or stressed volume), which should not be the indicator if a precise analysis of the load transfer mechanism was required. Varanasi and Rajadurai [85] made an analysis on a prosthetic hip joint using fracture and stress analysis using cast iron as the prosthesis material and found the stress distributions at different loads in the prostheses hip joint. Scannell and Prendergast [86] made a simulation study of changes in bone around hip replacement implants and offered an approach for computational pre-clinical testing of these implants. Li *et al.* [26-27] and Zhou *et al.* [28] used FEM to study numerically the progressive failure of thick laminated composite femoral components in an anatomical femur model by incorporating different failure criteria and material degradation models. Gross and Abel [87] have done finite element analysis of hollow stemmed hip prostheses as a means of reducing stress shielding of the femur. They used a hollow stemmed hip implant for reducing the effects of stress shielding, while maintaining the acceptably low levels of stress in the cement.

Peters *et al.* [88] carried out a finite element analysis to find the effect of femoral prosthesis design on cement strain in cemented total hip arthroplasty. They found that the finite element studies showing the highest cement stresses were located at the most proximal and distal ends of the prosthesis. Joshi *et al.* [89] did an analytical study of femoral hip prosthesis designed to reduce the stress shielding. In their study, they analyzed the hypothesis that through redesign, a total hip prosthesis could be developed

to substantially reduce stress shielding. Sakai *et al.* [90] reported a comparative study of different kinds of stems by experiments and FEM analysis with appropriate stress distribution on a hip prosthesis. Perez *et al.* [91] made a comparative finite element analysis of the debonding process in different concepts of cemented hip implants. In their work, they carried out a numerical study with debonding of the stem-cement interface and damage accumulation in the cement mantle. Hu *et al.* [92] developed a thermomechanical coupled finite element analysis model of total hip prosthesis and the model was used to simulate the wear test in a hip simulator to evaluate the transient contact stresses and to predict the rise of temperature elevated due to friction. The analysis served to further understand the tribological behavior of UHMWPE and the influence of temperature on contact interaction and wear process. Baleani *et al.* [93] investigated a theoretical protocol to predict the maximum stress induced in the stem by the ISO experimental test set-up. Stress was predicted using beam theory and finite element analysis (FEA) and strain measurements were used to assess the accuracy of the theoretical calculation. Fatigue testing was performed to verify the theoretical prediction about the fatigue stem performance. The results showed that FEA was more accurate than the beam model. Yoon *et al.* [94] searched for an optimal shape of the metal stem of a cemented total hip prosthesis minimizing stress concentration in the cement layer. A gradient projection method of numerical optimization and a finite element method of stress analysis were employed. Watanabe *et al.* [95] made a biomechanical study of the resurfacing hip arthroplasty using finite element analysis of the femoral component. The finite element analysis was performed using three-dimensional models to examine the biomechanical characteristics of the femoral component in resurfacing hip arthroplasty. Zannoni *et al.* [96] conducted an investigation on the possibility of developing finite element models of the human femur after hip joint arthroplasty using CT images acquired directly after surgery. Mathias *et al.* [97] performed a design study of hip joint prosthesis with the effect of stem introducers. The stress levels in the femoral component of a total hip prosthesis were calculated by finite element analysis (FEA). Taylor *et al.* [98] investigated the cancellous bone stresses surrounding the femoral component of total hip replacement using the finite element method. Four versions of a certain femoral hip prosthesis cemented, HA coated, press-fit,

and press-fit with ridges were analyzed. The results were also compared to clinical subsidence data for the Freeman femoral prosthesis to determine if the initial cancellous bone stress distribution could be used to predict the migration of the various versions of this prosthesis. Harrigan [99] conducted a study on analysis of the stresses within the cement-metal interface using a large-scale linear finite element analysis. To assess the effects of cement-prosthesis debonding, a 3D contact analysis was conducted which assessed the effect of several different areas of debonding between the prosthesis and the cement.

Prendergast and Taylor [100] have identified stress induced bone loss in the proximo-medial femur as a factor leading to loosening in the artificial hip joint using FE method. McNamara *et al.* [101] investigated the effect of bone-prosthesis bonding on proximal load transfer using a coupled experimental and finite element analysis on a synthetic femur. Prendergast *et al.* [102] studied the effects of Young's modulus of the stem and cement layer on the interfacial stresses in the prosthesis and developed some material selection criteria.

2.5.2 Finite element analysis of acetabular cup

Siegele *et al.* [103] did stress analyses on the ceramic hip joint heads under different loading conditions and reported the elastic deformation with corresponding stresses in the head by both experimental and numerical analyses as a basis of integrity tests of ceramic heads.

2.6 Fatigue analysis of hip prosthesis

Hertzler *et al.* [104] studied the femoral components using combination of experimental and computational methods to find the fatigue crack propagation process from stem-PMMA cement interface using a novel torsional loading model. Kim *et al.* [105] determined the fatigue damage response for cement bone constructs subjected to shear fatigue loading. Using von-Mises equivalent stress/strain concept, a general damage model was developed to describe the fatigue creep response of the cement bone interface under either shear or tensile fatigue loading. Kayabasi and Erzincanli [106] and Senalp *et al.* [107] designed four different stem shapes for hip prosthesis and investigated for the optimum stem shape. The static and dynamic finite element analyses were carried out for both static and dynamic loading conditions for four different stem shapes using FE

software ANSYS. Colombi [108-109] did a fatigue analysis, damage evaluation simulation and sensitivity analysis of cemented total hip arthroplasty using a quasi three dimensional finite element model. Numerical results showed a significant sensitivity to variations of the cement Young's modulus and stem–cement friction coefficient and a moderate sensitivity to the stem Young's modulus. Heida *et al.* [30] described about a new method for shape optimization of a hip prosthesis to maximize the fatigue life of the cement. In this study they described a method for numerical shape optimization whereby the finite element method was used to determine an optimal shape for the femoral stem of a hip prosthesis. Raimondi and Pietrabissa [110] reported about the in vivo fatigue failure of hip prosthesis stems. Their results suggested that the ISO 7206 testing specification would give experimental data of reasonable accuracy, with probably no more scatter than that found in typical specimen test results. Hung *et al.* [111] made a computer simulation study on fatigue behavior of cemented hip prostheses.

Tai *et al.* [112] carried out a finite element analysis of the cervico-trochanteric stemless femoral prosthesis and investigated the biomechanical performance of a newly designed cervico-trochanteric stemless prosthesis by comparing the stress distribution with that of the traditional stem-type porous-coated anatomic prosthesis. Culleton *et al.* [113] conducted a failure analysis on a cement mantle of an artificial hip joint, largely during a revision operation and subjected to detailed failure analysis. The results revealed a number of features, which were important to understand the failure of bone cement in situ and its consequences for prosthesis loosening.

2.7 Contact and wear analysis

Teoh *et al.* [114] studied the wear behavior of UHMWPE acetabular cup using finite element model and reported the effect of friction and the clearance between UHMWPE cup and the femoral head. Saikko and Calonius [115] did a slide track analysis of the relative motion between femoral head and acetabular cup in walking and in hip simulators. Bufford and Goswami [116] and Slonaker and Goswami [117] reviewed the wear mechanisms in hip implants which are the primary causes of premature failure in hip prostheses. Wear mechanisms were discussed as a function of contact stresses, lubricants and clearance, surface hardness and surface abrasions of both metal and polyethylene particulates.

Bevill *et al.* [118] developed a finite element model of hip replacement, and performed creep and wear simulation to 1 million gait cycles. From their results greater creep penetration was found with smaller heads, thicker liners, and larger clearance. Rapperport *et al.* [119] carried out a two dimensional finite element stress analyses of the hip joint using contact elements at the joint surface. The results explained the sensitivity of the hip contact pressures and stresses to imposed boundary conditions and indicated that care should be taken to simulate anatomic conditions in experimental and theoretical studies. Laurian and Tudor [120] analyzed the influence of the clearance in the pressure distribution in the total hip prostheses. Galvin *et al.* [121] made a comparison of wear of UHMWPE acetabular cups against alumina ceramic and chromium nitride coated femoral heads. Calonius [122] made a validation of wear simulation methods in the tribological aspect of prosthetic joints. Different methods had been taken to validate the wear simulation and all of them were validated. Reggiani *et al.* [123] made a phase transformation in explanted highly crystalline UHMWPE acetabular cups and debris after in vivo wear. They also examined retrieved Hylamer acetabular cups by differential scanning calorimetry and Raman micro-spectroscopy and compared with conventional UHMWPE cups to evaluate their crystallinity and crystal structure. Goswami and Alhassan [124] developed wear rate model for hip and knee prosthesis.

Jones *et al.* [125] did a simulation study on micro abrasion corrosion of CoCrMo alloy based artificial hip joint environments. Maxian *et al.* [126] used a three-dimensional, nonlinear contact finite element model of total hip replacement, linked to a sliding-distance-coupled wear algorithm, to study polyethylene wear rates for three different femoral head sizes. They observed that with increase in head diameter, though the wear depth remained almost same, the volumetric wear rate increased. Podra and Anderson [76] conducted a wear simulation approach with finite element software ANSYS. Spherical pin-on-disc unlubricated steel contact was analysed both experimentally and with FEM, and the Lim and Ashby wear map was used to identify the wear mechanism. It was shown that the FEA wear simulation results of a given geometry and loading could be treated on the basis of wear coefficient-sliding distance change equivalence. Podra and Anderson [127] developed a wear model considering surface topography and calculated wear in conical spinning contacts both analytically and with FEM, using the commercial

software ANSYS 5.0. Podra and Anderson [128] again made the wear simulation with the Winkler surface model and analyzed the advantages and disadvantages of using the simple Winkler surface model in wear simulations. Ogden *et al.* [129] conducted a study on wear properties of UHMWPE, which is generally used as a material for acetabular cup in total hip prosthesis. Sfantos and Aliabadi [130] analyzed an application of the boundary element method for simulating wear in total hip prosthesis. Several examples including different update periods of the worn acetabular cup, various femoral head sizes and various materials for both the femoral head and the acetabular cup were simulated under the same variable loading conditions for up to 20 years of service. Schmalzried and Callaghan [131] made a literature review of wear in total hip and knee replacements by reporting the review of more than 250 papers. Adegbile *et al.* [132] analyzed the failure of an uncemented acetabular prosthesis with a case study. They observed severe wear and aseptic loosening in an uncemented acetabular prosthesis in a revision surgery carried out at King Edwards VII hospital. They conducted a 3D FE analysis and the results showed high initial contact pressure along the periphery of the liner due to the oversize of the femoral head. The maximum contact pressure was found in the superior–posterior quadrant, which correlated well with the location and the direction of the wear. Wu *et al.* [73] used a pin-on-disk plate experiment, which was reconstructed to assess the efficiency and validity of the proposed algorithms.

Unsworth [133] made a study on the historical development of tribological aspects of artificial joints and compared with how those were lubricated with the mechanisms involved in human joints. It was concluded that while healthy human joints were lubricated by fluid film action, all current artificial joints at best were lubricated by mixed lubrication and hence wear is taking place through out the life of the prosthesis. Barbour *et al.* [134] conducted a study which combined pin-on-plate style wear testing with elastic-plastic finite element analysis in order to study the effects of a range of constant loads and contact stress on the wear factor of isotropic UHMWPE in conditions representative of those occurring in total replacement hip prostheses. The results showed that the wear factor had a tendency to decrease with increasing nominal contact stress. Yoshida *et al.* [135] studied the 3D dynamic hip contact area and pressure

distribution during activities of daily living. Some useful websites in these directions are given in [136-138].

2.8 Objectives of the present work

Literature review reveals that a large number of works have already been reported in the broad area of hip prosthesis. While these works could be classified as experimental and numerical, all these works aim at analyzing the hip prosthesis for more safety and more life. Many researchers have used different prosthesis materials and different models in their analysis. A need has been felt to have detailed discussions regarding the comparative performances of different prosthesis material and shape in terms of life and safety of the prosthesis. Literature review also clearly showed that material used, fatigue life, and wear of the prosthesis are important factors to be addressed in proper design of hip prosthesis. Keeping these in mind, the following specific objectives have been laid down for the present work.

1. 3D FE model for failure analysis of hip prosthesis in terms of assessing its fatigue life and wear volume rate of the acetabular cup.
2. To determine the comparative performances of different biocompatible materials used in hip prosthesis
3. To determine the influence of stem-shape on the strength and fatigue life of hip prosthesis
4. To understand the influence of different daily activities such as slow walking, fast walking, normal walking, upstairs climbing, downstairs coming, standing up, sitting down, standing on 2-1-2 legs and knee bend on the fatigue life of the hip prosthesis.
5. To study the influence of different materials used in hip prosthesis on the wear rate of the acetabular cup.
6. To study the influence of different daily activities on the wear rate of the acetabular cup.
7. To develop an empirical relation for wear rate calculation as a function of important parameters such as head radius, surface roughness and different activities.

CHAPTER 3

FINITE ELEMENT MODELING OF HIP PROSTHESIS

3.1 Introduction

This chapter gives a brief description about the finite element modeling of hip prosthesis for estimation of fatigue life of the prosthesis as well as the wear rate of acetabular cup. Two models have been considered for the stress analysis of hip prosthesis. In the first model a cylindrical stem with spherical head, cortical bone and a cement layer are considered. In the second model conical stem with spherical head and cement layer along with a cancellous and cortical bone have been considered. These prostheses are analyzed by 3D- finite element method using ANSYS. Three different shapes of stems have been considered in this study.

3.2 Finite element analysis of the prosthesis

Finite element (FE) modeling of the hip prosthesis has been carried out using ANSYS 9.0 general purpose FE Software. Solid 187 and Solid 92 elements (which are higher order 3-D 10 noded tetrahedral structural solid elements) embodied in ANSYS 9.0 have been used for modeling. For analysis of contact stress CONTA174 and TARGET170 elements have been used at the interface of the acetabular cup and the head. The following subsection describes the characteristics of the elements in brief.

3.2.1 Characteristics of tetrahedral element

A 10 noded tetrahedral element in space defined by *x*, *y* and *z* is shown in the Fig 3.1. Each node has three degrees of freedom. The state of displacement of a point is defined by three displacement components *u*, *v* and *w*, in the direction of the co ordinates *X*, *Y* and *Z*.

$$U = \begin{Bmatrix} u \\ v \\ w \end{Bmatrix} \tag{3.1}$$

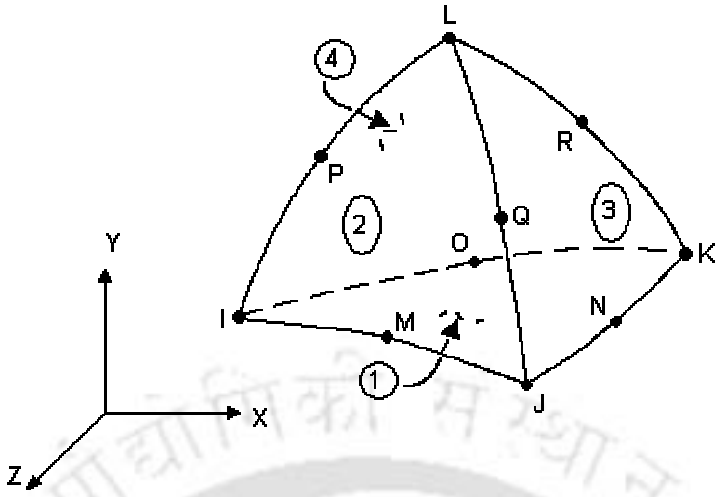

Fig 3.1: SOLID187 3-D 10-noded tetrahedral structural solid element

where

$$u = \alpha_1 + \alpha_2 x + \alpha_3 y + \alpha_4 z + \alpha_5 x^2 + \alpha_6 y^2 + \alpha_7 z^2 + \alpha_8 xy + \alpha_9 yz + \alpha_{10} zx \qquad (3.2)$$

Equating the values of the displacements at the nodes, ten equations of the type $u_i = \alpha_1 + \alpha_2 x_i + \alpha_3 y_i + \alpha_4 z_i + \alpha_5 x_i^2 + \alpha_6 y_i^2 + \alpha_7 z_i^2 + \alpha_8 x_i y_i + \alpha_9 y_i z_i + \alpha_{10} z_i x_i$ have been obtained and by solving these equations for α_1, α_2, α_3, α_4, α_5, α_6, α_7, α_8, α_9 and α_{10} in terms of the nodal displacements and finally U could be obtained .

The shape functions for the 10 noded tetrahedral elements are as follows:

$$N_I = L_I(2L_I - 1) \qquad N_J = L_J(2L_J - 1)$$
$$N_K = L_k(2L_k - 1) \qquad N_L = L_L(2L_L - 1)$$
$$N_M = 4L_I L_J \qquad N_N = 4L_J L_K$$
$$N_O = 4L_I L_K \qquad N_P = 4L_I L_L$$
$$N_Q = 4L_J L_L \qquad N_R = 4L_K L_L$$

where, N_I, N_J, N_K,N_L, N_M, N_O, N_P, N_Q, N_R are the shape functions at nodes I, J, K, L, M, N, O, P, Q, R respectively and L_I, L_J, L_K, L_L are the natural coordinates and satisfy the relation $L_I + L_J + L_K + L_L = 1$.

3.2.2 Characteristics of contact elements

In studying the contact between two bodies, the surface of one body is conventionally taken as a contact surface and the surface of the other body as a target surface. The "contact-target" pair concept has been widely used in finite element simulations. For rigid-flexible contact, the contact surface is associated with the deformable body; and the target surface must be the rigid surface. For flexible-flexible contact, both contact and target surfaces are associated with deformable bodies. The contact and target surfaces constitute a "Contact Pair".

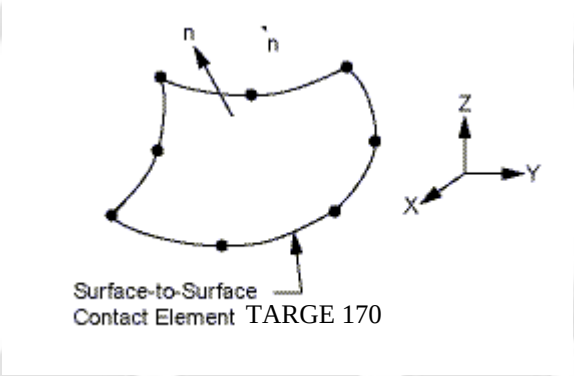

Fig 3.2: TARGE 170 3- D 8 noded surface-to-surface contact element.

TARGE 170 is used to represent various 3-D target surfaces for the associated contact elements (CONTA 174). The contact elements themselves overlay the solid elements describing the boundary of a deformable body that is potentially in contact with the rigid target surface, defined by TARGE 170. Hence, a "target" is simply a geometric entity in space that senses and responds when one or more contact elements move into a target segment element. The target surface is modeled through a set of target segments; typically several target segments comprise one target surface. Each target segment is a single element with a specific shape or segment type. TARGET 170 is an 8 noded element, for any target surface definition, the node ordering of the target segment element is critical for proper detection of contact. The nodes must be ordered so that the outward normal to the target surface is defined by the right hand rule Therefore, for general target segments, the outward normal by the right hand rule is consistent to the external normal.

For a rigid cylinder, cone, or sphere, contact must occur on the outside of the elements; internal contacting of these segments is not allowed.

Each target surface can be associated with only one contact surface, and vice-versa. However, several contact elements could make up the contact surface and thus come in contact with the same target surface. Likewise, several target elements could make up the target surface and thus come in contact with the same contact surface. For either the target or contact surfaces, you can put many elements in a single target or contact surface, but doing so may increase computational cost. For a more efficient model, localize the contact and target surfaces by splitting the large surfaces into smaller target and contact surfaces, each of which contain fewer elements.

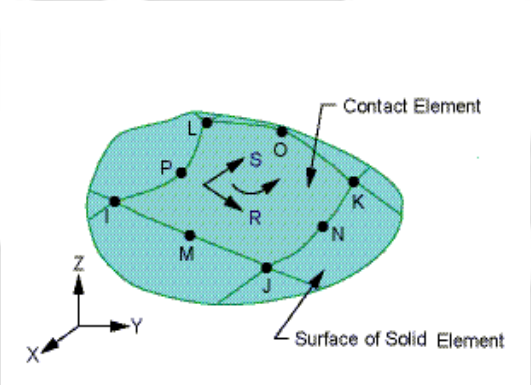

Fig 3.3: CONTA 174 8-noded surface to surface to contact element.

CONTA174 is used to represent contact and sliding between 3-D “target” surfaces. It is an 8-noded surface-to-surface contact element that is intended for general rigid-flexible and flexible-flexible contact analysis. This element is located on the surfaces of 3-D solid with mid side nodes (SOLID87, SOLID92). The node ordering is consistent with the node ordering for the underlying solid or shell element. The positive normal is given by the right-hand rule going around the nodes of the element and is identical to the external normal direction of the underlying solid. For solid shell elements, the same nodal ordering between shell and contact elements defines upper surface contact; otherwise, it represents bottom surface contact.

3.2.3 Modeling of the prosthesis

In order to compare the performance of different prosthesis material viz. Ti6Al4V, CoCr alloy and UHMWPE in terms of stress shielding initially a very simple model (Fig 3.4) of the prosthesis has been considered. It consists of a cylindrical stem, cement layer and cortical bone, the dimensions of which are given in Table 3.1. The model is similar to that considered by Senapati and Pal [17]. Properties of different materials used in the prosthesis are given in Table 3.2. All nodes at the bottom face of the model have been fully constrained in all directions and the load is applied in the top.

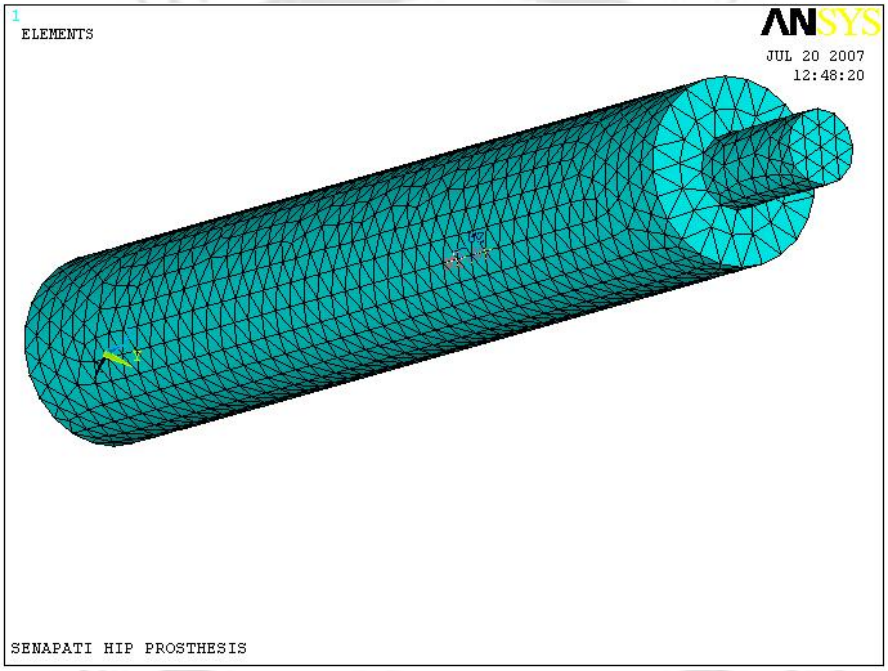

Fig 3.4: Model 1 of the cemented hip prosthesis

Table 3.1: Dimensions of different elements of the model in mm

Parts	Inner diameter, mm	Outer diameter, mm	Length, mm
Stem	0	12	105
Cement layer	12	20	80
Cortical bone	20	60	350

A second model is also considered as shown in Fig. 3.5, which a more realistic one having cortical bone, cancellous bone, stem and cement layers. As the stem shapes have a significant influence on the performance of prosthesis, three different types of stems viz., straight, stepped and conical shapes are considered which are similar to the work of Senalp *et al.* [107]. It may be noted that stem with smooth surfaces generally reduce stress concentrations and lead to high fatigue life of prosthesis, stem with sharp or non-smooth surfaces provide good bonding capability at the interface and prevent possible sliding at the interface. In this study, three different stem shapes as mentioned above are generated in ANSYS finite element software as shown in Fig 3.6. In addition to the previous model the abductor muscle force has been applied in the greater trochanter and the illiotibial force has been applied in the bottom surface. All nodes at the bottom surface are fully constrained in all directions and a static force is applied in the top of femoral head. The basic dimensions of the straight stem model are listed in Table 3.2. The dimensions of other stems are shown in Fig 3.6.

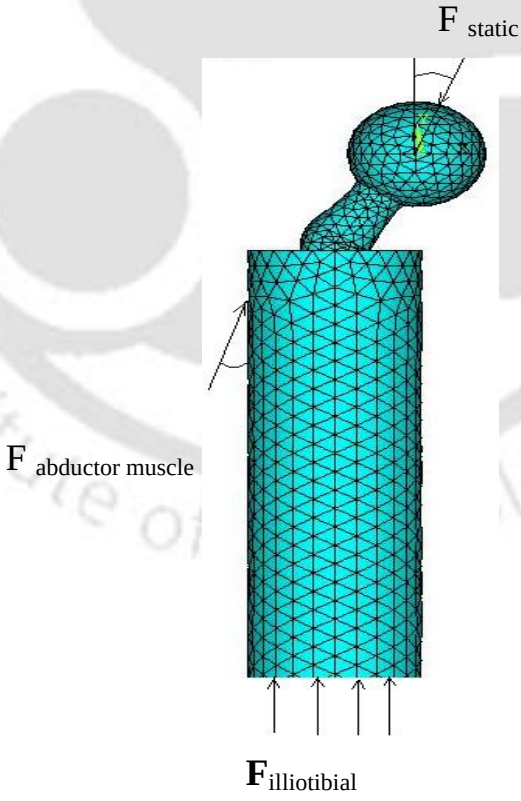

Fig 3.5: Model 2 of implanted cemented hip prosthesis

Table 3.2: Dimensions of the basic prosthesis model (straight stem)

Parts	Inner diameter, mm	Outer diameter, mm	Length, mm
Head	0	40	-
Stem	0	16	100
Cement layer	16	24	100
Cancellous bone	24	32	350
Cortical bone	32	50	350

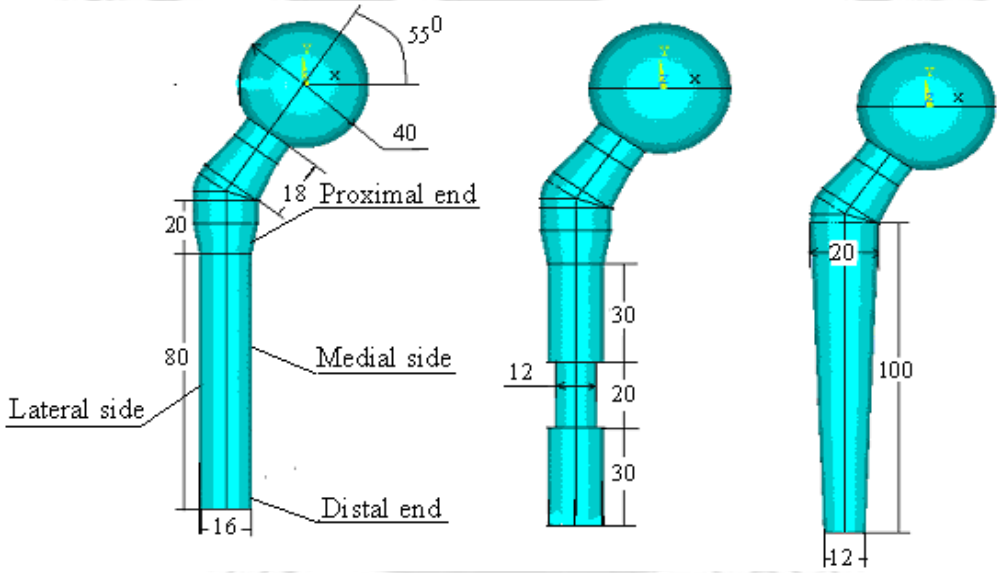

(a) Straight stem (b) Stepped stem (c) Conical stem

Fig 3.6: Different stems shapes

The acetabular model considered in the present work is shown in Fig 3.7. It consists of a spherical head, a polyethylene layer and a metal backing. It is very much essential to determine the contact stresses between the head and polyethylene layer. The finite element analysis of acetabular cup will be discussed in details in chapter 6.

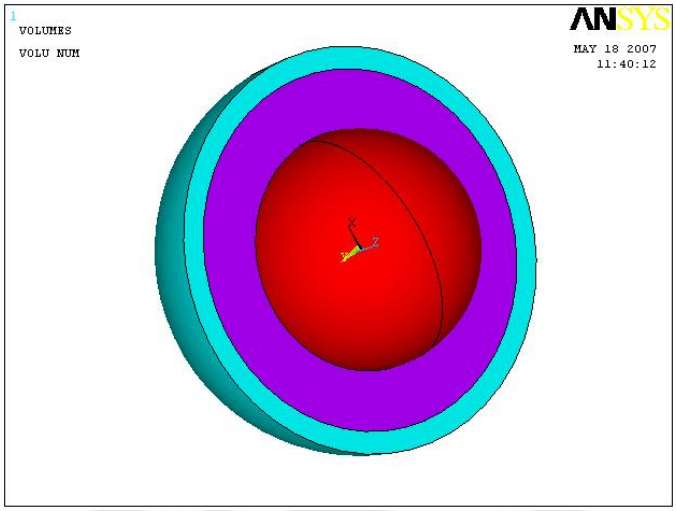

Fig 3.7: Acetabular model of the hip prosthesis

3.2.4: Materials used in the prosthesis

The material properties of the cortical bone, cancellous bone, cement layer and prosthesis are given in the Table 3.3. The femoral component consisting of a stem and spherical head is modeled with different materials like Ti6Al4V, Cobalt chromium alloy and UHMWPE. Cancellous bone is modeled with isotropic material and cortical bone is modeled with orthotropic material [107].

Table 3.3: Material properties used in the FE analysis

Parts	Material	Young's modulus (GPa)	Density (kg/m^3)	Poisson's ratio
Head and Stem	Ti6Al4V	110	$4.5x10^3$	0.32
	Co-Cr alloy	220	$8.4\ x10^3$	0.3
	UHMWPE	0.63497	$0.941\ x10^3$	0.45
Cement Layer	PMMA	2.7	1.19	0.35
Cancellous bone	----------	2.13	1.7	0.3
Cortical Bone	----------	$E_x = E_y$ =11.5, E_z =17, G_{xy} =3.6 $G_{xz} = G_{yz}$ =3.3	1.7	ν_{xy} =0.51 $\nu_{yz} = \nu_{xz}$ =0.31

3.3. Stress analysis of the hip prosthesis

Depending on the activities such as normal walking, fast walking, slow walking, etc. different loading conditions are applied on the femoral head. One may get these forces from actual experiments. In the present work, these loading conditions corresponding to different activities are taken similar to that of Bergmann *et al*. [3].

3.3.1 Stress analysis of model 1

Fig 3.4 shows FE model of hip prosthesis corresponding to model 1 considered in this work. It consists of axisymmetric cortical bone tube with solid stem. Bone cement and prosthesis material are linear elastic, isotropic and homogenous. Slow walking condition has been considered and a load of 3 KN has been applied on the surface of the implant bearing for a patient 70 kg body weight as shown in Figure 3.4. All nodal points at distal end are rigidly fixed. Finite element analysis and the model has been done considering three materials, *viz* Ti6Al4V, CoCr alloy and UHMWPE for the stem and head.

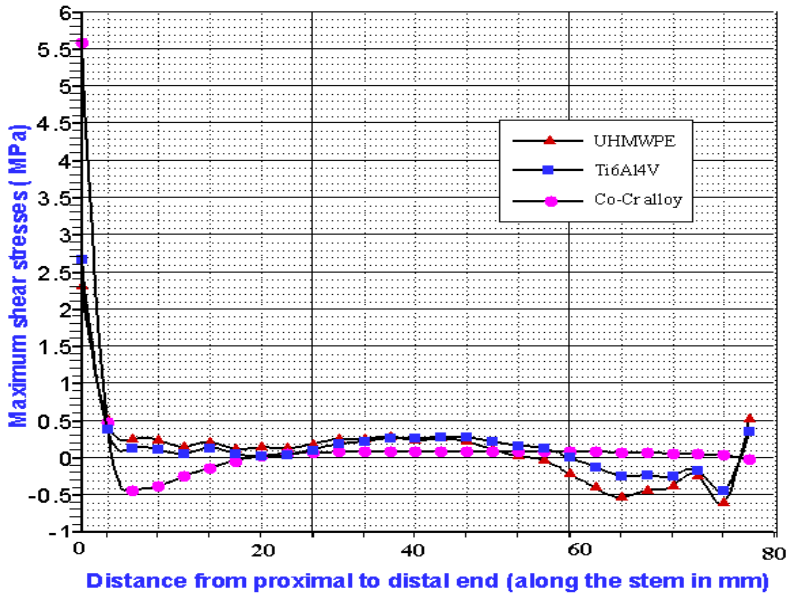

Fig 3.8: Variation of interfacial shear stresses on stem-cement interface for model

Fig 3.8 shows the variation of interfacial shear stresses along the stem from proximal to distal end on medial side model. UHMWPE stem has maximum shear stress at proximal end and is 5.5892MPa where as at distal end it is -1.65E-02MPa. Ti6Al4V stem has maximum at proximal end is 2.67MPa where as at distal end is 0.36106MPa. CoCr stem has maximum at proximal end is 2.3073MPa where as at the distal end it is 0.51951MPa. From Fig 3.8, it could be observed that the flexible implant peak interfacial shear stresses occurs at proximal end of stem i.e., more proximal load transfer using less stiff material.

Table 3.4 also lists the interfacial shear stresses developed for model 1. From Table 3.4 and Fig. 3.8, it could be observed that the interfacial shear stress is minimum for UHMWPE material. So to avoid stress shielding it is advisable to use UHMWPE material.

Table 3.4: Maximum interfacial shear stresses in model

S. No	CoCr (MPa)	UHMWPE (MPa)	Ti6Al4V (MPa)
1	2.3073	5.5892	2.67
2	0.50653	0.47701	0.39536
3	0.25215	-0.4342	0.13436
4	0.24116	-0.38359	0.11581
5	0.15148	-0.24844	5.97×10^{-2}
6	0.21398	-1.32×10^{-1}	0.13964
7	0.1228	-3.99×10^{-2}	5.94×10^{-2}
8	0.14241	2.65×10^{-2}	2.61×10^{-2}
9	0.12877	5.80×10^{-2}	3.94×10^{-2}
10	0.18366	7.43×10^{-2}	0.10937
11	0.2528	8.21×10^{-2}	0.18844
12	0.25448	8.48×10^{-2}	0.22457
13	0.28703	8.70×10^{-2}	0.26767
14	0.24017	8.68×10^{-2}	0.26314
15	0.26202	8.73×10^{-2}	0.28705
16	0.22061	8.74×10^{-2}	0.27684
17	0.12508	8.70×10^{-2}	0.22227
18	2.90×10^{-2}	8.66×10^{-2}	0.16867
19	-2.95×10^{-2}	8.63×10^{-2}	0.12925
20	-0.21212	8.49×10^{-2}	1.07×10^{-2}
21	-0.39451	8.31×10^{-2}	-0.11476
22	-0.53415	7.83×10^{-2}	-0.24286
23	-0.43445	7.21×10^{-2}	-0.23174
24	-0.37935	6.21×10^{-2}	-0.24189
25	-0.24455	5.22×10^{-2}	-0.17065
26	-0.60112	3.79×10^{-2}	-0.43909

3.3.2: Stress analysis of model 2

As explained before, three different stem shapes as shown in Fig 3.6 have been considered for the analysis purpose using a more realistic model i.e., model 2 (Fig. 3.5). Here, slow walking condition has been considered and a load of 3 kN with an angle of 20^0 is applied on the surface of the implant bearing for a patient 70 kg body weight. An

abductor muscle load of 1.25 kN was applied at an angle of 20^0 to the proximal area of the greater trochanter. An iliotibial-tract load of 250 N is also applied to the bottom of the femur in the longitudinal femur direction as shown in Figure 3.5. Distal end of the femur was constrained not to move in horizontal direction [107]. Fig 3.9 shows the stress distribution on medial side of stem for different materials under static loading. The maximum von Mises stresses developed in stems are given in Table 3.5.

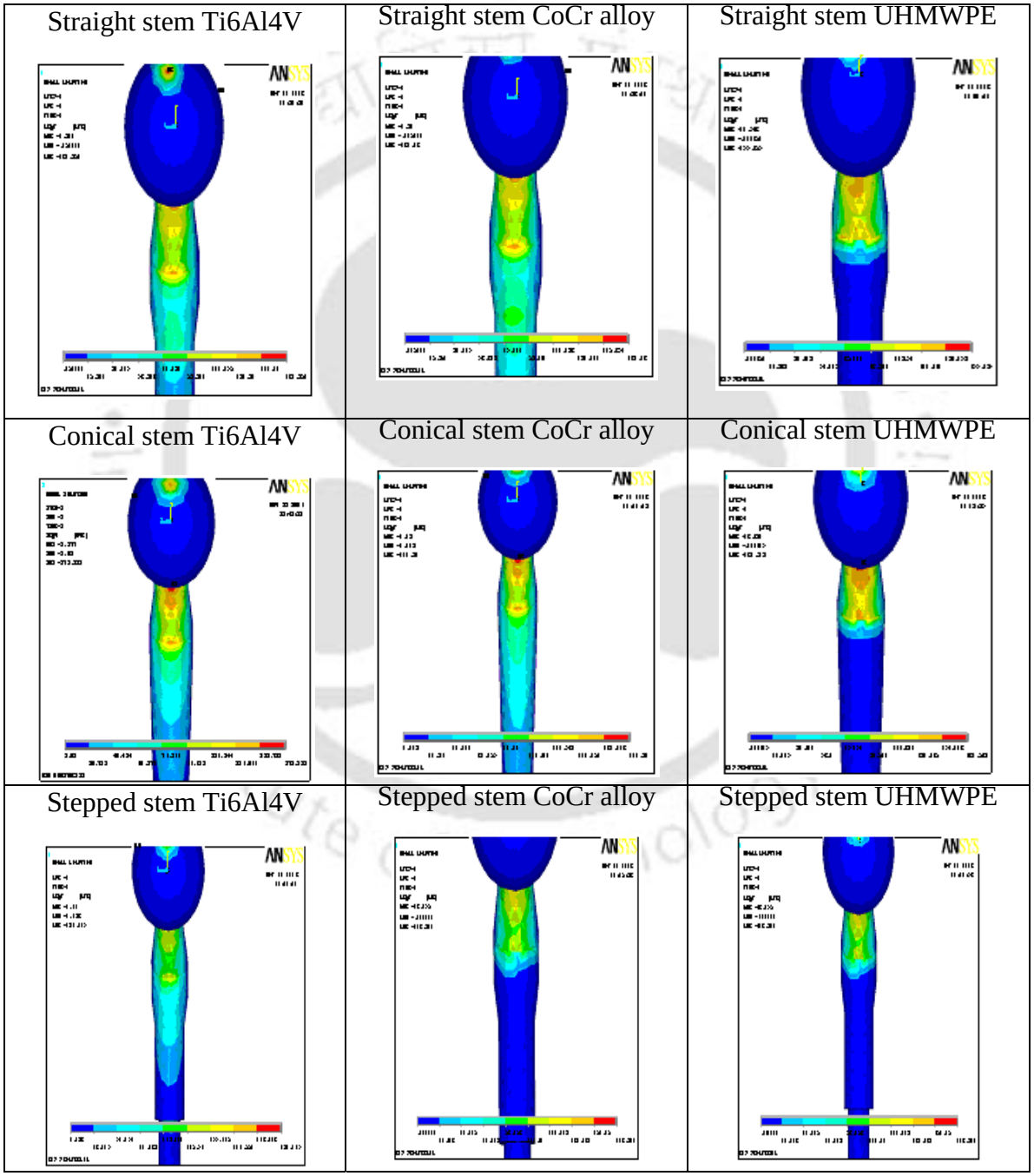

Fig 3.9: Stress distribution on medial side of stem for different materials under static loading

From Table 3.5 it could be observed that the minimum stress is developed in straight stem in comparison to conical and stepped stems. It has also been observed that the maximum stress occurs in neck region of the stem where it enters in to the cement layer. So straight stem has more life in compared to the other two stems.

The Young's modulus of prosthesis material is a critical design variable because, for a given stem geometry design, it largely determines how load is transferred, via the cement, to bone. Bending is the primary deformation mode in prosthesis stem. Due to bending, the medial side is subjected to compressive stress and lateral side is subjected to tensile stress. Figs 3.10-3.12 show the variation of maximum von Mises stresses in prosthesis, which occurs at the prosthesis-cement interface, for different prosthesis materials for different stem shapes.

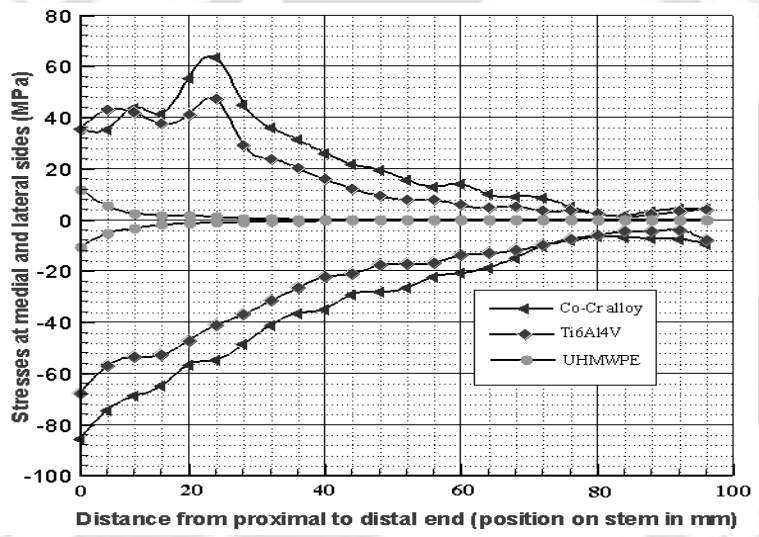

Fig 3.10: Stress distribution in lateral and medial sides of a straight stem

The maximum and minimum von Mises stresses are plotted directly from the above nodal stresses. The Young's moduli for CoCr alloy, Ti6AlV, UHMWPE are 220GPa, 110GPa and 0.63497GPa respectively. In the three cases it could be observed that if the prosthesis is made of lower stiffness material (UHMWPE), maximum stresses occurs just beneath the neck region for both medial and lateral sides and continuously decreases towards the distal end. If the prosthesis is made of higher stiffness materials (Ti6Al4V, CoCr alloy), the maximum stress occurs just beneath the neck for medial side, and for the lateral side,

the maximum stress occurs about one-third distance from the neck region. Figs 3.10-3.12 also show that compressive stresses on medial side are greater in magnitude than tensile stresses on lateral side. Increase in the prosthesis stiffness leads to higher stress in the prosthesis.

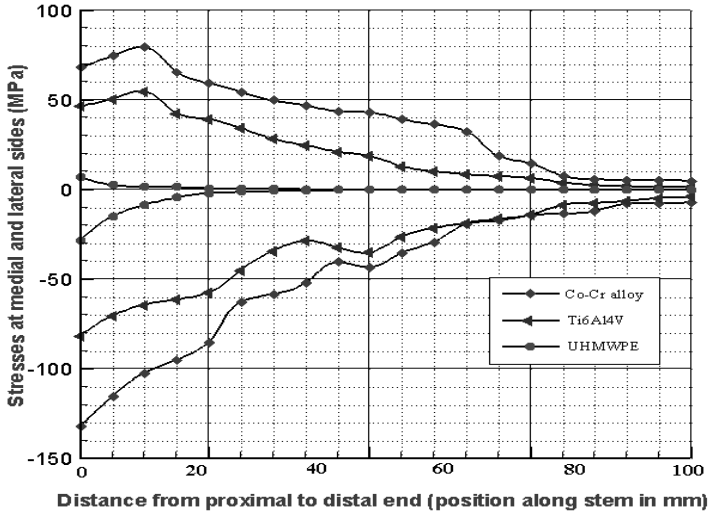

Fig 3.11: Stress distribution in lateral and medial sides of a stepped stem

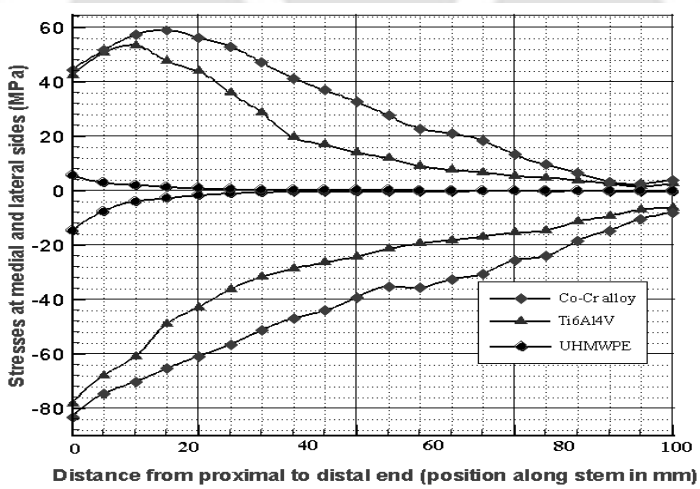

Fig 3.12: Stress distribution in lateral and medial sides of a conical stem

Increase in the prosthesis stiffness leads to lower stress in cement mantle. This is because a stiffer stem undergoes less bending displacements, and so the magnitude of the bending stress transferred to cement decreases.

Table 3.5: Maximum von Mises stresses for static loading

Type of stem	Maximum von Mises stress (in MPa)		
	Ti6Al4V	Co-Cr	UHMWPE
Straight stem	139.385	143.631	127.578
Stepped stem	164.202	166.403	151.184
Conical stem	147.107	154.557	122.374

Table 3.5 describes the maximum von Mises stresses developed in the prosthesis for different materials with three different stem shapes. It may be observed that maximum stress is developed in stepped stem in comparison to conical and straight stems. Since, insertion of stem inside the bone, could be performed more easily using a conical stem compared to a straight stem, in the further analysis conical stems have been considered.

It has also been observed from Table 3.5 that the ratio of the stress induced to the yield stress is very high for UHMWPE and hence this could not be used as stem material and it was decided to study, only Ti6Al4V and CoCr materials as the prosthesis materials.

3.4 Summary

In this chapter, the 3D finite element analyses of hip prosthesis were carried out by considering two models with three different prosthesis materials. It has been observed that though UHMWPE material is the best option for stem materials to avoid stress shielding, but it performs very poorly from strength point of view. Hence it cannot be considered as a stem material, which has been proposed by many authors to use as stem materials. It has also been shown that a conical stem shape is a better option than that of straight and stepped stem for a given loading condition.

CHAPTER 4

FATIGUE ANALYSIS OF HIP PROSTHESIS USING EQUIVALENT STATIC LOADING

4.1 Introduction

In this chapter, the fatigue life of hip prosthesis has been evaluated using equivalent static loading. Residual strength degradation model [65-66] has been used for determination of fatigue life of hip prosthesis for three different patients [3] corresponding to nine different daily activities using three dimensional finite element analyses. The constants involved in the residual strength degradation model have been evaluated using simulation data for different prosthesis materials.

4.2 Residual Strength degradation model

Following Yang and Liu [65], Yang [66] and Tai *et al.* [67], the residual strength $R_i(n)$ of the i^{th} specimen at the n_i^{th} cycle can be expressed in terms of the initial strength $R_i(0)$, maximum stress developed due to fatigue loading *S,* and material constant parameters *c, b, K* by the following equation.

$$R_i^c(n_i) = R_i^C(0) - X_0{}^c S^b n_i K \tag{4.1}$$

Here X_0 is a scale parameter or characteristic ultimate strength. The constants *c, b, K* and X_0 are to be determined for a given material by conducting experiments. In the present work, the material constants *c, b,* and *K* have been determined form the simulated data obtained from the known range of ultimate strength and the S-N curves without performing any experiment for three biocompatible materials, viz., Ti6Al4V, CoCr alloy and ultrahigh molecular weight poly ethylene (UHMWPE), which are extensively used in the development of different prostheses. The algorithm used for the same has been described in the following subsection.

4.2.1 Algorithm for determination of *K, b, c*

An algorithm has been developed to determine the fatigue parameters *K, b,* and *c* is given below.

1. Simulated data for static testing are obtained by assuming the ultimate strength of the specimen to be varying between $X_{\max}$ and $X_{\min}$.

2. Assuming that the tests have been performed for *m* specimen, *m* random numbers are generated between $X_{\max}$ and $X_{\min}$. These numbers correspond to the ultimate strengths of *m* specimen used in any experimental testing.

3. A table is prepared with specimen number and ultimate strength.

4. Using these data, the first moment, second and third central moments m_1, m_2, m_3 are calculated using the following expressions.

$$m_1 = \mu = \frac{1}{m}\sum_{i=1}^{m} X_i, \quad m_2 = \frac{1}{m}\sum_{i=1}^{m}\left(X_i - \mu\right)^2, \text{ and } \quad m_3 = \frac{1}{m}\sum_{i=1}^{m}\left(X_i - \mu\right)^3 \tag{4.2}$$

Here X_i (i =1 to m) is the ultimate strength of the i^{th} specimen.

5. The shape parameter and scale parameter are determined by the maximum likelihood estimation (MLE) technique using the two-parameter Weibull distribution, which is given by

$$R_{fx}(x) = 1 - \exp\left[-\left(\frac{X_i}{X_0}\right)^{\alpha}\right]. \tag{4.3}$$

Here $R_{fx}(x)$ is the distribution function, α is the shape parameter and X_0 is the scale parameter.

6. A set of *J* data points of residual strengths, denoted by $(R_1, S_1, n_1), (R_2, S_2, n_2) \cdots (R_J, S_j, n_j)$ are required to be obtained from the specimens subjected to fatigue loading. The i^{th} data point (R_i, S_i, n_i) indicates that the i^{th} specimen is subjected to a maximum cyclic stress S_i for n_i cycles and its residual strength is R_i. Since a point on the S-N curve of a material gives the information regarding the maximum developed stress S_i corresponding to the life of the specimen at fracture (number of cycles n_i), S_i has been taken to be equal to R_i [65]. Hence, without performing any experiment, these data $(R_1, S_1, n_1), (R_2, S_2, n_2) \cdots (R_J, S_j, n_j)$ have been simulated from the available S-N curve of the material.

7. A table has been prepared using these simulated data for number of cycles to fracture, n and residual strength, $R_i(n)$.

8. The residual strength of fatigue specimens $R_i(n)$ has been converted into equivalent ultimate strength $R_i(0)$ using the following equation.

$$R_i(0) = \left[R_i^c(n) + X_0{}^c S^b n K \right]^{1/c}. \quad i = 1, 2 \ldots J \tag{4.4}$$

9. The first moment, second and third central moments for fatigue data have been calculated using the following equations.

$$\mu_1 = \frac{1}{J}\sum_{i=1}^{J} R_i(0), \qquad \mu_2 = \frac{1}{J}\sum_{i=1}^{J}\left[R_i(0) - \mu_1 \right]^2, \quad \text{and } \mu_3 = \frac{1}{J}\sum_{i=1}^{J}\left[R_i(0) - \mu_1 \right]^3 \tag{4.5}$$

10. μ_1, μ_2 and μ_3 are functions of *c*, *b* and *K* and these parameters can be determined by minimizing the mean square difference Δ of the first three central moments (given in (4.2) and (4.5)) which is given by

$$\Delta = (m_1 - \mu_1)^2 + g_1\left(\sqrt{m_2} - \sqrt{\mu_2}\right)^2 + g_2\left(\sqrt[3]{m_3} - \sqrt[3]{\mu_3}\right)^2 \tag{4.6}$$

Here g_1 and g_2 are weighting parameters which are having positive values to indicate the relative importance of matching the mean, the standard deviation and the skewness.

4.2.2 Validation of the algorithm

The algorithm described in the previous section has been used to develop a code in MATLAB for determination of *K, b, c* values for different materials. Initially, the code has been validated by finding these values for graphite/epoxy for which the experimental data are available [65]. As it is known from experimental data from Table 4.1 that the ultimate strength of graphite/epoxy varies from 60 to 85 ksi [65], a random set of data has been generated assuming the number of specimen *m* equal to 14 and they are given in Table 4.2

Table 4.1: Experimental Ultimate strength data for graphite/epoxy [65]

S. No	1	2	3	4	5	6
Ultimate strength (ksi)	63.152	66.312	71.900	72.323	72.626	75.050
S. No	7	8	9	10	11	12
Ultimate strength (ksi)	77.743	78.316	80.052	81.324	81.742	84.154

Table 4.2: Ultimate strength data for graphite/epoxy

S. No	1	2	3	4	5	6	7
Ultimate strength (ksi)	63.394	64.844	66.771	67.849	68.570	69.889	70.366
S. No	8	9	10	11	12	13	14
Ultimate strength (ksi)	71.686	72.286	73.614	75.064	77.002	80.881	82.336

The first moment, second and third central moments have been calculated using Equation (4.2). They are found to be $m_1 = 71.7541$, $m_2 = 29.3415$, $m_3 = 70.9981$, $\mu = 71.7541$.

Table 4.3: Experimental Fatigue and residual strength data for graphite / epoxy [65]

S. No	No of cycles to fracture (n)	Residual strength (ksi) $R_i(n)$	S. No	No of cycles to fracture (n)	Residual strength (ksi) $R_i(n)$
1	1650	64.012	14	18790	52.716
2	1950	64.012	15	3840	52.716
3	1320	64.012	16	161000	50.456
4	2050	60.246	17	110000	50.456
5	50980	56.481	18	523500	48.950
6	6480	56.481	19	863200	48.950
7	155000	52.716	20	1346300	46.691
8	228500	52.716	21	1007000	460.201
9	88000	52.716	22	30000	61.455
10	117580	52.716	23	30000	64.544
11	228700	52.716	24	30000	62.4
12	221200	52.716	25	30000	61.62
13	310000	52.716			

Using the randomly generated data in Table 4.2, the shape and scale parameters in the Weibull distribution are determined and they are found to be $\alpha = 13.4285$, $X_0 = 74.3502$.

Taking the experimental data for the fatigue test (Yang and Liu) [65] from the Table 4.3, for 25 specimens, the S-N curve has been plotted as shown in Fig 4.1. The simulated data have been developed which are given in Table 4.4. These data have been used for finding

the fatigue parameters for graphite/epoxy. It could be noted that these data are not same as the experimental data taken in [65].

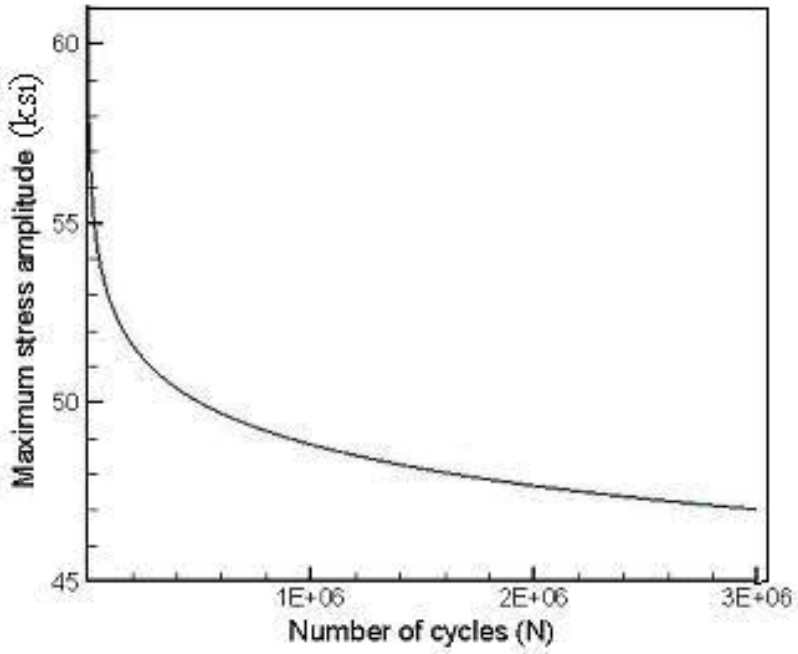

Fig.4.1: Developed S-N curve for graphite/ epoxy

These residual strengths $R_i(n_i),\quad i=1,2,3,....J$ of fatigue specimens have been converted into equivalent ultimate strength $R_i(0)$, using Equation (4.4). Similar to Equation (4.2) for static data, here also the first three central moments have been calculated with the help of the data given in Table 4.2 using the Equations (4.5).

Following the algorithm given in the previous section, for graphite/epoxy, the values of c, b and K are obtained as c=12, b=19, and K=1.34X10^{-38}. It may be noted that the c, b, and K values obtained in Yang and Liu [6] are c=10.818, b=17.78 and K=1.8285X10^{-36}. Using the values of K, b and c in residual strength degradation Equation (4.1), the fatigue life curves have been determined and are shown in Fig. 4.2. These curves have been obtained for 99%, 90% and 80% of residual strength. For 99% residual strength, $R_i(0)$ is taken as 99% of the mean ultimate strength (μ). In the case of glass/epoxy, the mean ultimate strength is found to be 71.7541 ksi. Here the maximum developed stress (S) is taken as 85% of mean ultimate strength. Fig.4.3 shows residual strength degradation vs.

the number of cycles by taking the *K*, *b* and *c* values obtained in the work of Yang and Liu [65] under similar conditions.

Table 4.4: Simulated Fatigue and residual strength data for graphite / epoxy

S. No	No of cycles to fracture (n)	Residual strength (ksi) R_i (n)	S. No	No of cycles to fracture (n)	Residual strength (ksi) R_i (n)
1	2805.94	57.1637	18	726493	49.3466
2	18187.9	55.8445	19	761770	49.2727
3	18255.5	56.1376	20	812733	49.1985
4	18323.1	56.4307	21	851923	49.0878
5	18399	56.7604	22	887209	49.0506
6	25946.5	55.478	23	934234	48.9031
7	33730.4	55.2214	24	993040	48.8288
8	37575.9	54.8916	25	1.02E+06	48.7916
9	41412.9	54.5251	26	1.06E+06	48.6809
10	45266.9	54.2319	27	1.12E+06	48.57
11	53033.9	53.902	28	1.22E+06	48.5325
12	64731	53.6087	29	1.26E+06	48.4217
13	72498	53.2788	30	1.17E+06	48.421
14	88125.1	53.0221	31	1.30E+06	48.3102
15	99847	52.8387	32	1.35E+06	48.3093
16	111553	52.3618	33	1.40E+06	48.2351
17	131110	52.1049	34	1.47E+06	48.1605

Here it may be noted that in the work of Yang and Liu [65], experimental data have been used and in the present case the simulated data have been used for finding the fatigue life of the specimen. From these figures and Table 4.3, it could be observed that the present method predicts life, which is within 8% of the life predicted, by Yang and Liu [65]. It could also be observed that for a specimen with lower initial residual strengths, the difference has been observed to be very less.

Hence, simulated data could be used to predict the fatigue life of a specimen in absence of experimental data if the S-N curve for the material is available. In the following sections, simulated data are generated to determine these fatigue constants for Ti6Al4V, CoCr alloy and UHMWPE materials.

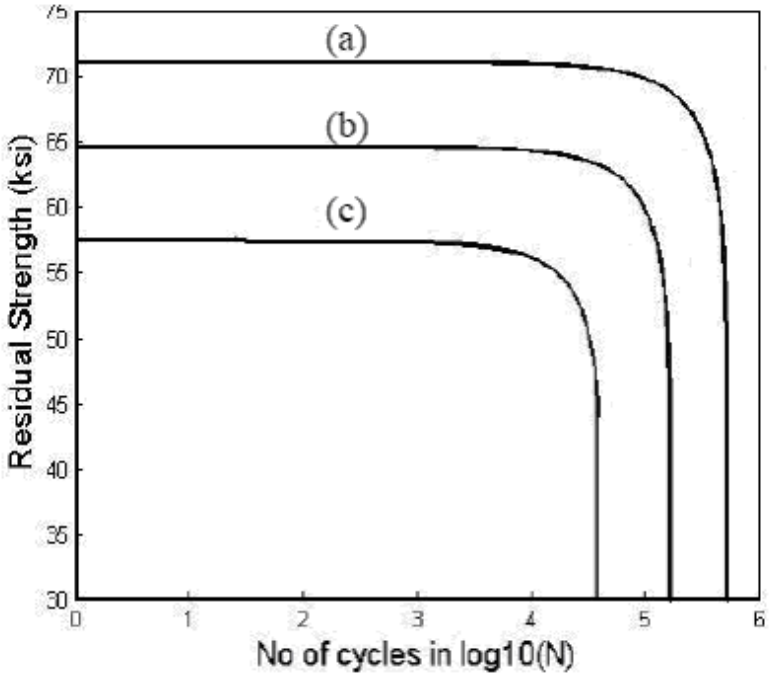

Fig.4.2: Residual strength vs. number of cycles for graphite / epoxy with *K*, *b*, *c* value obtained from the present analysis; (a) 99% residual strength, (b) 90% residual strength, (c) 80% residual strength.

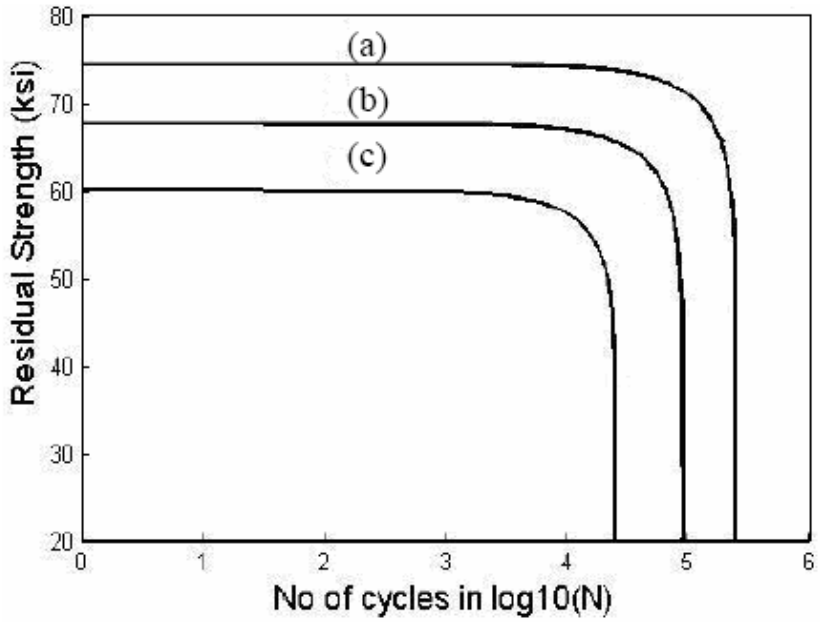

Fig.4.3: Residual strength vs number of cycles for graphite /epoxy with *K*, *b*, *c* value taken from [65] (a) 99% residual strength, (b) 90% residual strength, (c) 80% residual strength.

4.2.3 Determination of fatigue parameter *c, b, K* for Ti6Al4V

In order to determine the parameters *c*, *b* and *K* in residual strength degradation model (Equation (4.1)), two sets of specimen are required to be tested. One set of *m* specimen, referred to as static specimens subjected to static loading should be taken to determine ultimate strength $(x_1, x_2 \cdots x_m)$. As it is known from experimental data that the ultimate strength of Ti6Al4V material varies 900 to 1200 MPa [39,106], a random set of data has been generated taking 12 specimens and they as listed in Table 4.5.

Table 4.5: Ultimate strength data for Ti6Al4V

S. No	1	2	3	4	5	6
Ultimate strength (MPa)	969.905	979.147	986.967	993.365	993.365	993.365
S. No	7	8	9	10	11	12
Ultimate strength (MPa)	1009	1013.98	1020.38	1028.91	1063.03	1079.38

Following Yang and Liu [65], the first three central moments have been calculated using the Equation (4.2). They are found to be $m_1 = 1014.5$, $m_2 = 969.84$, $m_3 = 1.8986 \times 10^4$, $\mu = 1014.5$.

This technique has been used to estimate the values of the parameters that maximize the likelihood for the observed sample data. In the present work, using Table 4.3, these parameters have been calculated by using least square fitting in MATLAB and are found to be α=31.3, x_0 =1030.4.

Table 4.6 shows 42 different sets of data for residual strength and number of cycles to fracture, which are obtained from the S-N curve of Ti6Al4V [107].

These data are similar to the data obtained by testing 42 different specimens under fatigue loading as the S-N curve is obtained from the experimental data.

Following similar procedure as in the previous section 4.2.2, for Ti6Al4V *c*, *b* and *K* are calculated and they are found to be $c=34.1$, $b=15.4$, $K=1.823X10^{-44}$.

The residual strength could be obtained under any maximum stress level *S* at any number of cycles *n* using Equation (4.1).

Table 4.6: Simulated Fatigue and residual strength data for Ti6Al4V

S. No	No of cycles to fracture(N)	Residual strength (MPa) $R_i(n)$	S. No	No of cycles to fracture (N)	Residual strength (MPa) $R_i(n)$
1	175	676.4180	22	12489	511.393
2	216	670.5320	23	15966	503.541
3	248	660.6930	24	21133	493.722
4	295	654.8020	25	27042	487.842
5	339	646.9350	26	35858	481.966
6	419	639.0780	27	44200	472.137
7	499	633.1870	28	54530	464.28
8	709	621.4060	29	64923	456.417
9	785	611.5620	30	95879	452.529
10	1004	605.6810	31	1090020	395.693
11	1153	595.8420	32	1396070	391.785
12	1424	589.9570	33	1781590	379.989
13	1884	580.1370	34	2450240	376.09
14	2165	572.2700	35	3251950	372.187
15	2967	560.4840	36	4468390	366.317
16	3663	554.5980	37	5517780	360.432
17	4213	548.7030	38	7849570	352.595
18	5016	540.8400	39	12001900	346.74
19	6424	536.9320	40	16521200	344.813
20	8510	529.0850	41	25306300	342.902
21	10132	521.2230	42	34772500	337.032

4.2.4 Determination of fatigue parameter *c, b, K* for CoCr alloy

Similar procedure as described in previous sections has been followed for determination of fatigue parameters of CoCr alloy. Since, it is known from experimental data that the ultimate strength of CoCr alloy varies between 650 and 750 MPa [39,106], a random set of data has been generated taking 12 specimens as shown in Table 4.7.

The first moment, second and third central moments have been calculated using the Equation (4.2) and they are m_1=694.4906, m_2=262.4902, m_3=2.5664×10^3, μ =694.4906.

Scale parameter and shape parameters are found to be α=41.0968, x_0 =702.7998, respectively.

Table 4.7: Ultimate strength data for CoCr alloy

S.No	Ultimate Strength (MPa)
1	670.931
2	675.817
3	679.939
4	683.299
5	685.904
6	689.267
7	694.104
8	697.466
9	701.580
10	710.225
11	719.272
12	728.323

Table 4.8 shows 42 different sets of data for residual strength and number of cycles to failure, which are taken from the S-N curve of CoCr alloy [107].

After minimizing the mean square difference of the first three central moments given in Equation (4.2) and (4.5) the parameters of residual strength degradation model are obtained as follows.

c= 48, b= 16.9, K=1.413×10^{-46}

Table 4.8: Simulated fatigue and residual strength data for CoCr alloy

S. No	No of cycles to fracture (N)	Residual strength (MPa) $R_i(n)$	S. No	No of cycles to fracture(N)	Residual strength (MPa) $R_i(n)$
1	175	492.957	22	12489	390.76
2	216	492.957	23	15966	386.75
3	248	486.946	24	21133	378.74
4	295	484.942	25	27042	366.71
5	339	480.934	26	35858	366.71
6	419	474.922	27	44200	358.7
7	499	470.914	28	54530	352.69
8	709	466.907	29	64923	346.67
9	785	460.895	30	95879	340.66
10	1004	456.887	31	1090020	336.65
11	1153	448.872	32	1396070	330.64
12	1424	442.86	33	1781590	322.626
13	1884	430.837	34	2450240	314.611
14	2165	426.829	35	3251950	310.603
15	2967	436.848	36	4468390	304.591
16	3663	430.837	37	5517780	298.58
17	4213	418.813	38	7849570	292.568
18	5016	410.8	39	12001900	288.56
19	6424	408.794	40	16521200	280.545
20	8510	404.786	41	25306300	278.541
21	10132	398.774	42	34772500	272.529

4.2.5 Determination of fatigue parameter *c, b, K* for UHMWPE

Above procedure is also followed for finding of fatigue parameters of UHMWPE. Since, it is known from experimental data that the ultimate strength of CoCr alloy varies between 35 and 45 MPa, a random set of data has been generated taking 12 specimens as shown in Table 4.9.

Table 4.9: Ultimate strength data for UHMWPE

S. No	1	2	3	4	5	6
Ultimate strength (MPa)	38.8009	39.1738	39.4901	39.7500	40.0103	40.2413
S. No	7	8	9	10	11	12
Ultimate strength (MPa)	40.3866	40.6177	40.8488	41.1662	41.7680	43.1698

The first moment, second and third central moments have been calculated using the Equation (4.2) and they are m_1 =40.5994, m_2 =1.4791, m_3 =1.0281, μ =40.5994. Scale parameter and shape parameters are found to be α=41.0968, x_0 =41.2170. Table 4.10shows 34 different sets of data for residual strength and number of cycles to failure, which are taken from the S-N curve of UHMWPE.

Table 4.10: Simulated Fatigue and residual strength data for UHMWPE

S. No	No of cycles to fracture (N)	Residual strength (MPa) R_i(n)	S. No	No of cycles to fracture (N)	Residual strength (MPa) R_i(n)
1	100	21.7	18	1163	17.42
2	133	21.425	19	13335	17.375
3	178	21.15	20	17783	17.15
4	237	20.875	21	23714	16.925
5	316	20.6	22	31623	16.7
6	421	20.35	23	42170	16.45
7	562	20.1	24	56234	16.2
8	750	19.85	25	74989	15.95
9	1000	19.6	26	100000	15.7
10	1333	19.3	27	133353	15.45
11	1778	19	28	177828	15.2
12	2371	18.7	29	237137	14.95
13	3162	18.4	30	316228	14.7
14	4216	18.2	31	421696	14.5
15	5623	18	32	562341	14.3
16	7499	17.8	33	749894	14.1
17	10000	17.6	34	1000000	13.9

After minimizing the mean square difference of the first three central moments given in Equation (4.2) and (4.5) one may obtain c = 10.6, b= 26.5, K=1.783×10^{-37}.

Table 4.11: *c*, *b*, *K* values for three different materials

Type of material	*c*	*b*	*K*
Ti6-Al4-V	34.1	15.4	1.823×10^{-44}.
Co-Cr alloy	48	16.9	1.413×10^{-46}
UHMWPE	10.6	26.5	1.783×10^{-37}

The *c*, *b*, *K* constant values obtained for the three different biomaterials viz., Ti6-Al4-V, CoCr alloy and UHMWPE using simulated data have been listed in Table 4.11. These data will be useful for the researchers working on fatigue life estimation of different prostheses using the residual strength degradation model.

4.3 Evaluation of fatigue life

Fatigue life of different prosthesis has been evaluated using 3D finite element analysis along with residual strength degradation model. In this analysis, static loading has been considered and the maximum load experienced by the prosthesis during one cycle (Bergman *et al*. [3]) has been applied. Equivalent von Mises stresses have been obtained from the finite element analysis and have been used in the residual strength degradation model for the determination of fatigue life. For a given loading, factor of safety values have also been calculated using Goodman, Soderberg and Gerber relations.

In the present work, two different models of prosthesis have been considered. These models have been used for the analysis of three different patients for nine different daily activities. Two different types of prosthesis materials viz., Ti6Al4V and CoCr alloys have been considered for the analysis.

Table 4.12 describes the details of different patients in terms of their ages, body weights, and anatomical specifications. Table 4.13 shows details of two models considered in the present case and Figs 4.4 and 4.5 show the FE meshes of two models, respectively. The orientations and the magnitudes of the equivalent static load are different for different activities and for the same activity the magnitude of the load acting varies from patient to patient. Description of various activities is given in Table 4.14 (Bergmann *et al*. [3]). Table 4.15 shows the magnitude and directions of the equivalent static load (Bergmann *et al.* [3]) for different patients corresponding to different activities. These values are obtained by multiplying the body weight with the magnification factor given in the

experimental work of Bergmann *et al.* [3]. It may be noted that the magnification factors are different for different patients and different activities.

Table 4.12 Personal data of different patients [3].

Patient	Patient 1	Patient 2	Patient 3
Gender	Male	Male	Male
Age	55	51	61
Operated Joint	Right	Left	Right
Body weight (N)	860	980	702

Table 4.13 Dimensions of the two models of the hip prosthesis used in the analysis

Parts	Model 1	Model 2
Stem and Head	Sphere radius 20 Stem length 100 Stem outer radius 8 Stem inner radius 6.5 Neck length 50 Neck inclination 45^0	Sphere radius 20 Stem length 100 Stem outer radius 8 Stem inner radius 0
Cement Layer	Length 100 Outer radius 12 Inner radius 8	Length 100 Outer radius 12 Inner radius 8
Cancellous bone	-	Length 350 Outer radius 16 Inner radius 12
Cortical bone	Length 350 Outer radius 25 Inner radius 16	Length 350 Outer radius 25 Inner radius 16

In the present analysis, solid 92 and solid 187 elements were used, for model 1 the solid 92 element has been used and for model 2, solid 187 element has been used. All nodes at the bottom face has been constrained fully in all degrees of freedom and the load have been applied from the top of the femoral head. In model 2, additionally the abductor muscle force has been applied in the great trochanter position.

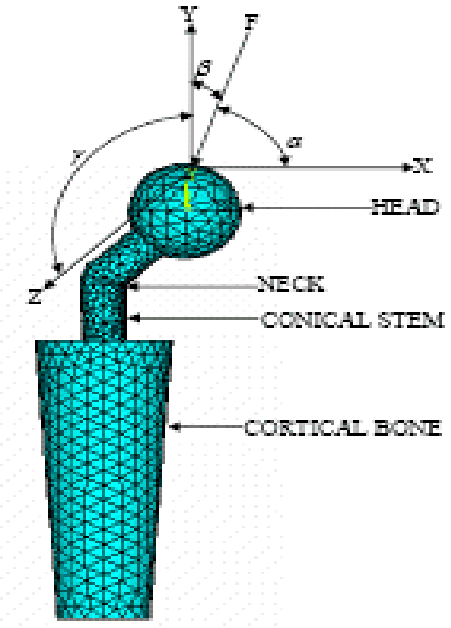

Fig 4.4: Finite Element mesh for model 1 of cemented hip prosthesis

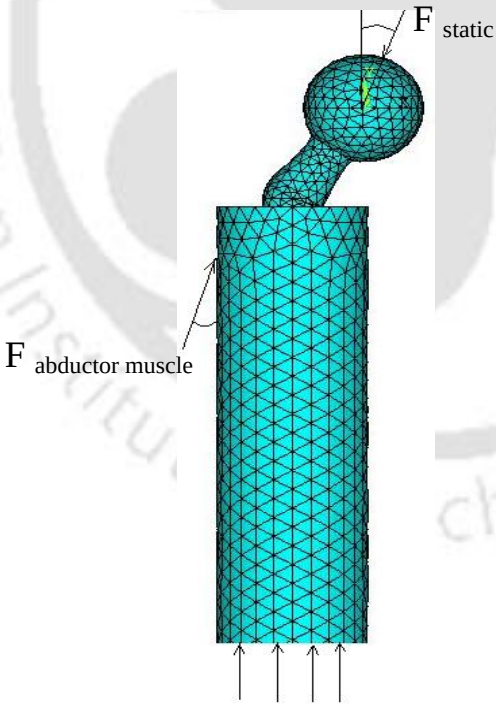

Fig 4.5: Finite element mesh for Model 2 of implanted cemented hip prosthesis

Table 4.14 Description of various activities [3]

Sl. No	Activity	Description
1	Slow walking (SW)	Walking at slow speed on level ground, average speed of all patients =3.5 kmph (0.98m/s)
2	Normal walking (NW)	Walking at normal speed on level ground, average speed of all patients =3.9 kmph (1.09m/s)
3	Fast walking (FW)	Walking at fast speed on level ground, average speed of all patients =5.3 kmph (1.46m/s)
4	Up stairs (US)	Walking upstairs, stair length 17 cm, no support at hand rail.
5	Down stairs (DS)	Walking downstairs, stair length 17 cm, no support at hand rail.
6	Standing up (SU)	Standing up, chair height 50 cm, arms hold at chest height
7	Sitting down (SD)	Sitting down, chair height 50 cm, arms hold at chest height
8	Standing on 2-1-2 legs (SL)	Two-legged stance- One legged stance-Two legged stance
9	Knee bend (KB)	Two-legged stance Bending knees Two legged stance

Table 4.15 Magnitude and direction of applied load for different activities for different patients

Patients	Peak load (N)								
	Activities								
	1 **SW** $\alpha = 36^0$ $\beta = 12^0$	**2** **NW** $\alpha = 31^0$ $\beta = 13^0$	**3** **FW** $\alpha = 30^0$ $\beta = 12^0$	**4** **US** $\alpha = 46^0$ $\beta = 14^0$	**5** **DS** $\alpha = 35^0$ $\beta = 12^0$	**6** **SU** $\alpha = 16^0$ $\beta = 14^0$	**7** **SD** $\alpha = 16^0$ $\beta = 1^0$	**8** **SL** $\alpha = 28^0$ $\beta = 7^0$	**9** **KB** $\alpha = 16^0$ $\beta = 7^0$
1	2055.4	2132.8	2399.4	2279	2261.8	1556.6	1513.6	2175.8	1522.2
2	2499	2067.8	2136.4	2224.6	2214.8	2038.4	1499.4	2185.4	1146.6
3	1712.88	1698.84	1930.5	1909.44	2218.32	1277.64	1045.98	2590.38	1031.94

4.3.1 Fatigue life of Ti6Al4V prosthesis

Finite element models have been developed using ANSYS 9.0 for the two different prosthesis models using SOLID 92 elements and SOLID 187 elements (as described in chapter 3). The distal end of the prosthesis has been constrained and the peak load has been applied with proper orientation and magnitude depending upon the type of patients and the corresponding activities. Material properties and dimensions of the prosthesis made of Ti6Al4V used for the analysis are as described in Tables 3.3 (chapter 3) and 4.13, respectively. The finite element model consists of 24942 nodes and 16324 elements for model 1. From the FE analysis, maximum von Mises stresses obtained for different models and different patients corresponding to different activities have been tabulated in Table 4.16. The von Mises stresses thus obtained from the FE analysis have been used in the residual strength degradation model for calculating the fatigue life of the prosthesis corresponding to different activities.

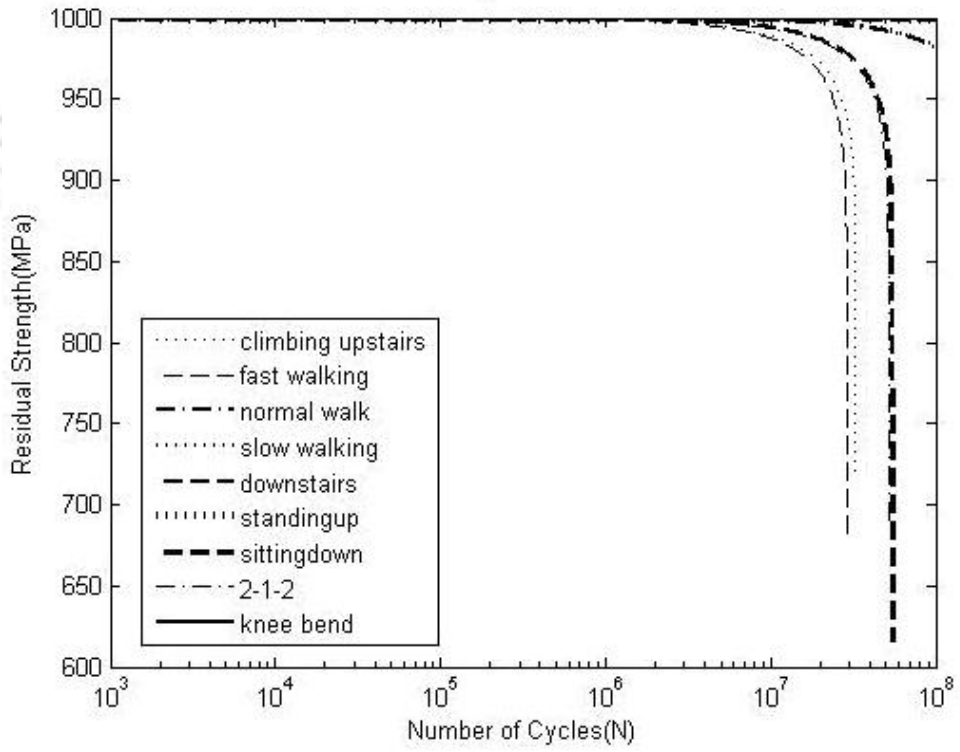

Fig 4.6: Fatigue life of Ti6Al4V made hip prosthesis for patient1 and model 1

Figures 4.6, 4.7 and 4.8 show the fatigue life curves for patient 1, patient 2 and patient 3 respectively with Ti6Al4V prosthesis material corresponding to nine different activities.

It could be observed from the table 4.16 that in the model 1 of the prosthesis, fatigue life of the prosthesis for patient 1 is minimum corresponding to fast walking, which is 5×10^6 cycles.

However, for patient 2 and patient 3, minimum fatigue lives correspond to standing 2-1-2 posture. For other activities the fatigue life is comparatively more.

For model 2, it has been observed that for patient 1 minimum fatigue life corresponds to first working conditions, whereas for patient 2 and patient 3, minimum fatigue life corresponds to climbing upstairs.

From the above observations, it could be inferred that model 2 has more fatigue life compared to model 1 for the three patients studied in the present work under different activities.

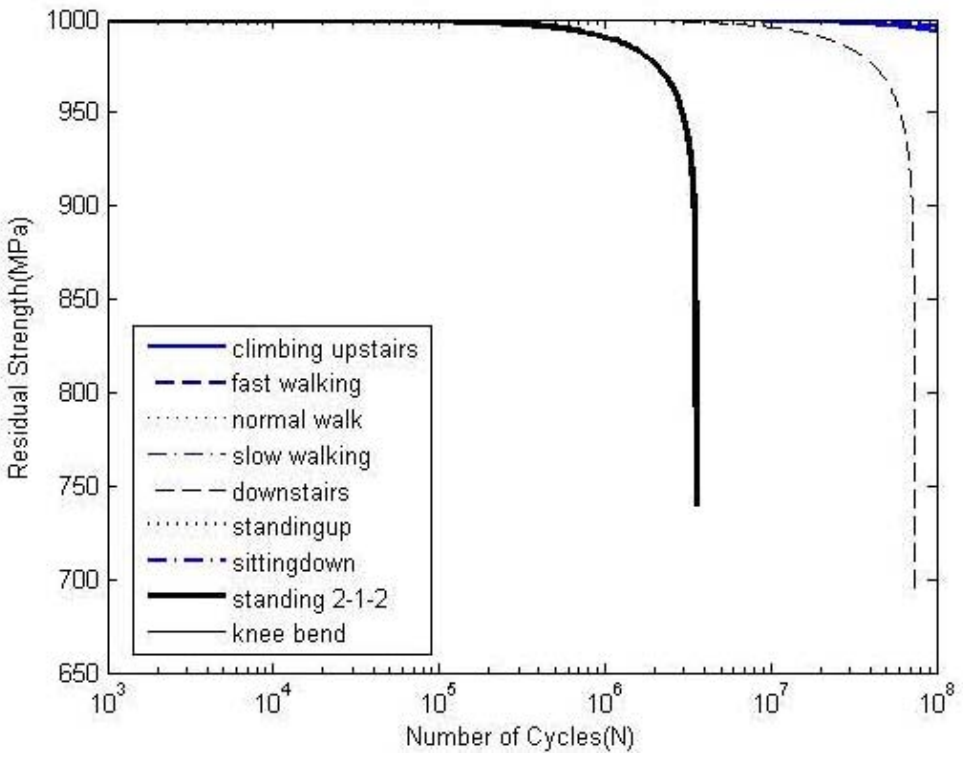

Fig 4.7: Fatigue life of Ti6Al4V made hip prosthesis for patient 2 and model 1

Table 4.16: Maximum von Mises stresses for Ti6Al4V prosthesis for different activities and models

Patients	Activities	Maximum von Mises Stress(MPa)	
		Model 1	Model 2
1	Slow walking	198.606	141.308
	Normal walking	199.573	144.709
	Fast walking	226.793	164.435
	Climbing upstairs	225.004	155.411
	Downstairs	217.736	155.395
	Standing up	135.082	104.486
	Sitting down	119.058	128.31
	Standing on 2-1-2 legs	218.392	161.457
	Knee bend	122.181	111.209
2	Slow walking	165.509	171.805
	Normal walking	158.966	140.299
	Fast walking	182.472	146.411
	Climbing upstairs	188.517	151.702
	Downstairs	213.551	152.166
	Standing up	110.874	136.827
	Sitting down	82.275	127.106
	Standing on 2-1-2 legs	260.005	162.169
	Knee bend	82.83	83.773
3	Slow walking	241.469	117.76
	Normal walking	193.491	115.265
	Fast walking	201.934	132.301
	Climbing upstairs	219.633	130.21
	Downstairs	213.212	152.408
	Standing up	176.892	85.761
	Sitting down	117.941	88.675
	Standing on 2-1-2 legs	219.355	192.218
	Knee bend	92.033	75.398

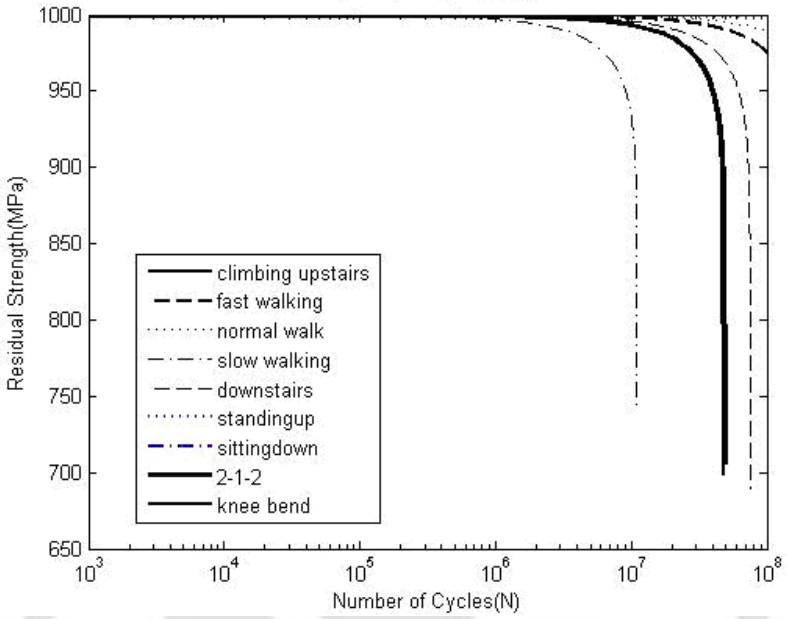

Fig 4.8: Fatigue life of Ti6Al4V made hip prosthesis for patient 3 and model 1

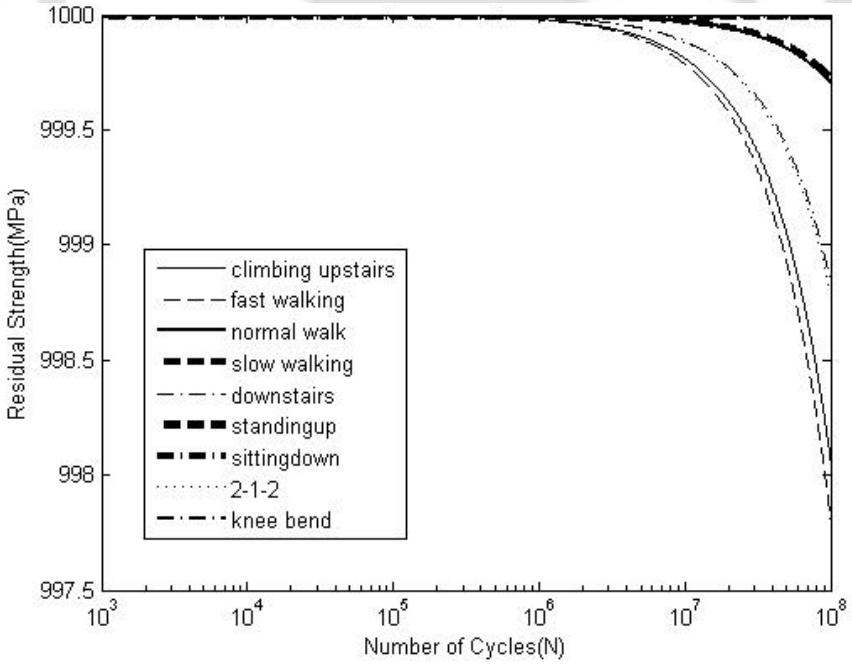

Fig 4.9 Fatigue life of hip prosthesis made of Ti6Al4V for patient 1 and model 2

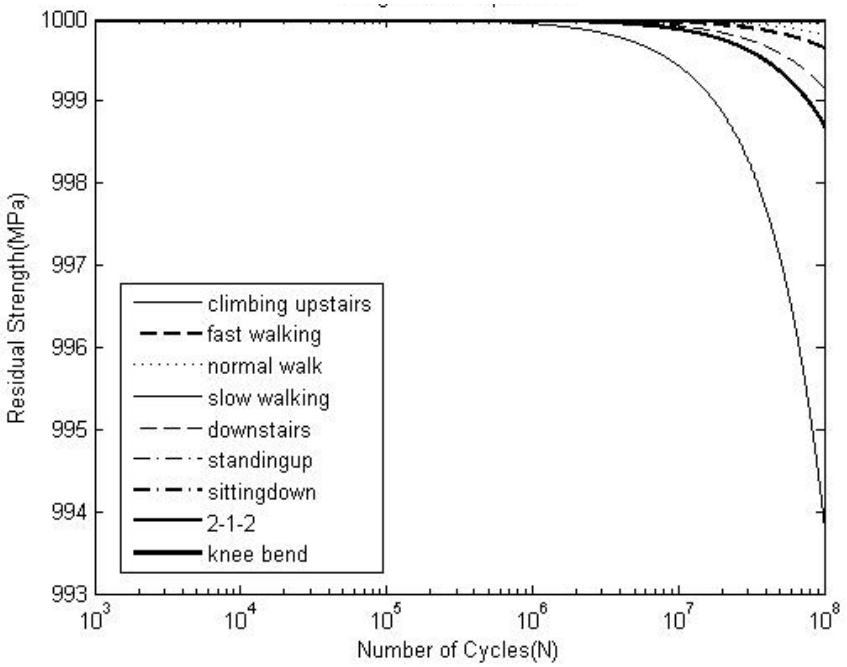

Fig 4.10 Fatigue life of hip prosthesis made of Ti6Al4V for patient 2 and model 2

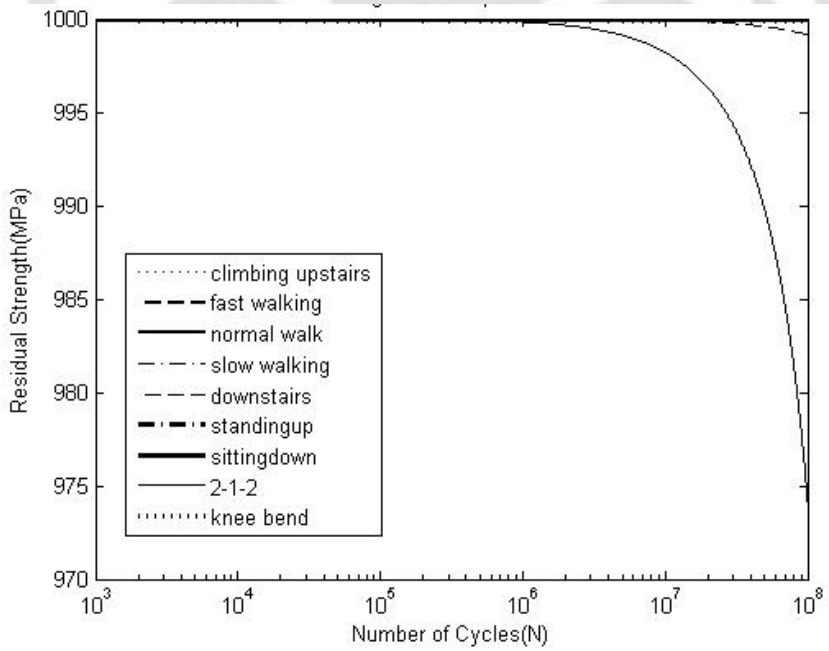

Fig 4.11 Fatigue life of hip prosthesis made of Ti6Al4V for patient 3 and model 2

After determination of fatigue lives using residual strength degradation model, the results could be qualitatively compared by finding the factor of safety using Soderberg, Goodman and Gerber relations. These relations are as given below.

1. Soderberg relation: $(\sigma_a/\sigma_e)+(\sigma_m/\sigma_y)=1/FOS$
2. Goodman relation: $(\sigma_a/\sigma_e)+(\sigma_m/\sigma_u)=1/FOS$
3. Gerber relation: $(FOS\,\sigma_a/\sigma_e)+(FOS\sigma_m/\sigma_u)^2=1$

Here, $\sigma_e, \sigma_u, \sigma_{y,} \sigma_m$ and σ_a are endurance limit, ultimate strength, yield stress, mean stress and alternate stress respectively for the specimen. *FOS* is the factor of safety.

Using the maximum von Mises stress and other material properties, the factor of safety values for different patients with different activities having prosthesis made of Ti6Al4V have been calculated using the above relations and are listed in Table 4.17. It could be observed from the Table 4.17, that the operating factor of safety varies from patient to patient and for a particular patient, the factor of safety varies with the type of prosthesis model. From Table 4.17 it could also be observed that for patient1, minimum factor of safety occurs corresponding to fast waking but model 2 perform better compared to model 1. For patient 2, minimum factor of safety occurs corresponding to standing 2-1-2 for model 1 and slow walking for model 2. For patient 3, minimum factor of safety occurs corresponding to slow walking for model 1 and corresponding to standing 2-1-2 for model 2. These observations are qualitatively similar to the observations made using the residual strength degradation model, in terms of determination of fatigue lives.

4.3.2 Fatigue life of CoCr alloy prosthesis

Similar to the prostheses made of Ti6Al4V, for the CoCr alloy prosthesis also, the maximum von-Mises stresses for two different models with nine different loading conditions have been found out from equivalent static stress analysis, these stresses are listed in Table 4.16.

Table 4.17: Factor of safety values for two different materials, models and three different patients

Patient	Activities	Soderberg		Goodman		Gerber	
		Model 1	Model 2	Model 1	Model 2	Model 1	Model2
1	Slow walking	2.197	3.088	2.323	3.266	2.789	3.92
	Normal walking	2.186	3.015	2.312	3.189	2.775	3.828
	Fast walking	1.924	2.654	2.0350	2.807	2.442	3.369
	Climbing upstairs	1.939	2.808	2.0512	2.97	2.462	3.565
	Downstairs	2.004	2.808	2.119	2.97	2.544	3.565
	Standing up	3.230	4.176	3.416	4.417	4.100	5.302
	Sitting down	3.665	3.401	3.876	3.597	4.652	4.317
	Standing on 2-1-2 legs	1.998	2.703	2.113	2.859	2.536	3.431
	Knee bend	3.571	3.924	3.777	4.15	4.533	4.981
2	Slow walking	2.636	2.54	2.789	2.686	3.347	3.224
	Normal walking	2.745	3.11	2.903	3.29	3.485	3.948
	Fast walking	2.391	2.98	2.529	3.152	3.036	3.784
	Climbing upstairs	2.315	2.876	2.448	3.042	2.939	3.652
	Downstairs	2.043	2.868	2.161	3.033	2.594	3.641
	Standing up	3.936	3.189	4.163	3.373	4.996	4.049
	Sitting down	5.304	3.433	5.61	3.631	6.733	4.358
	Standing on 2-1-2 legs	1.678	2.691	1.775	2.846	2.131	3.416
	Knee bend	5.268	5.209	5.572	5.509	6.688	6.613
3	Slow walking	1.807	3.706	1.911	3.919	2.294	4.704
	Normal walking	2.255	3.786	2.385	4.004	2.863	4.806
	Fast walking	2.161	3.298	2.286	3.489	2.743	4.187
	Climbing upstairs	1.987	3.351	2.101	3.545	2.522	4.254
	Downstairs	2.047	2.863	2.165	3.028	2.598	3.635
	Standing up	2.467	5.088	2.609	5.382	3.132	6.459
	Sitting down	3.7	4.921	3.913	5.205	4.697	6.247
	Standing on 2-1-2 legs	1.989	2.27	2.104	2.401	2.525	2.882
	Knee bend	4.741	5.787	5.015	6.121	6.019	7.347

Table 4.18: Maximum von Mises stresses for CoCr prosthesis for different activities

Patient	Activities	Maximum von Mises stress (MPa)	
		Model 1	Model 2
1	Slow walking	198.607	141.308
	Normal walking	199.575	144.709
	Fast walking	226.794	164.435
	Climbing upstairs	225.005	155.411
	Downstairs	217.738	155.395
	Standing up	135.083	104.486
	Sitting down	119.059	128.31
	Standing on 2-1-2 legs	218.394	161.457
	Knee bend	122.182	111.209
2	Slow walking	165.51	171.805
	Normal walking	158.967	140.299
	Fast walking	182.473	146.411
	Climbing upstairs	188.518	151.702
	Downstairs	213.552	152.166
	Standing up	110.874	136.827
	Sitting down	82.276	127.106
	Standing on 2-1-2 legs	260.007	162.169
	Knee bend	82.83	83.773
3	Slow walking	241.471	117.76
	Normal walking	193.492	115.265
	Fast walking	201.935	132.301
	Climbing upstairs	219.634	130.21
	Downstairs	213.213	152.408
	Standing up	176.893	85.761
	Sitting down	117.942	88.675
	Standing on 2-1-2 legs	219.357	192.218
	Knee bend	92.034	75.398

Figures 4.12 to 4.17 show the fatigue life curves for CoCr prosthesis for three different patients under different activities. Two models of the prosthesis have been considered. It could be observed that in model 1 of the prosthesis, fatigue life of the prosthesis for patient 1 is minimum corresponding to fast walking, which is 5×10^6 cycles. However for patient 2 and patient 3, minimum fatigue life corresponds to standing 2-1-2 posture. For other activities the fatigue life is comparatively more. For model 2, it has been observed that for patient 1, minimum fatigue life corresponds a first working condition, whereas for patient 2 and patient 3, minimum fatigue life corresponds to climbing upstairs. From the above observations, it could be inferred that the model 2 leads to more fatigue life

compared to model 1 for the different patients studied in the present work under different activities.

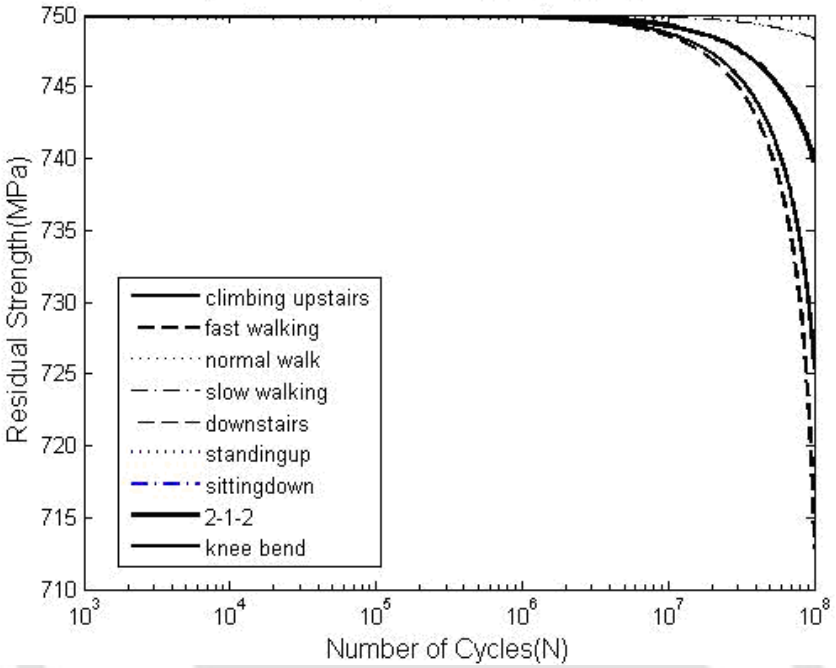

Fig 4.12: Fatigue life of hip prosthesis made of CoCr for patient1 and model1

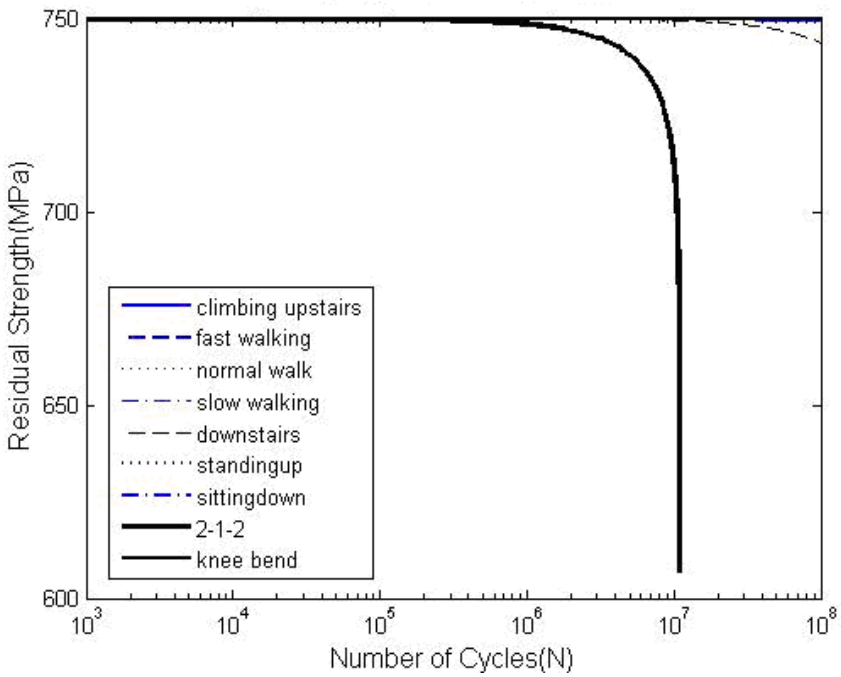

Fig 4.13: Fatigue life of hip prosthesis made of CoCr for patient2 and model1

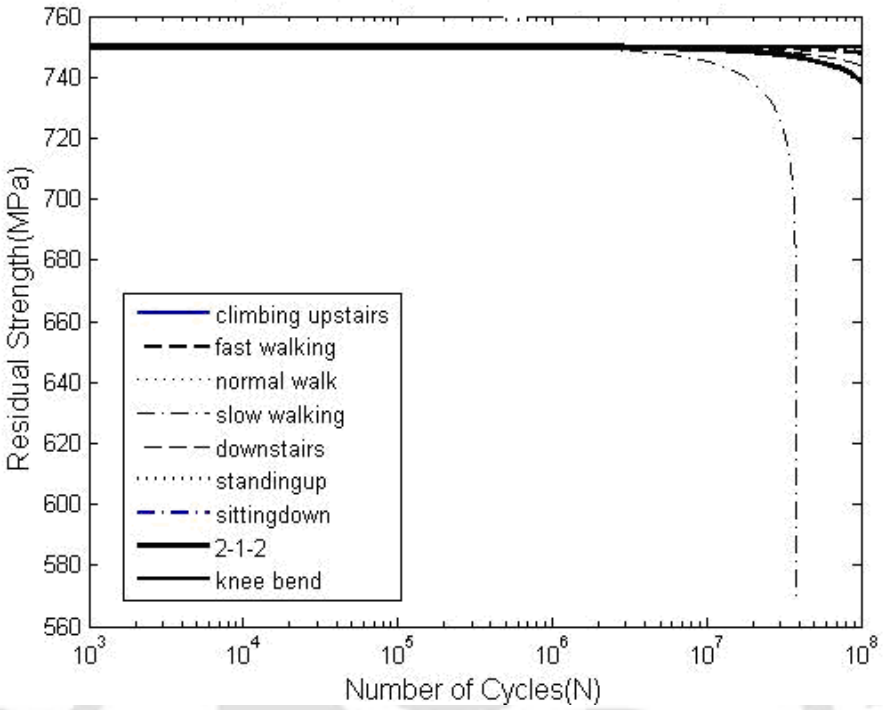

Fig 4.14: Fatigue life of hip prosthesis made of CoCr for patient3 and model1

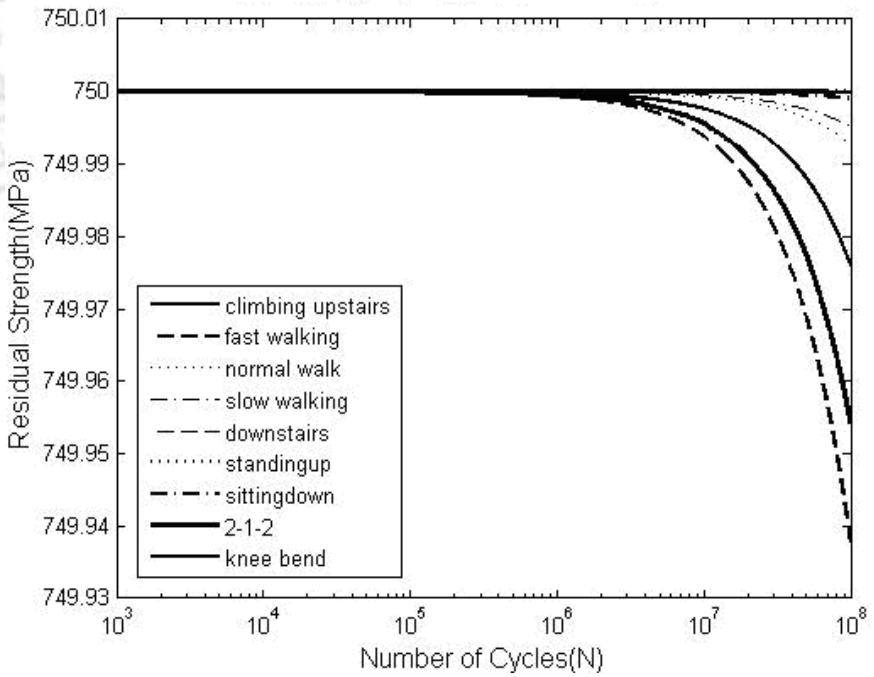

Fig 4.15: Fatigue life of hip prosthesis made of CoCr for patient1 and model2

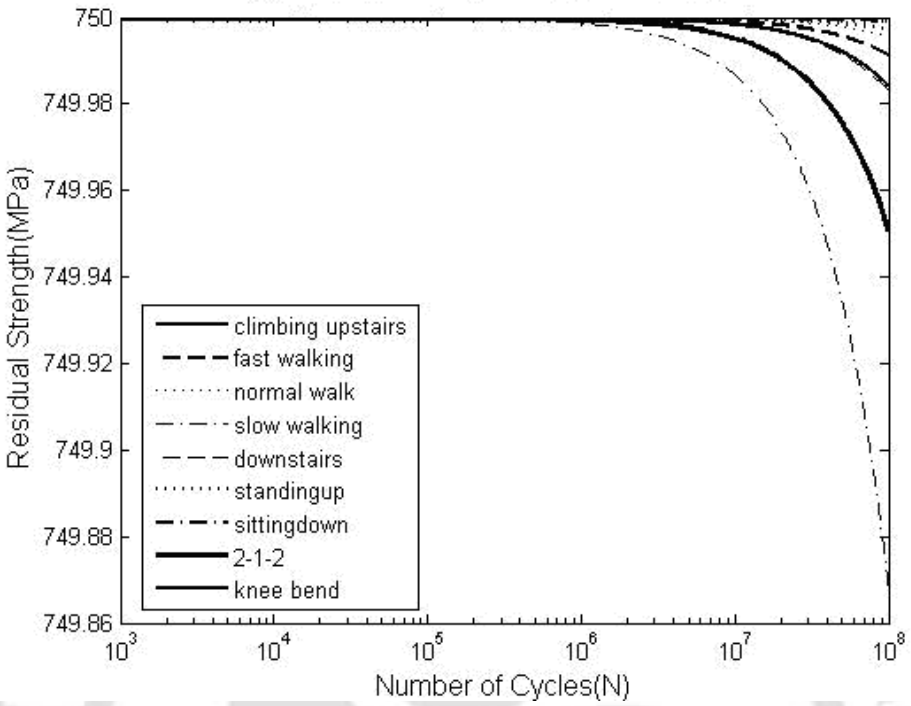

Fig 4.16: Fatigue life of hip prosthesis made of CoCr for patient2 and model2

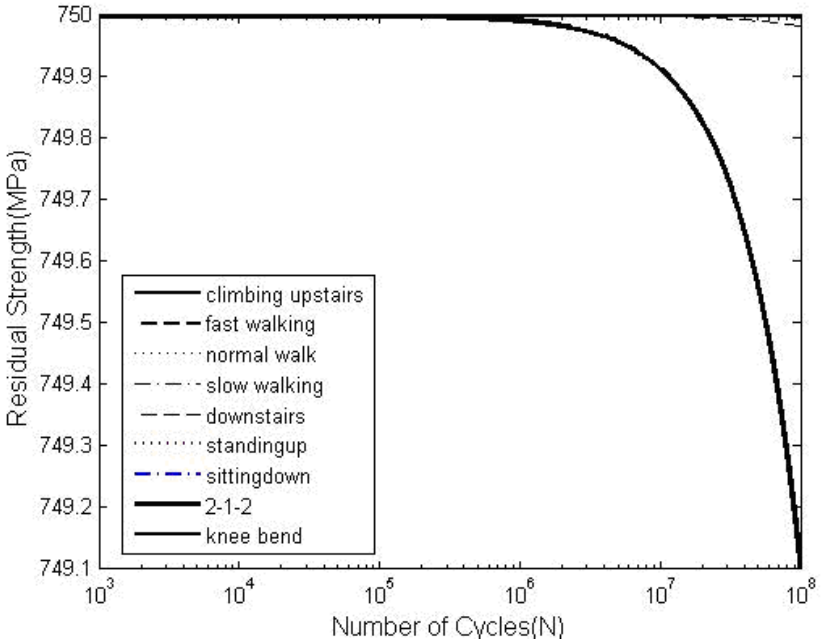

Fig 4.17: Fatigue life of hip prosthesis made of CoCr for patient3 and model2

Table 4.19 show the factor of safety values compared using the three relations for the prosthesis made of CoCr alloy for different patients under different activities.

Table 4.19: Factor of safety value for CoCr material for three different patients

Patient	Activities	Soderberg		Goodman		Gerber	
		Model 1	Model 2	Model 1	Model 2	Model 1	Model 2
1	Slow walking	1.576	2.215	1.648	2.316	1.923	2.703
	Normal walking	1.569	2.163	1.64	2.262	1.914	2.64
	Fast walking	1.38	1.904	1.443	1.99	1.684	2.323
	Climbing upstairs	1.391	2.014	1.455	2.106	1.698	2.458
	Downstairs	1.438	2.015	1.503	2.106	1.754	2.458
	Standing up	2.317	2.996	2.423	3.132	2.828	3.656
	Sitting down	2.629	2.44	2.749	2.551	3.208	2.977
	Standing on 2-1-2 legs	1.433	1.939	1.499	2.027	1.749	2.366
	Knee bend	2.562	2.815	2.679	2.943	3.126	3.435
2	Slow walking	1.891	1.822	1.977	1.905	2.308	2.223
	Normal walking	1.969	2.231	2.059	2.333	2.403	2.723
	Fast walking	1.716	2.138	1.794	2.235	2.093	2.609
	Climbing upstairs	1.661	2.064	1.736	2.157	2.026	2.518
	Downstairs	1.466	2.057	1.533	2.151	1.789	2.51
	Standing up	2.823	2.288	2.952	2.392	3.445	2.792
	Sitting down	3.805	2.463	3.978	2.575	4.643	3.005
	Standing on 2-1-2 legs	1.204	1.93	1.259	2.018	1.469	2.355
	Knee bend	3.779	3.737	3.951	3.907	4.612	4.56
3	Slow walking	1.296	2.658	1.355	2.779	1.582	3.244
	Normal walking	1.618	2.716	1.691	2.839	1.974	3.314
	Fast walking	1.55	2.366	1.621	2.474	1.892	2.887
	Climbing upstairs	1.425	2.404	1.49	2.513	1.739	2.934
	Downstairs	1.468	2.054	1.535	2.147	1.792	2.506
	Standing up	1.77	3.65	1.85	3.816	2.159	4.454
	Sitting down	2.654	3.53	2.775	3.691	3.239	4.308
	Standing on 2-1-2 legs	1.427	1.629	1.492	1.703	1.741	1.987
	Knee bend	3.401	4.152	3.556	4.341	4.15	5.066

Table 4.20: Fatigue life comparison of Ti6Al4V and CoCr alloy

Patient	Fatigue life in cycles			
	Ti6Al4V		Co Cr alloy	
	Model 1	Model 2	Model 1	Model 2
1	$1.1x10^6$	10^6	10^6	$8x10^5$
2	$6x10^5$	$9x10^5$	$5x10^5$	$8x10^5$
3	$5x10^6$	10^6	$6x10^6$	$5.5x10^5$

Table 4.20 shows the comparative performances of two different prosthesis materials viz. Ti6Al4V and CoCr alloy in terms of fatigue lives for different daily activities. It could be observed from table 4.20 that Ti6Al4V has more fatigue life compared to CoCr alloy in all the cases. The same observations could also be made from the factor of safety values.

4.4. Summary

In this chapter, residual strength degradation model has been used for calculation of fatigue lives of hip prosthesis for different patients under different daily activities for two different prosthesis models. Constants of strength degradation model viz *c*, *b* and *K* have been evaluated and the simulated values are obtained to be close to the experimental values. 3D finite element method is used to find the maximum von Mises stress in the prosthesis. The developed constant values along with the maximum von Mises stress have been used for fatigue life calculation of different prosthesis. Also the factor of safety calculation has been made using Goodman, Soderberg and Gerber relation which are in good agreement with the trend observed in fatigue life calculation using strength degradation model. It has been observed that fatigue life of prosthesis varies from patient to patient and also depend upon the activities. A detailed fatigue life and factor of safety calculations for different patients under different activities has been presented which will be useful for hip prosthesis in determining the kind of activities the patient can perform.

CHAPTER 5
FATIGUE ANALYSIS OF HIP PROSTHESIS USING DYNAMIC LOADING

5.1 Introduction

In this chapter, fatigue life has been determined for two different prosthesis models corresponding to three patients under nine different activities considering the actual load history during those activities. 3D dynamic finite element analysis has been performed and the stress values obtained have been used for evaluation of fatigue life with the help of residual strength degradation model. Factor of safety has been calculated using Soderberg, Goodman, and Gerber relations. Fatigue life and factor of safety values obtained have also been compared with those obtained using equivalent static loading condition.

5.2 Finite Element Analysis

3D Finite element analysis has been carried out using ANSYS finite element software for dynamic analysis of hip prosthesis. SOLID 92 and 187 elements embedded in ANSYS have been used for FE modeling of the prosthesis.

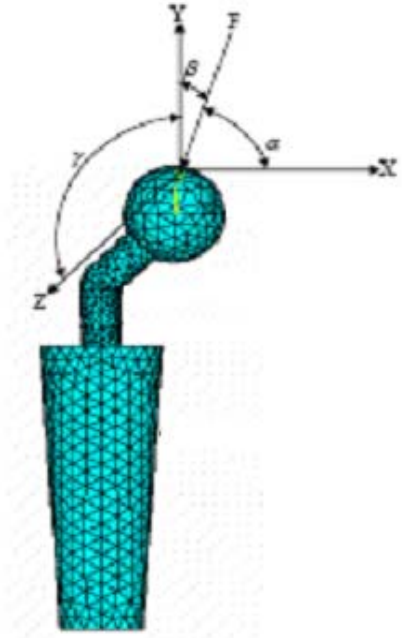

Fig 5.1: Finite element model 1 of cemented hip prosthesis

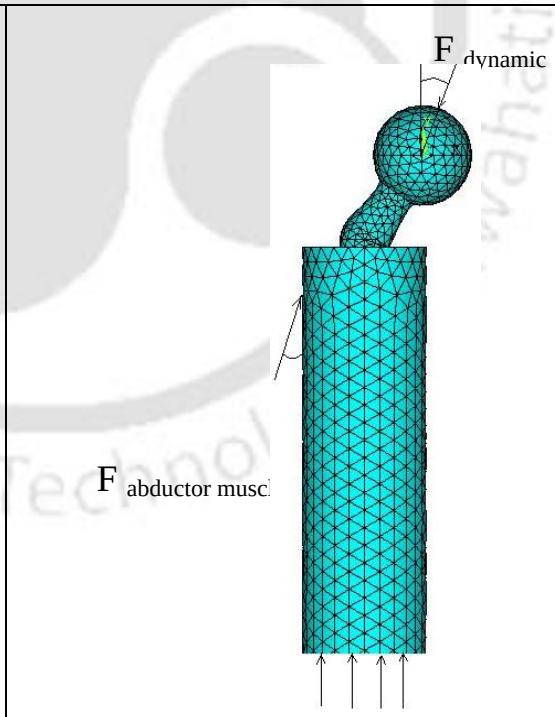

Fig 5.2: Model 2 of implanted cemented hip prosthesis

Two different models have been considered and for each model Ti6Al4V alloy and CoCr alloy have been considered as prosthesis materials in order to study the comparative performance of the materials and models. Figures 5.1 and 5.2 show the FE meshes of model 1 and model 2 respectively. Distal end of the prosthesis has been constrained and time varying dynamic load has been applied on this spherical head. Load histories of three components of forces (F_x, F_y, F_z) acting on the spherical head for nine different activities have been listed in Tables 5.1-5.9. Equivalent von Mises stresses have been calculated corresponding to different activities, different patients and corresponding to two different types of prosthesis. Fig 5.3 shows the stress distribution for a typical case of patient 1, model 1 and for slow walking condition. It could be observed that the maximum stress occurs near the neck region. These maximum stress values have been used in residual strength degradation model for calculation of fatigue life as well as factor safety for a given loading.

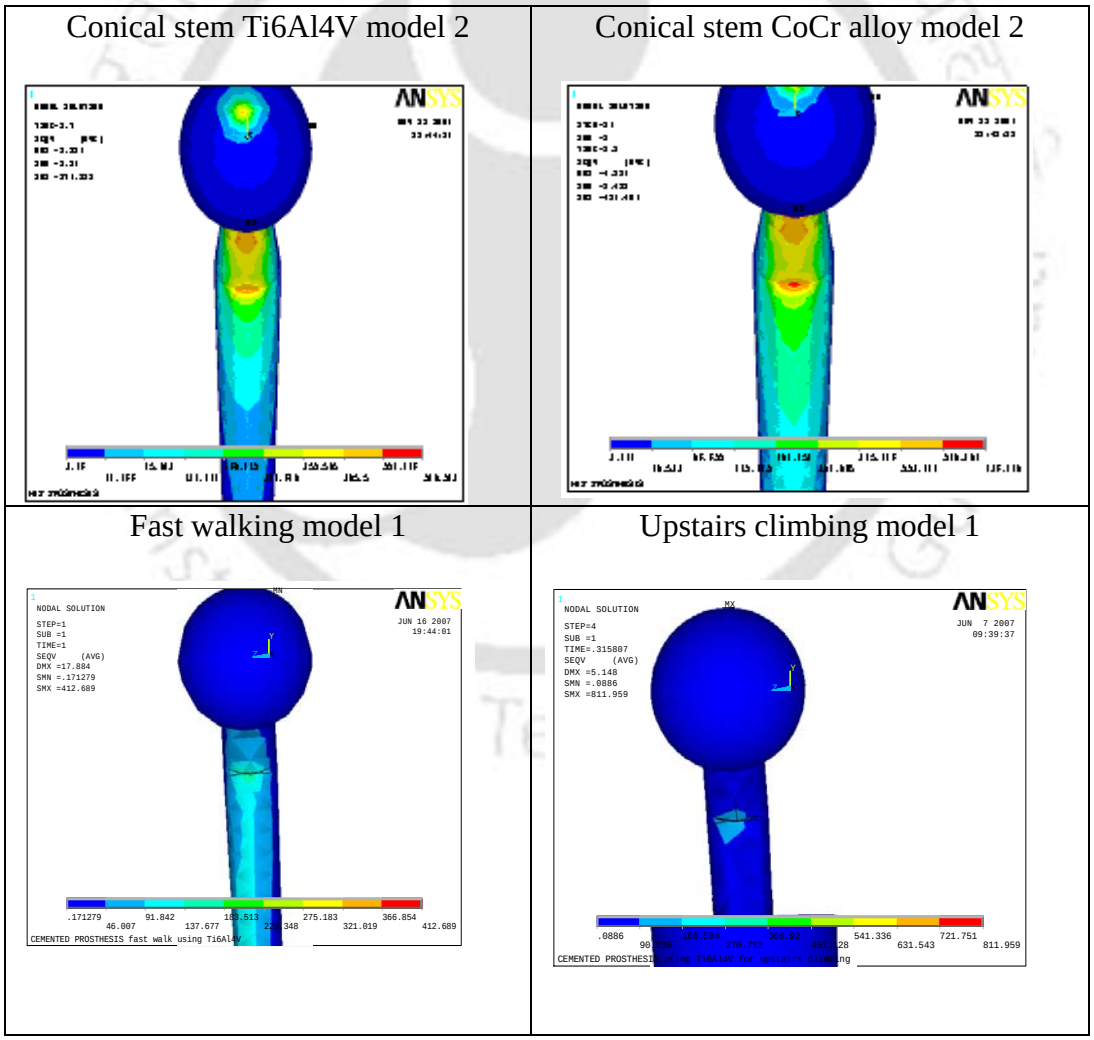

Fig 5.3: Stress distribution on medial side of stem for different materials

Table 5.1: Applied load for fast walking condition

Time(Sec)	F_y (N)	F_x (N)	F_z (N)
0.000587	105.392	30.4852	-3.3809
0.012505	109.841	32.7004	-1.13658
0.024445	120.209	33.4388	-1.12027
0.036393	132.798	36.3924	0.37187
0.045689	143.164	39.346	3.34799
0.056306	153.532	40.8228	3.36226
0.066935	166.859	43.038	6.34042
0.077583	185.366	44.5148	9.31654
0.090877	203.876	48.2068	10.0728
0.101503	216.463	49.6835	13.051
0.11477	228.313	51.8987	16.7711
0.124071	240.159	52.6371	20.4892
0.134661	243.127	54.1139	21.9834
0.143923	244.614	54.1139	22.7376
0.163769	247.589	53.3755	26.468
0.174347	247.597	51.8987	26.4863
0.184909	243.166	51.1603	28.7245
0.196799	240.215	51.1603	28.7408
0.207358	235.044	48.2068	29.4991
0.219234	228.393	48.2068	29.5134
0.232429	221.004	48.2068	28.7959
0.244299	212.873	48.2068	26.5944
0.256183	208.443	47.4684	24.3969
0.269387	203.273	46.73	19.9715
0.282593	198.844	45.9916	16.2962
0.295797	193.674	45.9916	12.6147
0.310328	189.985	45.9916	9.67531
0.324857	185.557	45.2532	6.73791
0.335435	185.565	45.2532	3.05446

Table 5.2: Applied load for climbing upstairs condition

Time(Sec)	F_y (N)	F_x (N)	F_z (N)
0	80.42	28.1053	5.26316
0.0263172	87.8017	30.3158	8.21053
0.0482483	92.9697	31.7895	9.68421
0.0614069	97.3969	33.2632	11.1579
0.0833379	106.249	36.9474	14.8421
0.103076	123.943	39.8947	18.5263
0.122814	140.162	43.5789	24.4211
0.142552	162.277	48.7368	30.3158
0.16229	184.391	53.8947	36.2105
0.179834	201.346	56.8421	41.3684
0.199572	216.092	59.7895	45.7895
0.214924	227.152	61.2632	51.6842
0.230276	236.738	62	54.6316
0.250014	242.642	62	56.1053
0.267559	247.808	62	56.8421
0.28291	250.763	62	59.0526
0.298262	250.77	62.7368	58.3158
0.315807	252.252	62.7368	58.3158
0.339931	250.789	62.7368	56.8421
0.359669	247.851	61.2632	56.8421
0.379407	244.913	59.0526	54.6316
0.396952	239.763	56.1053	52.4211
0.414497	235.35	54.6316	50.2105
0.438621	233.151	53.1579	47.2632
0.456166	230.948	51.6842	43.5789
0.47371	227.272	51.6842	39.8947
0.495641	225.072	49.4737	36.2105
0.513186	221.396	49.4737	33.2632
0.532924	219.194	49.4737	27.3684
0.552662	214.782	48.7368	25.1579

Table 5.3: Applied load for slow walking condition

Time(Sec)	F_y (N)	F_x (N)	F_z (N)
0	61.2642	23.8397	-2.74086
0.0241379	70.091	26.7932	-0.55416
0.0482759	89.2347	29.0084	0.894149
0.0689655	112.801	34.1772	6.77281
0.0896552	140.052	37.8692	10.4444
0.113793	170.249	43.038	15.5806
0.141379	207.811	46.73	22.9361
0.160345	227.695	48.2068	28.0804
0.175862	236.528	48.2068	30.2793
0.196552	240.2	51.8987	34.6832
0.217241	243.872	51.1603	35.3952
0.237931	242.386	51.1603	36.1132
0.258621	237.953	51.1603	36.0868
0.286207	229.094	51.1603	28.6703
0.313793	223.92	50.4219	25.6862
0.343103	217.271	49.6835	20.4829
0.362069	214.313	49.6835	14.5493
0.386207	211.351	49.6835	12.3138
0.403448	209.131	46.73	7.86107
0.425862	206.907	46.73	3.40631
0.446552	206.895	46.73	2.63944
0.468966	206.145	46.73	-1.81126
0.489655	205.396	45.2532	-3.31652
0.512069	204.646	44.5148	-4.08339
0.532759	204.633	45.2532	-4.1078
0.55	204.623	45.2532	-4.86857
0.57069	204.611	43.038	-2.67576
0.591379	204.599	43.038	-3.43857
0.613793	199.428	43.038	-1.98212
0.627586	194.998	41.5612	-1.27221

Table 5.4: Applied load for normal walking condition

Time(Sec)	F_y (N)	F_x (N)	F_z (N)
0	67.4051	20.8867	2.40681
0.024497	76.2658	23.0855	4.60978
0.045931	95.4641	27.4995	7.55114
0.064303	114.662	30.4429	9.75818
0.079614	131.646	32.6489	11.2258
0.093393	147.89	37.0711	13.4329
0.102579	172.996	40.7559	17.1147
0.119421	191.456	43.6982	20.0581
0.134731	204.008	46.6426	25.2146
0.150041	223.207	50.3213	27.4176
0.168414	232.068	52.5262	28.8883
0.179131	235.759	52.516	31.0933
0.195972	237.236	54.723	32.5599
0.209752	237.236	55.4502	34.0244
0.228124	237.236	56.1773	31.7981
0.243434	233.544	56.1661	31.7879
0.258745	229.114	56.8943	26.6099
0.272524	224.684	56.8851	25.8634
0.287834	221.73	56.1375	22.1612
0.301614	218.038	56.1273	19.9348
0.318455	214.346	55.3787	16.2337
0.330703	211.392	55.3685	11.0557
0.349076	205.485	54.6209	8.82831
0.362855	204.008	54.6107	6.60294
0.379697	202.532	54.6015	3.63917
0.393476	201.055	54.5923	2.15626
0.407255	199.578	53.0961	1.40768
0.417972	200.316	50.8656	-3.03696
0.440938	199.578	50.116	-3.04714
0.454717	199.578	50.8452	-2.31995

Table 5.5: Applied load for downstairs coming condition

Time(Sec)	F_y (N)	F_x (N)	F_z (N)
-0.00113382	102.941	36.9474	-11.4407
0.029035	96.3235	-50.7368	-11.4407
0.0692516	86.0294	36.2105	-11.4407
0.0893557	80.1471	31.7895	-11.4407
0.117511	73.5294	30.3158	-9.2161
0.143652	66.9118	27.3684	-8.47458
0.167779	60.2941	25.8947	-8.47458
0.203964	49.2647	22.2105	-7.73305
0.228104	44.8529	20.7368	-6.99153
0.248225	41.9118	19.2632	-5.50847
0.270373	41.1765	19.2632	-3.2839
0.294547	42.6471	19.2632	-1.80085
0.312684	44.8529	19.2632	0.423729
0.334844	46.3235	19.2632	1.90678
0.359009	46.3235	19.2632	2.64831
0.379147	46.3235	21.4737	4.13136
0.399285	46.3235	19.2632	4.13136
0.417414	47.0588	19.2632	4.13136
0.437552	47.0588	19.2632	4.87288
0.457689	47.0588	19.2632	4.87288
0.477832	47.7941	19.2632	4.87288
0.49797	47.7941	21.4737	2.64831
0.520121	47.7941	24.4211	1.90678
0.540259	47.7941	24.4211	0.423729
0.560414	50.7353	24.4211	0.423729
0.580569	53.6765	24.4211	0.423729
0.600753	61.7647	27.3684	0.423729
0.618945	73.5294	28.1053	1.90678
0.641198	91.1765	28.1053	2.64831
0.661548	127.941	29.5789	6.35593

Table 5.6: Applied load for sitting down condition

Time(Sec)	F_y (N)	F_x (N)	F_z (N)
0.00707645	83.367	18.6707	-9.38807
0.0993507	86.2961	18.6503	-7.15151
0.186458	86.2789	21.5876	-6.39684
0.247978	88.4772	22.3148	-6.38362
0.304341	88.466	22.3016	-6.37345
0.365839	89.1907	23.7661	-6.36023
0.422203	89.1795	23.7519	-7.08642
0.478566	89.1684	23.7437	-7.07523
0.529817	89.8951	24.4709	-7.06811
0.591336	92.0934	25.1961	-5.57911
0.663136	96.5002	25.1849	-3.35069
0.709274	97.9648	27.3899	-3.3395
0.760546	100.165	28.117	-3.32933
0.822055	101.627	28.1079	-3.31916
0.868202	103.828	28.8371	-3.30696
0.914361	106.766	30.3037	-1.82304
0.970789	111.176	31.0299	-1.07345
1.02723	116.323	33.9733	0.416566
1.0632	123.684	33.9631	0.42572
1.11958	124.41	34.6903	1.17226
1.17089	129.558	36.1599	1.18243
1.21707	133.969	37.6255	1.1926
1.27353	140.59	37.6174	1.20175
1.31965	140.581	56.08	1.21192
1.37095	144.992	40.5516	1.22108
1.40683	145.721	40.5435	1.23125
1.45298	147.923	41.2706	1.23837
1.50424	149.386	41.2625	0.511154
1.55552	152.323	41.2533	0.520308
1.5914	153.053	41.9856	0.527428

Table 5.7: Applied load for stand up condition

Time(Sec)	F_y (N)	F_x (N)	F_z (N)
0.00342503	21.3235	6.11814	-3.57895
0.0685007	22.0588	6.85654	-2.84211
0.126726	22.7941	7.59494	-3.57895
0.178102	23.5294	6.11814	-2.10526
0.219202	23.5294	6.11814	-2.10526
0.246602	25	6.11814	-2.10526
0.294553	25	8.33333	-1.36842
0.339078	25	7.59494	-1.36842
0.380179	26.4706	8.33333	-1.36842
0.417854	28.6765	9.81013	-1.36842
0.44868	30.8824	9.81013	-1.36842
0.472655	32.3529	9.81013	-1.36842
0.513755	36.0294	10.5485	-2.10526
0.561706	38.2353	11.2869	-2.10526
0.595956	46.3235	12.7637	-0.63158
0.633631	53.6765	15.7173	-0.63158
0.667882	64.7059	17.1941	0.105263
0.705557	76.4706	18.6709	2.31579
0.736382	85.2941	20.8861	3.78947
0.760358	92.6471	22.3629	3.78947
0.787758	98.5294	24.5781	3.78947
0.811733	109.559	29.0084	3.78947
0.842558	119.853	29.0084	6.73684
0.876809	131.618	31.962	8.21053
0.911059	143.382	34.9156	8.21053
0.928184	148.529	37.1308	8.94737
0.955585	162.5	40.0844	10.4211
0.98641	170.588	43.038	10.4211
1.02066	177.941	44.5148	12.6316
1.04464	185.294	48.2068	12.6316

Table 5.8: Applied load for stand on 2-1-2 leg condition

Time(Sec)	F_y (N)	F_x (N)	F_z (N)
0.00626159	67.8941	19.2638	-2.74262
0.108502	67.8828	19.2505	-2.00422
0.229292	67.1328	18.5015	-2.74262
0.312943	67.1236	18.4923	-2.74262
0.424516	67.8482	18.4801	-2.00422
0.517853	75.2064	19.2047	-1.26582
0.620837	89.1951	19.1956	1.68776
0.74284	111.287	22.8665	5.37975
0.874138	133.378	25.0628	11.2869
0.986573	150.313	25.7874	12.7637
1.09893	165.774	28.7226	15.7173
1.20195	180.5	30.9239	15.7173
1.29545	190.805	31.6475	15.7173
1.42596	198.159	33.8458	16.4557
1.52836	201.096	32.3599	16.4557
1.61224	205.507	32.3518	14.2405
1.69601	207.709	32.3396	13.5021
1.81719	214.327	32.3284	13.5021
1.91022	215.791	32.3172	13.5021
1.98477	219.467	32.3101	13.5021
2.0685	220.931	33.0357	12.7637
2.16156	223.131	33.0276	12.7637
2.24529	224.596	31.5437	14.9789
2.35679	223.847	30.0609	14.9789
2.43102	221.628	30.0517	14.9789
2.53311	218.67	29.3037	14.2405
2.63531	217.922	29.2925	12.0253
2.71916	221.597	27.8086	12.0253
2.7752	226.748	27.8015	12.0253
2.86834	230.422	27.7913	12.0253

Table 5.9: Applied load for knee bend condition

Time(Sec)	F_y (N)	F_x (N)	F_z (N)
0.00642366	76.9382	23.6842	-1.36842
0.0963549	79.1253	25.1579	-2.84211
0.186286	84.2475	25.1579	-2.84211
0.26337	86.4366	25.1579	-3.57895
0.346878	88.6247	25.1579	-3.57895
0.417538	90.8149	25.1579	-5.78947
0.501045	91.5355	28.1053	-5.78947
0.578129	91.5234	28.1053	-7.26316
0.661637	90.0428	28.1053	-8
0.751568	90.0287	28.8421	-7.26316
0.835076	88.548	31.0526	-4.31579
0.91216	89.2697	31.0526	-3.57895
0.98282	89.9923	31.7895	-3.57895
1.05348	91.4487	34	-3.57895
1.11772	94.3737	34	-3.57895
1.1948	98.7641	36.2105	-3.57895
1.27831	108.29	38.4211	-3.57895
1.38109	117.079	39.8947	-3.57895
1.47102	125.136	42.1053	-3.57895
1.53525	128.794	42.8421	-3.57895
1.61234	133.919	44.3158	-3.57895
1.69585	135.373	43.5789	-4.31579
1.76651	134.628	43.5789	-3.57895
1.85001	130.946	43.5789	-5.05263
1.92067	130.935	40.6316	-6.52632
2.00418	130.188	40.6316	-8
2.07484	130.911	39.8947	-7.26316
2.16477	133.098	39.1579	-5.05263
2.2547	133.818	39.1579	-2.10526
2.34464	133.804	39.1579	0.842105

5.3 Fatigue Life of Ti6Al4V prosthesis

Here the prosthesis has been considered to be made of Ti6Al4V material with properties given in Table 3.3. Two different models have been considered and FE analysis has been carried out to evaluate stresses. Table 5.10 shows the maximum von Mises stress induced for two different models for three different patients corresponding to nine different activities. Figures 5.8 to 5.13 show the fatigue life curves for three different patients corresponding to nine different activities for model 1 and model 2.

Table 5.10: Maximum von Mises stress values for the dynamic loading condition

Patient	Activities	Maximum stress (σ_a) (MPa) Ti6Al4V	
		Model 1	Model 2
1	Fast Walking	280.665	177.140
	Normal Walking	245.660	169.789
	Slow Walking	230.410	174.415
	Upstairs	276.260	180.503
	Downstairs	245.766	170.562
	Stand up	180.336	130.637
	Sit down	160.116	164.361
	Stand on 2-1-2	262.336	192.634
	Knee bend	157.334	135.466
2	Fast Walking	229.400	170.361
	Normal Walking	219.337	165.731
	Slow Walking	269.334	197.864
	Upstairs	245.447	175.443
	Downstairs	239.437	175.661
	Stand up	210.525	160.632
	Sit down	140.233	150.208
	Stand on 2-1-2	244.422	185.336
	Knee bend	114.365	114.651
3	Fast Walking	202.116	156.432
	Normal Walking	182.635	140.625
	Slow Walking	189.483	143.460
	Upstairs	212.202	160.365
	Downstairs	239.236	192.665
	Stand up	137.466	118.272
	Sit down	112.652	112.629
	Stand on 2-1-2	283.043	218.684
	Knee bend	110.625	100.433

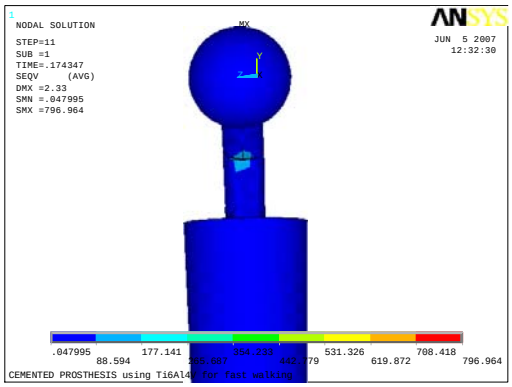

Fig 5.4: Fast walking

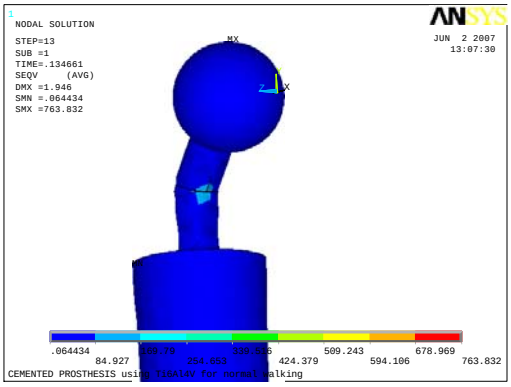

Fig 5.5: Normal Walking

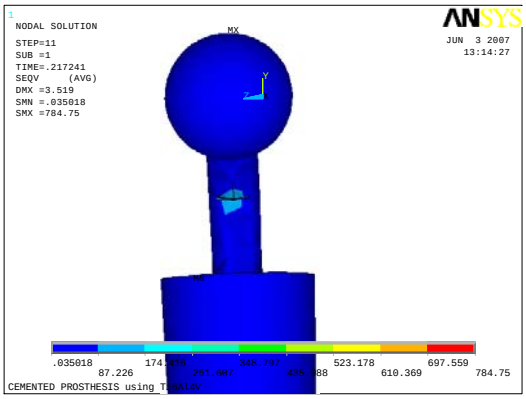

Fig 5.6: Slow Walking

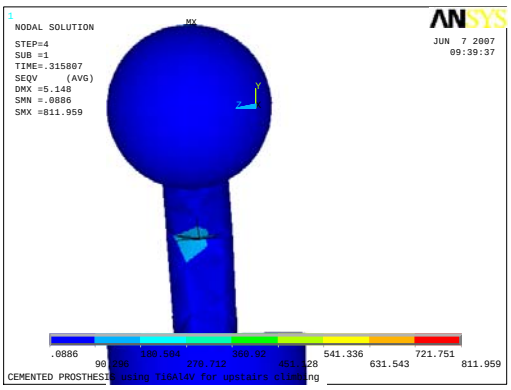

Fig 5.7: Upstairs Climbing

Figures 5.4 to 5.7 show the maximum von Mises stress in the hip prosthesis models for four different postures

In Fig 5.8, for patient 1 in model 1 using Ti6Al4V material, the fatigue life is minimum in fast walking condition and is $2x10^5$ cycles.

It has been observed that activities corresponding to minimum fatigue life vary from patient to patient and for the same patient it also depends upon the type of prosthesis model used. It could be seen from the fatigue life curves as well as from Table 5.10 that for model 1 minimum fatigue life corresponds to fast walking in patient 1, slow walking in patient 2 and standing in 2-1-2 legs in patient 3. However, for model 2, minimum fatigue life correspond to standing 2-1-2 for patient 1, slow walking for patient 2 and standing 2-1-2 for patient 3. In general, fatigue life of model 2 has been observed to be more than that of model 1.

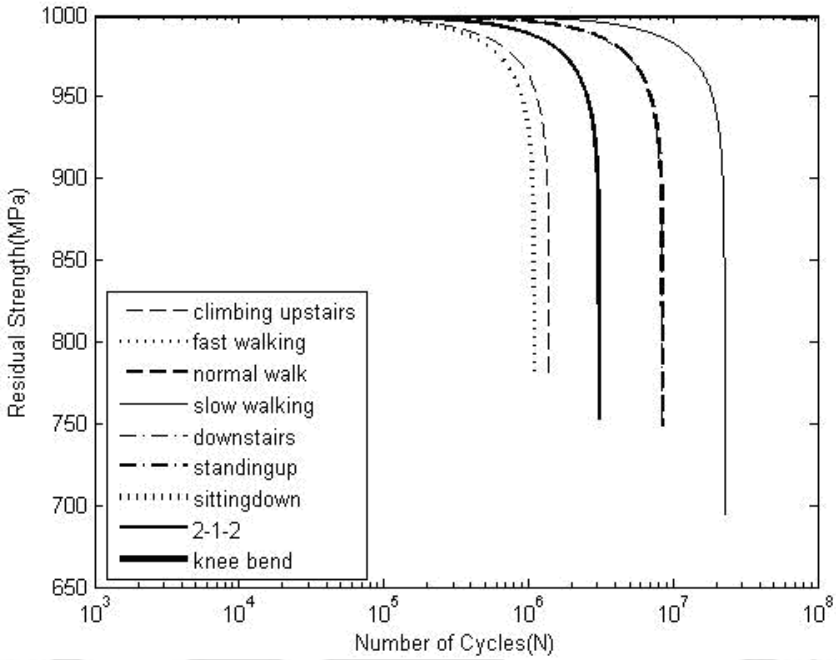

Fig 5.8: Fatigue lives of Ti6Al4V prosthesis using model 1 for patient 1 with 9 different activities under dynamic loading

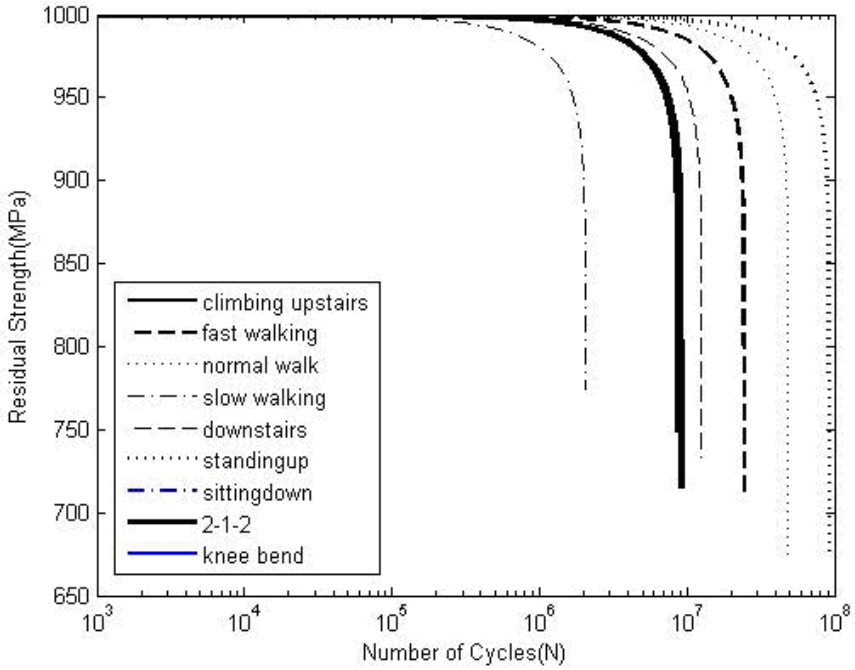

Fig 5.9: Fatigue lives of Ti6Al4V prosthesis using model 1 for patient 2 with 9 different activities under dynamic loading

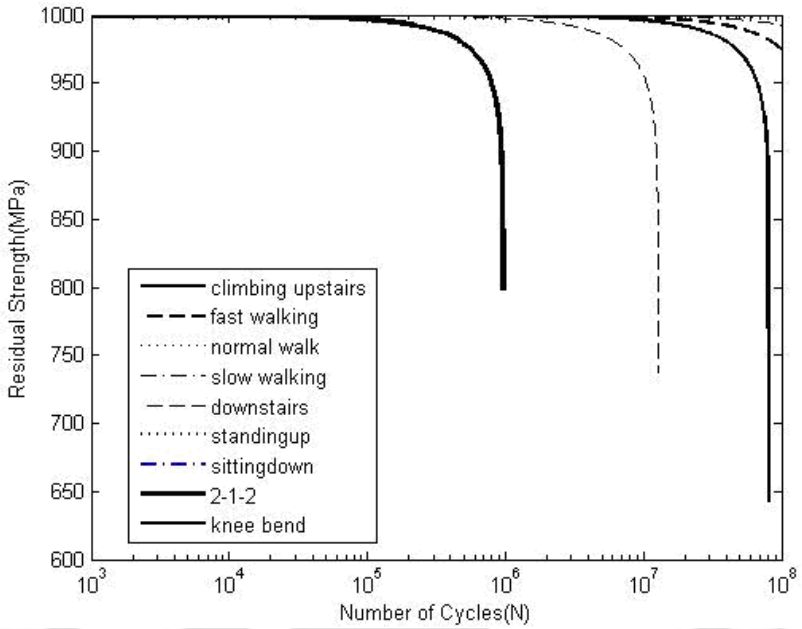

Fig 5.10: Fatigue lives of Ti6Al4V prosthesis using model 1 for patient 3 with 9 different activities under dynamic loading

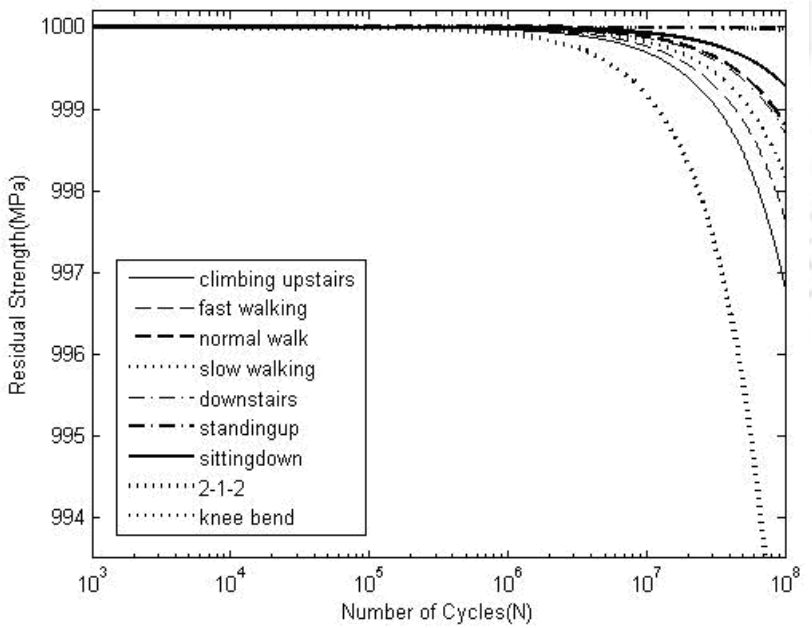

Fig 5.11: Fatigue lives of Ti6Al4V prosthesis using model 2 for patient 1 with 9 different activities under dynamic loading

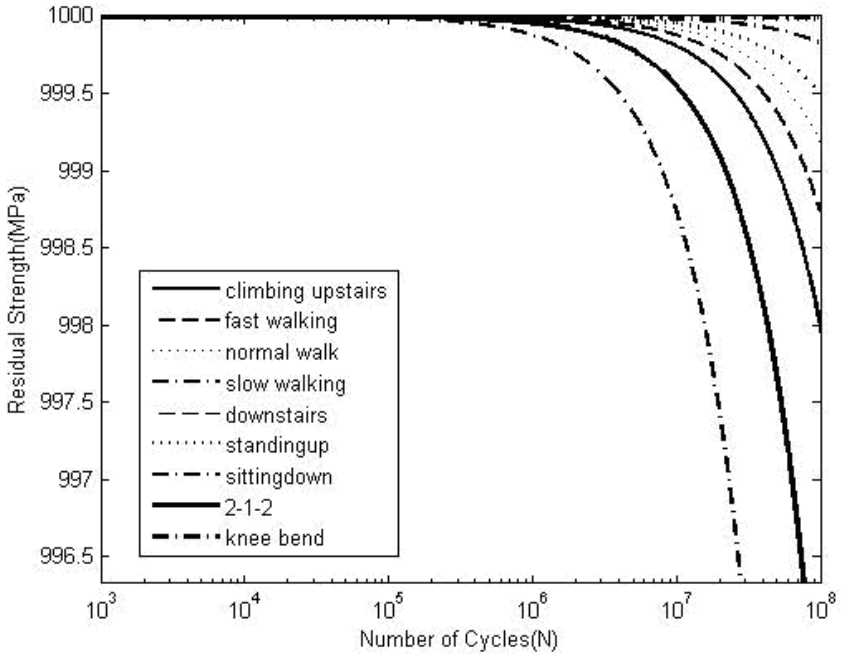

Fig 5.12: Fatigue lives of Ti6Al4V prosthesis using model 2 for patient 2 with 9 different activities under dynamic loading

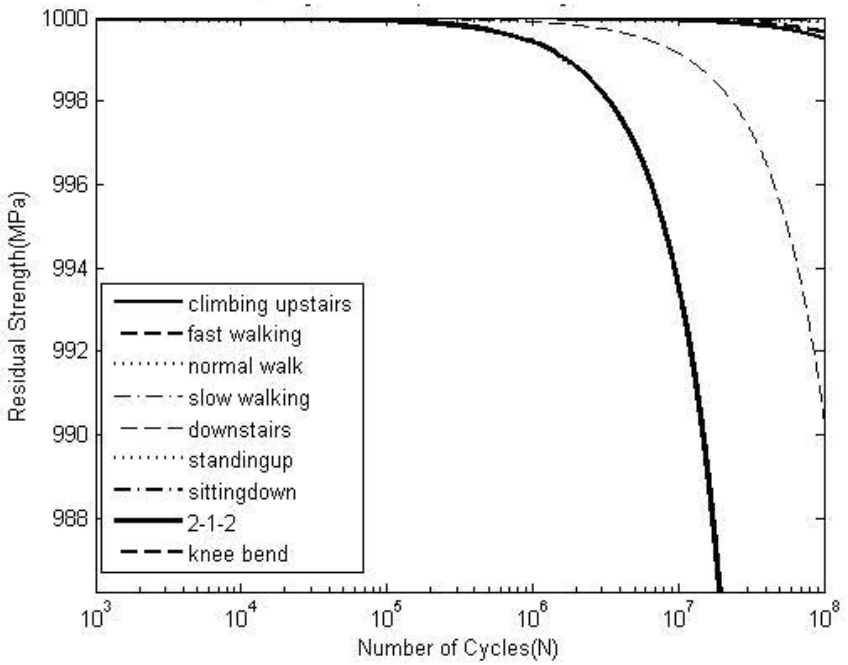

Fig 5.13: Fatigue lives of Ti6Al4V prosthesis using model 2 for patient 3 with 9 different activities under dynamic loading

Based on maximum von Mises stress calculated from FE analysis, factor of safety values have been calculated for all the cases of patient, activities and models using Soderberg, Goodman and Gerber relations and are listed in Table 5.11.

Table 5.11: Factor of safety for prosthesis with Ti6Al4V

Patient	Activities	Soderberg		Goodman		Gerber	
		Model 1	Model 2	Model 1	Model 2	Model 1	Model 2
1	Fast Walking	1.555	2.463	1.644	2.606	1.974	3.127
	Normal Walking	1.776	2.57	1.879	2.718	2.255	3.263
	Slow Walking	1.894	2.502	2.003	2.646	2.404	3.176
	Upstairs	1.58	2.417	1.671	2.557	2.005	3.069
	Downstairs	1.776	2.558	1.878	2.706	2.254	3.248
	Stand up	2.42	3.34	2.559	3.533	3.072	4.241
	Sit down	2.725	2.655	2.883	2.808	3.46	3.37
	Stand on 2-1-2	1.663	2.265	1.759	2.396	2.112	2.876
	Knee bend	2.773	3.221	2.933	3.407	3.521	4.089
2	Fast Walking	2.159	2.561	2.284	2.709	2.741	3.252
	Normal Walking	2.389	2.633	2.527	2.785	3.033	3.343
	Slow Walking	2.303	2.205	2.436	2.333	2.924	2.8
	Upstairs	2.056	2.487	2.175	2.631	2.611	3.158
	Downstairs	1.824	2.484	1.929	2.627	2.316	3.154
	Stand up	3.174	2.717	3.357	2.873	4.03	3.449
	Sit down	3.874	2.905	4.097	3.073	4.918	3.688
	Stand on 2-1-2	1.542	2.354	1.631	2.49	1.957	2.989
	Knee bend	3.945	3.806	4.172	4.026	5.008	4.832
3	Fast Walking	1.902	2.789	2.012	2.95	2.415	3.541
	Normal Walking	1.989	3.103	2.104	3.282	2.526	3.939
	Slow Walking	1.62	3.042	1.714	3.217	2.057	3.861
	Upstairs	1.778	2.721	1.88	2.878	2.257	3.454
	Downstairs	1.822	2.265	1.928	2.396	2.314	2.875
	Stand up	2.073	3.689	2.192	3.902	2.631	4.684
	Sit down	3.112	3.874	3.291	4.098	3.95	4.919
	Stand on 2-1-2	1.785	1.995	1.888	2.111	2.266	2.533
	Knee bend	3.816	4.345	4.036	4.595	4.844	5.516

5.4 Fatigue Life of CoCr alloy prosthesis

The von Mises stresses obtained for CoCr alloy prosthesis under dynamic loading for three patients with nine different activities are obtained using 3D FE analysis and are given in Table 5.12.

Table 5.12: Maximum von Mises stress for CoCr alloy prosthesis under different activities.

Patient	Activities	Maximum stress (σ_a) (MPa) CoCr	
		Model 1	Model 2
1	Fast Walking	280.687	177.141
	Normal Walking	245.673	169.79
	Slow Walking	230.425	174.416
	Upstairs	276.265	180.504
	Downstairs	245.769	170.562
	Stand up	180.609	130.638
	Sit down	160.258	164.362
	Stand on 2-1-2	262.487	192.635
	Knee bend	158.761	135.468
2	Fast Walking	229.437	170.362
	Normal Walking	217.532	165.732
	Slow Walking	267.773	197.865
	Upstairs	246.469	175.442
	Downstairs	240.437	175.662
	Stand up	210.863	160.634
	Sit down	140.463	150.209
	Stand on 2-1-2	245.498	185.333
	Knee bend	116.637	114.652
3	Fast Walking	203.461	156.434
	Normal Walking	183.259	140.626
	Slow Walking	190.463	143.461
	Upstairs	220.267	160.366
	Downstairs	235.462	192.666
	Stand up	133.652	118.273
	Sit down	105.369	112.630
	Stand on 2-1-2	285.337	218.685
	Knee bend	110.635	100.434

As in the case of Ti6Al4V prosthesis, here also the fatigue lives for these activities are determined using the residual strength degradation model for three different patients, under nine different activities and considering two models of prosthesis.

Figures 5.14 to 5.19 show the fatigue lives of the prosthesis model 1 and 2 with CoCr material in two different patients.

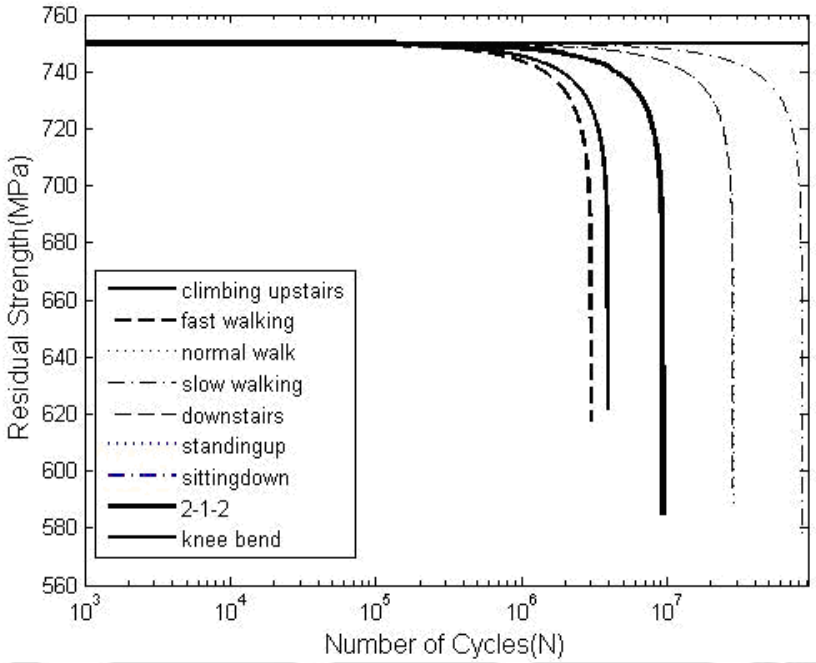

Fig 5.14: Fatigue lives of CoCr alloy prosthesis using model 1 for patient 1 with 9 different activities under dynamic loading

Fig 5.14 shows that for patient 1 and model 1, minimum fatigue life occurs corresponding to fast walking and is $1.1x10^5$ cycles. Fig 5.15 shows that for patient 2 and model 1, minimum fatigue life occurs corresponding to slow walking condition and is $1x10^5$ cycles. Fig 5.16 shows that for patient 3 and model 1, minimum fatigue life occurs corresponding to standing on 2-1-2 legs and is $7x10^4$ cycles.

Fig 5.17 shows that for patient 1 and model 2, minimum fatigue life occurs corresponding to standing on 2-1-2 legs and is $1.6x10^5$ cycles. Fig 5.18 shows that for patient 2 and model 2, minimum fatigue life occurs corresponding to slow walking condition and is $1x10^5$ cycles. Fig 5.19 shows that for patient 3 and model 2, minimum fatigue life occurs corresponding to standing on 2-1-2 legs and is $9x10^4$ cycles.

5.5 Comparison of performances of Ti6Al4V and Co Cr prosthesis

Table 5.14 shows the fatigue lives of Ti6Al4V and Co Cr prosthesis for three different patients corresponding to two models. Similar to our earlier observation, this analysis also revealed that Ti6Al4V made prosthesis are better in terms of fatigue life. This table also shows that model 2 prosthesis performs better than model 1 prosthesis. The same inference could also be drawn from the obtained factor of safety values. The factor of safety values for CoCr prosthesis corresponding to two models are listed in table 5.13

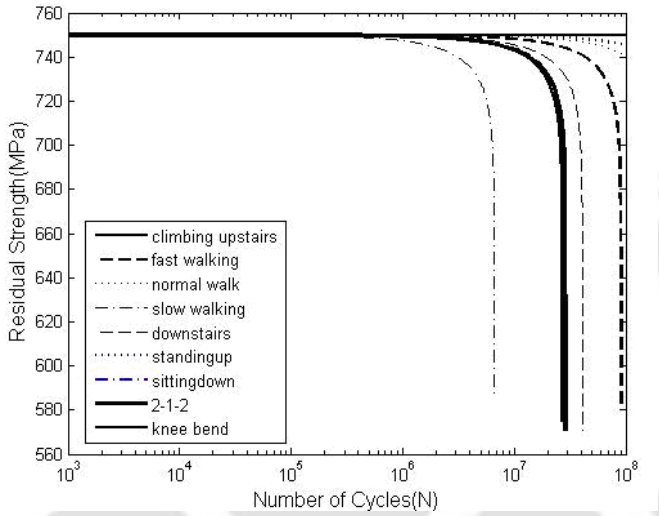

Fig 5.15: Fatigue lives of CoCr alloy prosthesis using model 1 for patient 2 with 9 different activities under dynamic loading

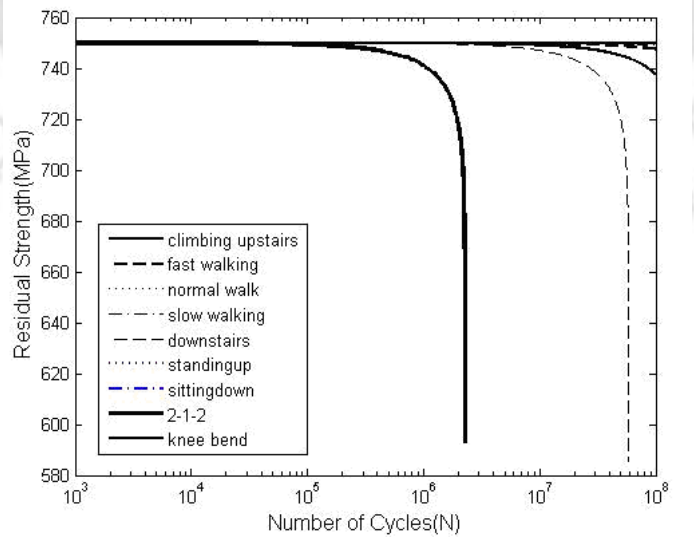

Fig 5.16: Fatigue lives of CoCr alloy prosthesis using model 1 for patient 3 with 9 different activities under dynamic loading

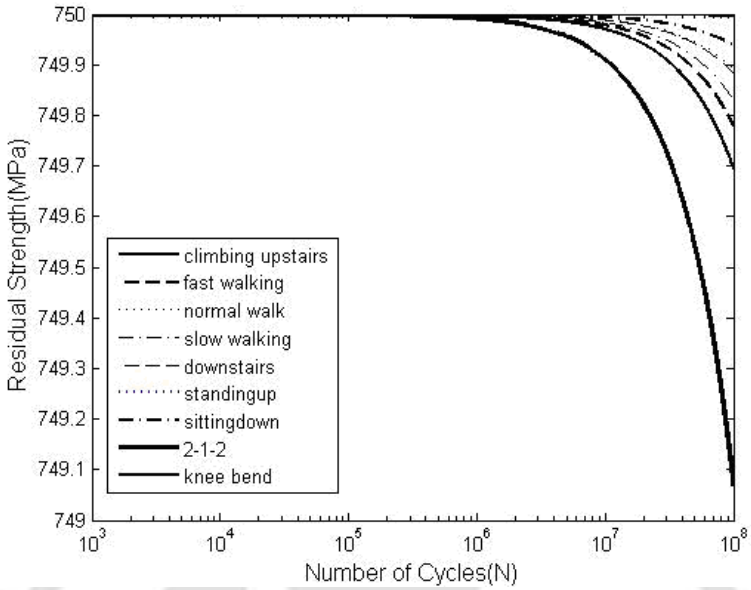

Fig 5.17: Fatigue lives of CoCr alloy prosthesis using model 2 for patient 1 with 9 different activities under dynamic loading

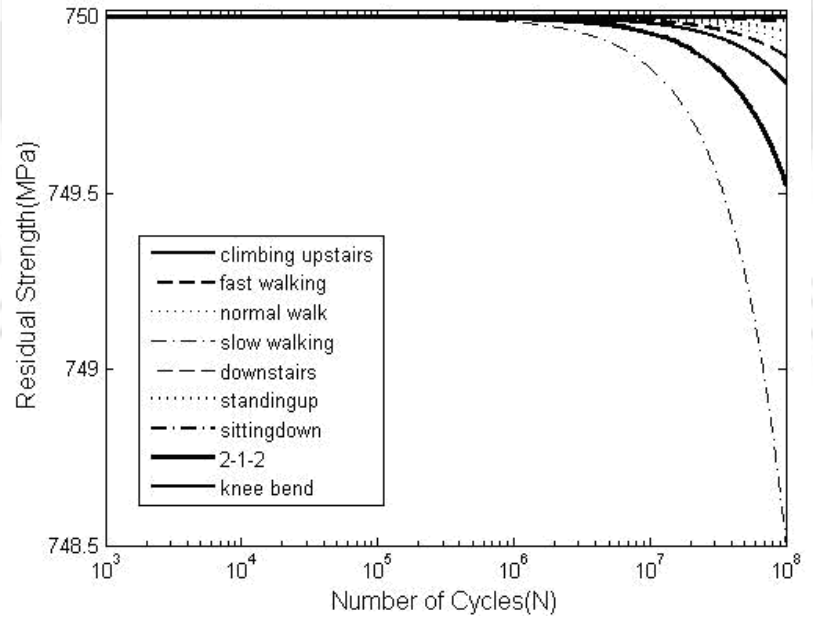

Fig 5.18: Fatigue lives of CoCr alloy prosthesis using model 2 for patient 2 with 9 different activities under dynamic loading

Table 5.13: Factor of safety for prosthesis with CoCr alloy

Patient	Activities	Soderberg		Goodman		Gerber	
		Model 1	Model 2	Model 1	Model 2	Model 1	Model2
1	Fast Walking	1.115	1.767	1.166	1.848	1.3609	2.156
	Normal Walking	1.274	1.844	1.332	1.928	1.5549	2.25
	Slow Walking	1.359	1.795	1.42	1.876	1.6577	2.19
	Upstairs	1.133	1.734	1.185	1.813	1.3827	2.116
	Downstairs	1.274	1.835	1.332	1.919	1.5542	2.24
	Stand up	1.733	2.396	1.812	2.505	2.115	2.924
	Sit down	1.953	1.905	2.042	1.991	2.3836	2.324
	Stand on 2-1-2	1.193	1.625	1.247	1.699	1.4553	1.983
	Knee bend	1.972	2.311	2.061	2.416	2.406	2.82
2	Fast Walking	1.364	2.001	1.426	2.092	1.665	2.442
	Normal Walking	1.439	2.226	1.504	2.327	1.756	2.716
	Slow Walking	1.169	2.182	1.222	2.281	1.427	2.663
	Upstairs	1.27	1.952	1.328	2.041	1.55	2.382
	Downstairs	1.302	1.625	1.361	1.699	1.589	1.983
	Stand up	1.485	2.647	1.552	2.767	1.812	3.23
	Sit down	2.229	2.779	2.33	2.906	2.719	3.392
	Stand on 2-1-2	1.275	1.431	1.333	1.497	1.556	1.747
	Knee bend	2.684	3.117	2.806	3.259	3.275	3.803
3	Fast Walking	1.539	1.838	1.609	1.921	1.877	2.242
	Normal Walking	1.708	1.889	1.786	1.975	2.084	2.305
	Slow Walking	1.644	1.582	1.718	1.654	2.006	1.931
	Upstairs	1.421	1.784	1.486	1.865	1.734	2.177
	Downstairs	1.329	1.782	1.39	1.863	1.622	2.175
	Stand up	2.342	1.949	2.449	2.037	2.858	2.378
	Sit down	2.971	2.084	3.106	2.179	3.625	2.543
	Stand on 2-1-2	1.097	1.689	1.147	1.766	1.339	2.061
	Knee bend	2.83	2.73	2.958	2.854	3.453	3.332

Table 5.14: Fatigue life of different patients under dynamic loading

Patient	Fatigue life in cycles			
	Ti6Al4V		Co Cr alloy	
	Model 1	Model 2	Model 1	Model 2
1	$2x10^5$	$3x10^5$	$1.1x10^5$	$1.6x10^5$
2	$8x10^4$	$2x10^5$	$1x10^5$	$1x10^5$
3	$1x10^5$	$2x10^5$	$7x10^4$	$9x10^4$

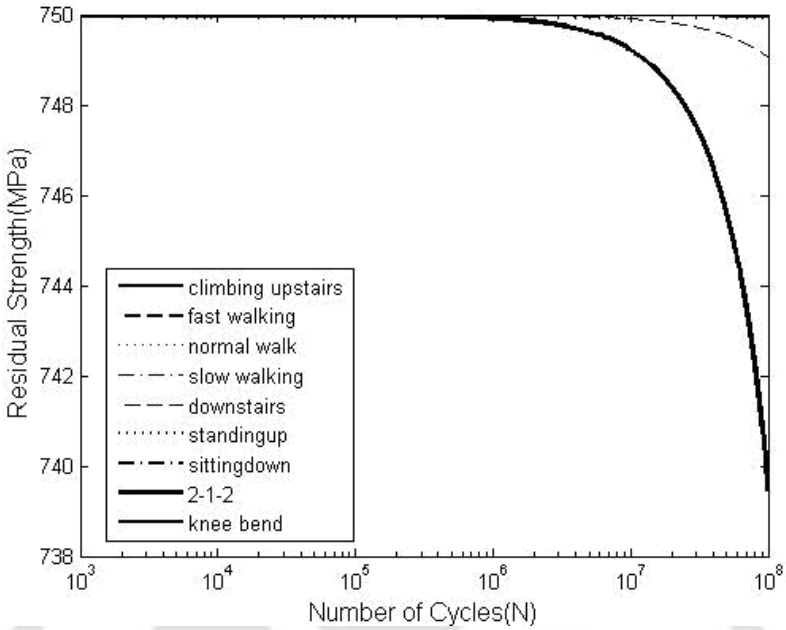

Fig 5.19: Fatigue lives of CoCr alloy prosthesis using model 2 for patient 3 with 9 different activities under dynamic loading

5.6. Summary

Maximum von Mises stresses in the hip prosthesis are determined under dynamic loading for nine different activities using a 3D finite element analysis for 3 patients, two models and two prosthesis materials. Residual strength degradation model has been used to determine the fatigue life of the prosthesis. The factors of safety values are also determined using three fatigue relations. It has been observed that von Mises stresses obtained from static loading and dynamic loading are different and hence the fatigue life obtained in this cases are also different from those observed in chapter 4. Similarly the factors of safety are also different for static and dynamic cases. For a given stem geometry, fatigue life is more in prosthesis made of Ti6Al4V compared to a prosthesis made of CoCr alloy. Model 2 gives a better fatigue life in comparison to model1.

CHAPTER 6
CONTACT AND WEAR ANALYSIS OF HIP PROSTHESIS

6.1 Introduction

In previous chapters, detailed analysis of hip prosthesis with regard to the failure of stem has been carried out for different materials under different activities. In an artificial hip joint, failure of the acetabular cup due to gradual wear caused by contact stresses is of significant importance. In this chapter detailed contact analysis using 3D FE method has been presented for evaluation of the contact stresses between the cup and the spherical head. The contact stress values thus obtained have been used to asses the wear volume. An empirical relation has also been developed to determine the wear volume as a function of body weight, head diameter and surface roughness factor.

6.2. Contact stress analysis and wear volume calculation using FEM

3D FEA has been carried out using ANSYS 9.0 to evaluate contact stresses developed at the interface of the cup and spherical head. Using these contact stresses and sliding distance modified Archard's law [73] has been used to determine the wear rate of the acetabular cup.

6.2.1. FE modeling of acetabular cup and spherical head

Total hip prosthesis contains femoral component and acetabulum. Femoral component contains spherical head, stem, cancellous bone and cortical bone. The acetabular cup acts as the female part of the bearing interface in the total hip arthroplasty.

Fig 6.1 shows the components of acetabulum model. It consists of femoral head, acetabular cup and metal backing. The ranges of dimensions of acetabulum model considered in the present work are shown in Table 6.1. TARGE 170 elements embodied in ANSYS have been used to model various 3-D target surfaces for the associated contact elements (CONTA 174 of ANSYS). The contact elements themselves overlay the solid elements describing the boundary of a deformable body that is potentially in contact with the rigid target surface, defined by TARGE 170. Hence, a "target" is simply a geometric entity in space that senses and responds when one or more contact elements move into a target segment element. The target surface is modeled through a set of target segments,

typically several target segments comprise one target surface. Each target segment is a single element with a specific shape or segment type. CONTA 174 is an 8-noded surface-to-surface contact element that is intended for general rigid-flexible and flexible-flexible contact analysis. In a general contact analysis, the area of contact between two (or more) bodies is generally not known in advance. CONTA 174 is applicable to 3-D geometries.

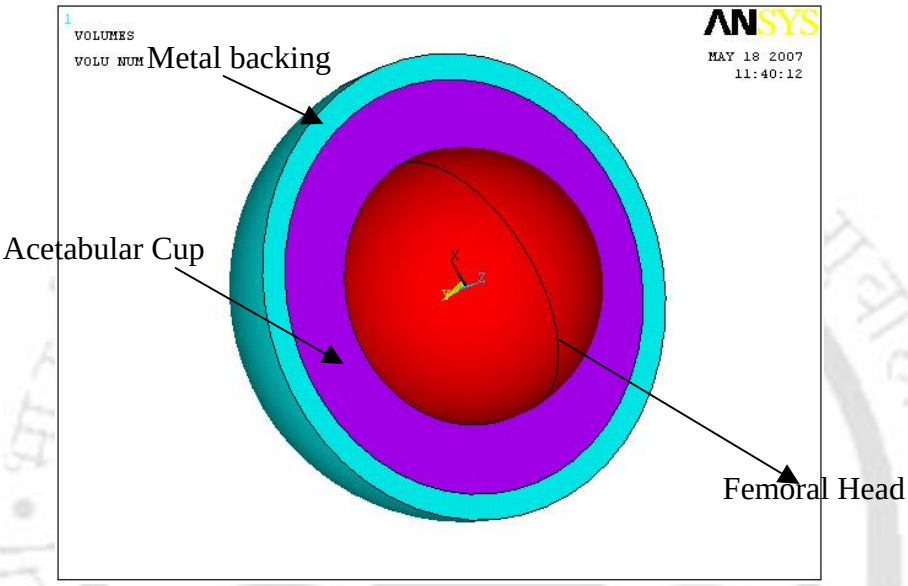

Figure 6.1 Acetabulum model

Four different patients with body weight of 860N, 980N, 800 N and 702N respectively (same as that of Bergmann et al [4]) are considered for the present analysis. The joint forces in terms of percentage of body weight corresponding to different activities are given in Table 6.2.

For example, in slow walking condition, a contact load of 242 percentage of patient's body weight is applied on the topmost node of metal backing. Bottom surface of the femoral head was constrained in all directions. Fig 6.2 shows meshed model of the acetabulum. Fig 6.3 shows the application of contact forces on the finite element mesh of the acetabulum assembly.

In the contact analysis femoral head and metal backing is considered to be made of Ti6Al4V, acetabular cup is considered to be made of UHMWPE. The material properties of these materials are shown in table 3.3 (chapter 3).

Table 6.1: Dimensions of acetabulum model

Parts	Inner diameter, mm	Outer diameter, mm
Femoral Head	0	32
Acetabular Cup	32	48
Metal backing	48	54

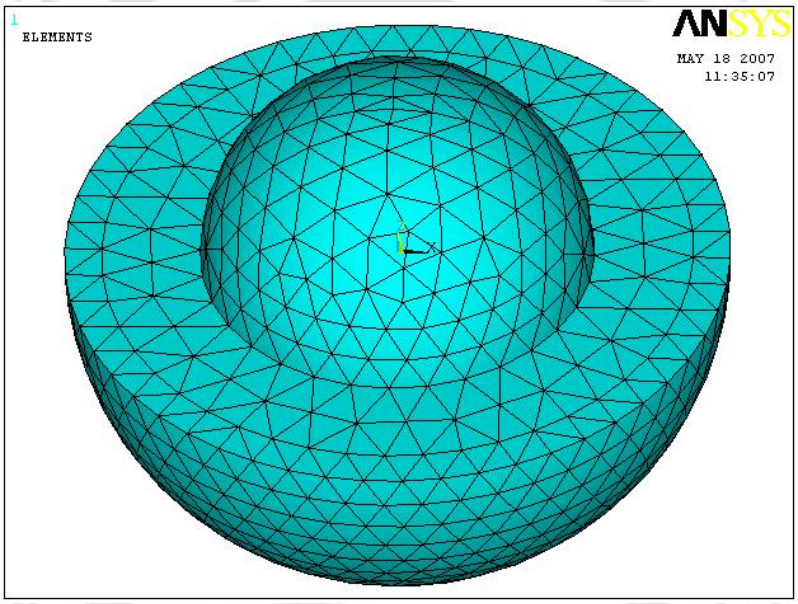

Fig 6.2 Meshed model of acetabulum cup

In this, the model has been constrained in the bottom surface in all degrees of freedom, and the force is applied from the top of the acetabular cup. The contact surface and target surface are meshed with contact and target elements.

Table 6.2: Maximum force at hip joint for various activities [4]

Activity	Maximum joint force (percentage of body weight)
Slow walking	242
Normal walking	238
Fast walking	250
Up stairs walking	251
Down stairs walking	260
Standing up	190
Sitting down	156
Standing on 212 legs	231
Knee bend	143

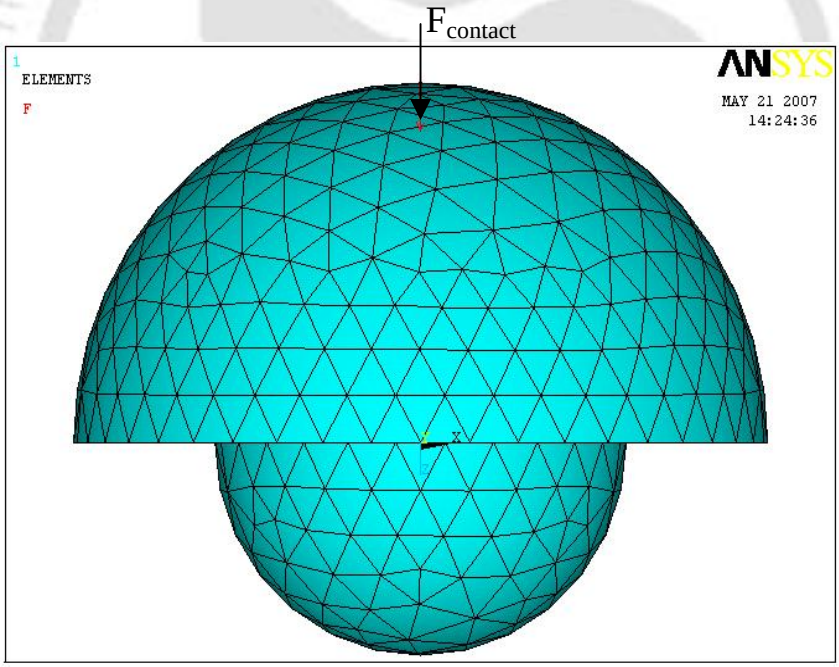

Fig 6.3: Applied forces on the acetabulum

6.2.2 Archard's Wear Equation

Considering two moving contact surfaces forming a circular junction of radius *a*. The contact stress on the junction is the yield stress of the softer material *p*, the load on the junction ,

$$w = \pi a^2 p \Rightarrow \pi a^2 = w/p \tag{6.1}$$

The two surfaces move, and assume after distance *2a*, a hemispherical particle is torn out, and this has volume of $\left(2/3\right)\pi a^3$. Let *v* be wear volume/unit distance.

$$v = \left(2/3\right)\pi a^3 / 2a = \pi a^2 / 3 \tag{6.2}$$

From (6.1) and (6.2), $v = w/3p$

This expression contains neither the junction nor the fragment dimensions. It applies to all junctions, and the total wear rate *V* is the sum of all *v*. Therefore $V = W_c/3p$ where W_c is total contact load. This expression assumes that every junction forms a wear fragment but actually only a fraction *K* of the volume is removed, hence wear volume rate is given by

$$V = \left(K/3p\right)W_c S_L \tag{6.3}$$

where S_L is the sliding distance

This equation applies to both adhesive and abrasive wear. It shows that the wear volume is proportional to the normal load and sliding distance and inversely proportional to the yield stress. It is modified for wear rate on softer material and is given as [73]

$$V = \left(K/3p\right)\sigma_c A S_L \tag{6.4}$$

$$V = K_w \sigma_c A S_L, \tag{6.5}$$

where $K_w = K/3p$. In equation (6.5), *V* is the wear volume removed from the softer material, *A* is the contact area and σ is the normal contact stress. K_w is known as the wear coefficient and its unit is mm^3/N-m. Many authors agree that, K_w is an exponential function of surface roughness (R_a) and is given by [114]

$$K_w = 0.235 * 10^{-4} R_a^{2.03} \tag{6.6}$$

where R_a is roughness expressed in μm.

Archard's law gives wear rate per cycle and can be converted into wear per day or per year. Using the contact stress values σ_c and sliding distance S_L obtained from FEA and knowing contact area *A*, wear volume *V* has been calculated in the present work.

6.3 Results and Discussions

In the present work, spherical head made of two different materials viz. Ti6Al4V and CoCr alloy has been considered against an acetabular cup made of UHMWPE with a Ti6Al4V metal backing. Four different types of patients under nine different activities have been considered to assess the performance of the acetabular cup in terms of wear volume. Different head diameters of the head along with different degree of surface roughness have been considered to study the effect of these parameters on the wear rate of the acetabular cup.

6.3.1. Wear of acetabular cup with Ti6Al4V head

Table 6.3 shows the maximum contact stress obtained from FEA for different patients undergoing different activities. In all these cases, the spherical head diameter considered was 32 mm and the surface roughness considered was $R_a = 0.7\mu m$. Corresponding sliding distances in all these cases have been listed in Table 6.4.

Figures 6.4 and 6.5 show the contact stress distribution for typical cases of patient 1 during standing up and up stairs climbing activities respectively. It could be observed that in all the cases considered in the present work, contact stresses as well as sliding distances are maximum during downstairs climbing.

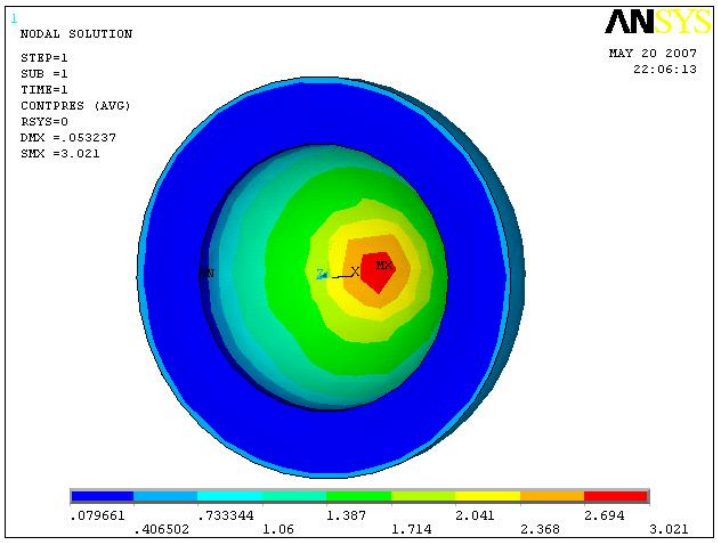

Fig 6.4: Distribution of contact stress in standing up condition

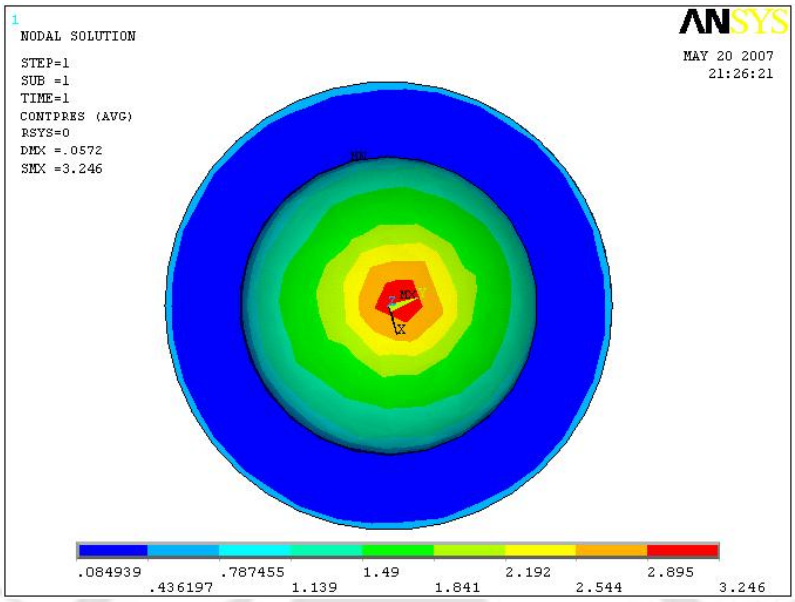

Fig 6.5: Distribution of contact stress in up stairs condition

Table 6.3: Maximum contact stress for four patients with nine different activities (R_a =0.7μm, R = 16mm)

Activities	Contact stress (MPa)			
	Patient 1	Patient 2	Patient 3	Patient 4
Downstairs	4.9946	5.6918	4.646	4.07662
Fast walking	4.8021	5.4723	4.467	3.91967
Knee bend	2.7457	3.1291	2.554	2.24089
Normal walking	4.5722	5.2106	4.253	3.73164
Sitting down	2.9951	3.4133	2.786	2.44447
Slow walking	4.6486	5.2978	4.324	3.79382
Standing on 2-1-2	4.4379	5.0577	4.128	3.62183
Standing up	3.6487	4.1581	3.394	2.97799
Upstairs	4.8216	5.4948	4.485	3.93522

Table 6.4: Sliding distance for four patients with nine different activities (R_a = 0.7 μm, R= 16mm)

Activities	Sliding distance (mm)			
	Patient 1	Patient 2	Patient 3	Patient 4
Downstairs	0.016448	0.018764	0.01529	0.013399
Fast walking	0.0158	0.01802	0.01469	0.012877
Knee bend	0.00899	0.01025	0.00836	0.007331
Normal walking	0.015039	0.017157	0.01398	0.0225
Sitting down	0.00982	0.0112	0.00913	0.008003
Slow walking	0.015297	0.017451	0.01422	0.012461
Standing on 2-1-2	0.014599	0.016657	0.01357	0.011889
Standing up	0.011983	0.013669	0.01114	0.009763
Upstairs	0.015863	0.018089	0.01475	0.012932

Figure 6.6 shows the variation of contact stresses in 9 different activities for four different patients for 32 mm femoral head diameter. The pattern of stress distribution is same for different body weights. It could be observed that contact stress is maximum for down stairs climbing followed by upstairs climbing. For each activity, contact stress happened to be maximum for patient 2. This is due to the fact that weight of patient 2 has been considered as maximum.

Using these stress values and sliding distances, wear volume has been calculated for all the cases. Tables 6.5 to 6.7 show the wear volume of acetabular cup for four different patients with body weights, 860N, 980N, 800 N and 702N respectively for different acetabular cup roughness ranging from 0.6μm to 0.8μm. From tables 6.5 to 6.7, it could be observed that out of 9 activities, downstairs activity has the maximum wear rate for a given roughness of acetabular cup and knee bend activity has the minimum wear rate for a given roughness. As body weight of patient increases, wear rate also increases.

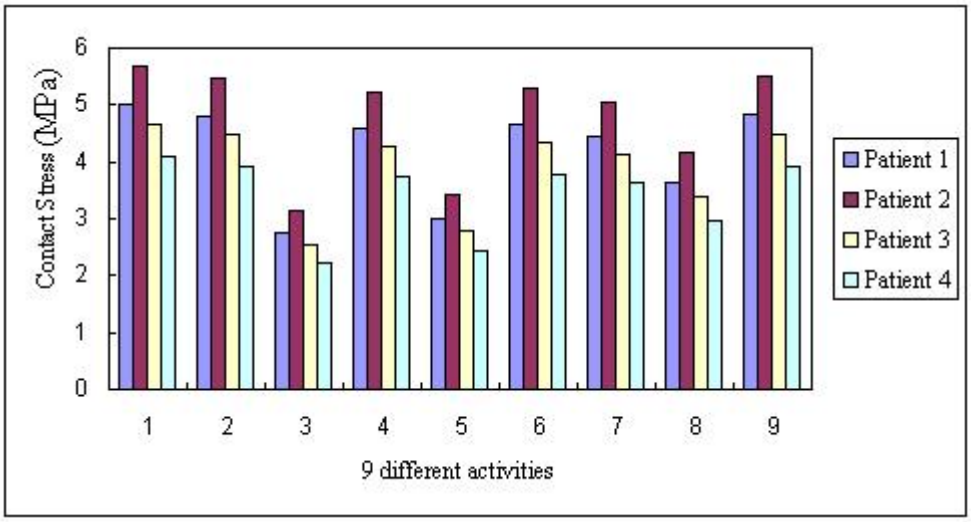

Fig 6.6: Contact stress distribution in different activities for four different patients

Table 6.5: Wear volume (mm^3/year) for four patients with nine different activities (R_a =0.6 μm, R=16mm)

Activities	Patient 1	Patient 2	Patient 3	Patient 4
Downstairs	4.018291	5.223994	3.474676	2.671697
Fast walking	3.711213	4.823389	3.209707	2.468833
Knee bend	1.20737	1.568812	1.044371	0.803547
Normal walking	3.363348	4.372771	2.908239	2.236012
Sitting down	1.438634	1.869907	1.244169	0.956897
Slow walking	3.478212	4.522135	3.00755	2.312351
Standing on 2-1-2	3.169044	4.120761	2.739978	2.10626
Standing up	2.138609	2.780093	1.849373	1.422128
Upstairs	3.741141	4.861766	3.235803	2.489234

Table 6.6: Wear volume (mm^3/year) for four patients with nine different activities (R_a = 0.7 μm, R = 16mm)

Activities	Patient 1	Patient 2	Patient 3	Patient 4
Downstairs	5.494692	7.143395	4.751342	3.653333
Fast walking	5.074788	6.595599	4.389018	3.375933
Knee bend	1.650982	2.145225	1.428094	1.098787
Normal walking	4.59911	5.979415	3.976785	3.057567
Sitting down	1.967218	2.556949	1.701302	1.30848
Slow walking	4.756177	6.183658	4.112585	3.161955
Standing on 2-1-2	4.333414	5.634812	3.746702	2.880142
Standing up	2.924377	3.801555	2.528871	1.944646
Upstairs	5.115712	6.648077	4.424702	3.403828

Table 6.7: Wear volume (mm^3/year) for four patients with nine different activities (R_a = 0.8 μm, R = 16mm)

Activities	Patient 1	Patient 2	Patient 3	Patient 4
Downstairs	7.205548	9.367599	6.230744	4.790853
Fast walking	6.6549	8.649239	5.755605	4.427081
Knee bend	2.16504	2.813174	1.872753	1.44091
Normal walking	6.031112	7.841196	5.215018	4.009588
Sitting down	2.579741	3.353094	2.231029	1.715895
Slow walking	6.237085	8.109034	5.393101	4.146478
Standing on 2-1-2	5.682689	7.389296	4.913294	3.776918
Standing up	3.834926	4.985227	3.316273	2.550141
Upstairs	6.708567	8.718057	5.8024	4.463662

Figures 6.7 to 6.9 show the variation of wear volume rate in 9 different activities for 4 different patients and roughness of acetabular cup ranging from 0.6μm to 0.8μm. It could

be observed that in all the cases, wear volume is maximum corresponding to down stair climbing which was also the case for contact stress amplitude. It is also clear that the wear volume increases as R_a value increases.

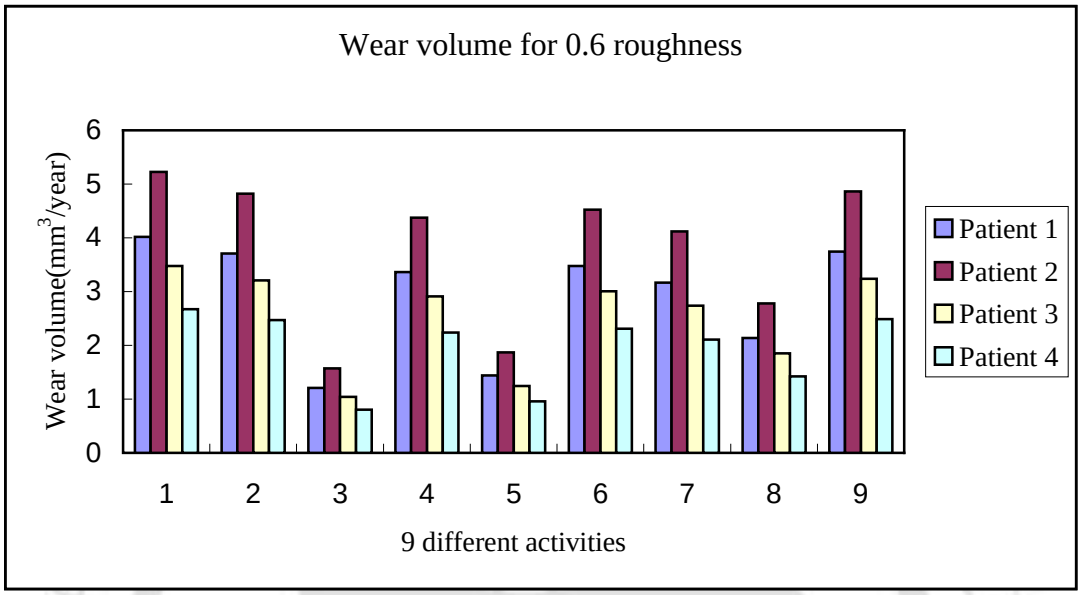

Fig. 6.7: Wear volume rate of acetabular cup for different patients with Ti6Al4V made head (R_a = 0.6 µm)

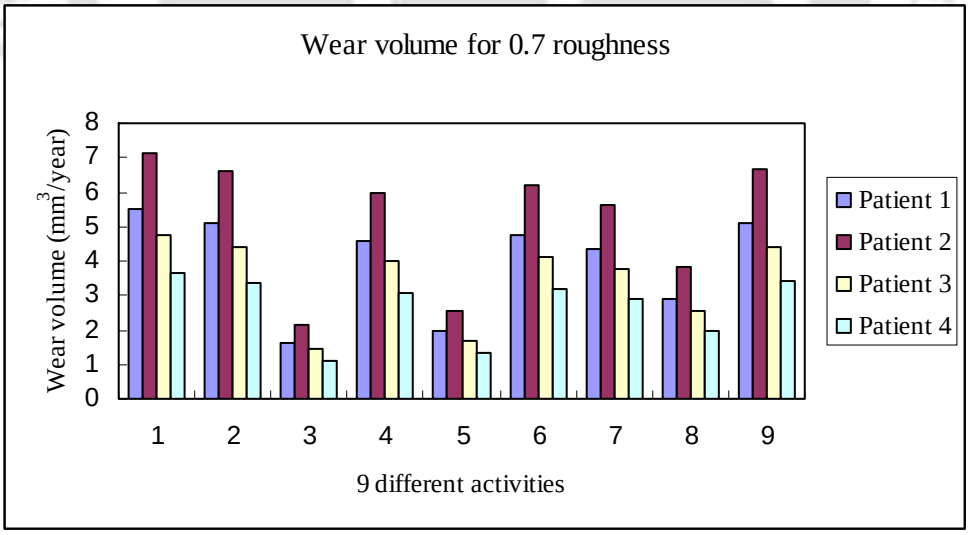

Fig. 6.8: Wear volume rate of acetabular cup for different patients with Ti6Al4V made head (R_a = 0.7 µm)

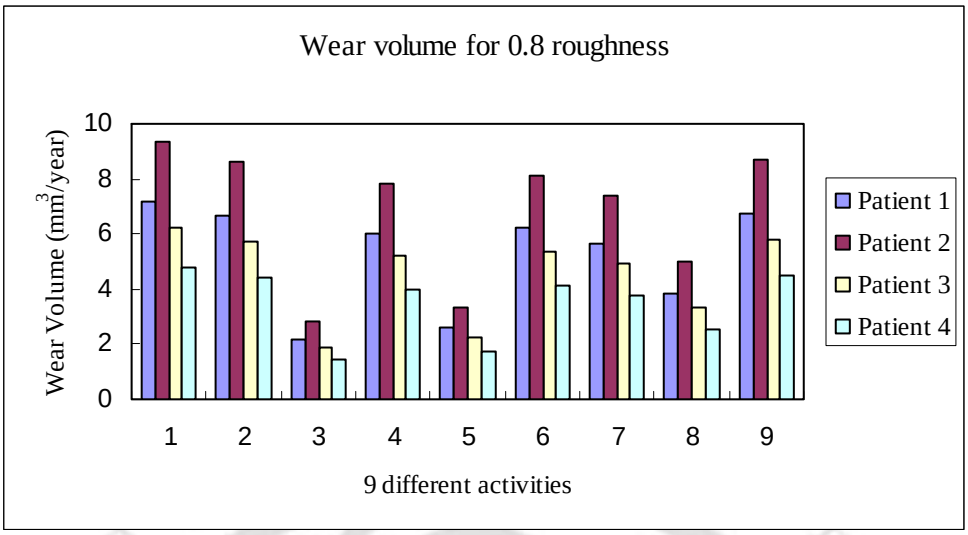

Fig. 6.9: Wear volume rate of acetabular cup for different patients with Ti6Al4V made head (R_a = 0.8 µm)

6.3.2. Wear Analysis with CoCr head with UHMWPE acetabular Cup

In the case of CoCr head, contact stress, sliding distance and wear volume for four different patients are tabulated below for nine different activities. Tables 6.8 to 6.11 show the contact stress, sliding distance, and wear volume for four different patients and nine different activities with CoCr head.

Table 6.8: Contact Stress for four patients with nine different activities
(*Ra*=0.8 µm, *R* = 16 mm)

Activities	Contact stress (MPa)			
	Patient 1	Patient 2	Patient 3	Patient 4
Downstairs	5.013	5.728	4.102	4.663
Fast walking	4.82	5.507	3.944	4.483
Knee bend	2.755	3.149	2.255	2.563
Normal walking	4.588	5.243	3.754	4.268
Sitting down	3.006	3.435	2.46	2.796
Slow walking	4.665	5.317	3.817	4.34
Standing on 2-1-2	4.453	5.088	3.644	4.142
Standing up	3.662	4.174	2.997	3.407
Upstairs	4.839	5.515	3.959	4.501

Table 6.9: Sliding distance for four patients with nine different activities
(R_a = 0.8 µm, R = 16mm)

Activities	Sliding distance (mm)			
	Patient 1	Patient 2	Patient 3	Patient 4
Downstairs	0.016297	0.018542	0.013236	0.015148
Fast walking	0.015663	0.017821	0.012721	0.014559
Knee bend	0.008912	0.010141	0.007302	0.008287
Normal walking	0.014902	0.01695	0.012105	0.013853
Sitting down	0.009728	0.011069	0.007913	0.009045
Slow walking	0.015156	0.017297	0.01231	0.014089
Standing on 2-1-2	0.01446	0.016452	0.011747	0.013442
Standing up	0.011872	0.013545	0.009648	0.011037
Upstairs	0.015726	0.017949	0.012772	0.014618

Table 6.10: Wear volume for four patients with nine different activities
(R_a = 0.8 µm, R = 16mm)

Activities	Wear volume (mm^3/year)			
	Patient 1	Patient 2	Patient 3	Patient 4
Downstairs	7.1657	9.315643	4.762178	6.195466
Fast walking	6.621787	8.607963	4.400595	5.72471
Knee bend	2.153525	2.800959	1.444247	1.862941
Normal walking	5.996823	7.794761	3.985771	5.185868
Sitting down	2.564872	3.334943	1.707377	2.218191
Slow walking	6.201396	8.066603	4.121293	5.363189
Standing on 2-1-2	5.647734	7.342079	3.754556	4.883455
Standing up	3.813252	4.958892	2.536164	3.298196
Upstairs	6.674629	8.682384	4.435041	5.770988

Table 6.11: Wear Volume for four patients with nine different activities
(R_a = 0.6 µm, R = 16mm)

Activities	Patient 1	Patient 2	Patient 3	Patient 4
Downstairs	3.996069	5.19502	3.455002	2.655706
Fast walking	3.692747	4.80037	3.192478	2.454063
Knee bend	1.200948	1.562	1.0389	0.805408
Normal walking	3.344226	4.346875	2.891984	2.22273
Sitting down	1.430343	1.859785	1.23701	0.952147
Slow walking	3.458309	4.498472	2.99087	2.298306
Standing on 2-1-2	3.149551	4.09443	2.723338	2.093789
Standing up	2.126522	2.765407	1.839292	1.414333
Upstairs	3.722215	4.841873	3.218286	2.473273

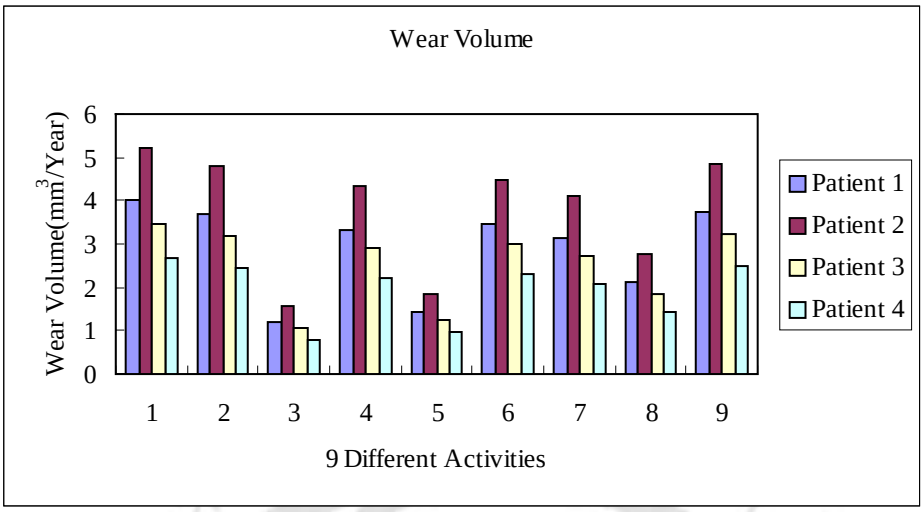

Fig. 6.10: Variation of CoCr alloy wear volume rate per year in 9 different activities at different body weights at R_a = 0.6 µm.

Table 6.12: Wear Volume for four patients with nine different activities (R_a = 0.6µ, R = 16mm)

Activities	Patient 1	Patient 2	Patient 3	Patient 4
Downstairs	3.996069	5.19502	3.455002	2.655706
Fast walking	3.692747	4.80037	3.192478	2.454063
Knee bend	1.200948	1.562	1.0389	0.805408
Normal walking	3.344226	4.346875	2.891984	2.22273
Sitting down	1.430343	1.859785	1.23701	0.952147
Slow walking	3.458309	4.498472	2.99087	2.298306
Standing on 2-1-2	3.149551	4.09443	2.723338	2.093789
Standing up	2.126522	2.765407	1.839292	1.414333
Upstairs	3.722215	4.841873	3.218286	2.473273

Table 6.12 shows the wear volume rate for four different patients with nine different activities for roughness value 0.6µ. Figure 6.10 shows the variation of wear volume rate per year in nine different activities for four different patients at 0.6µ roughness, for spherical head made of CoCr alloy.

6.4: Development of an empirical relation for determination of wear volume

In the previous sections, wear volumes have been calculated using modified Archard's law based on the contact stresses and sliding distances obtained from FEA. Large number of FEA was performed for different patients with different activities and different materials of

the prosthesis. In this section, an attempt has been made to develop an empirical relation which could be used to calculate the wear volume without actually performing the FE analysis.

Following Wu *et al.* [73], the modified Archard's wear volume equation for softer material in terms of contact stress, sliding distance can be given by

$$V = K_w \sigma_c A S_L \ . \tag{6.7}$$

Here V is the wear volume removed from the softer material in mm^3; K_w is known as the wear coefficient and its unit is mm^3/N-m, σ is normal contact stress in MPa, A is the contact area in mm^2, and S_L is the sliding distance in mm. Many authors (Pietrabissa *et al.* [76]) agree that, K_w is an exponential function of surface roughness (R_a). Assuming a person has an average movement of 10,000 cycles per day (Pietrabissa et al. [76]), the above equation can be written as

$$V = K_w \sigma_c A S_L \times 10000 \times 365 \times 10^{-3} \ \text{mm}^3 \text{/year} \ . \tag{6.8}$$

In this section, an empirical relation for the wear volume in terms of body weight, head radius and roughness has been developed using the maximum contact stress and sliding distance obtained by FE analysis for nine different activities.

Tables 6.3 and 6.4 show respectively the maximum contact stress and sliding distance for down stair climbing activity for different body weights and femoral head radius. In order to develop an empirical relation for contact stress in terms of body weight and femoral head radius, following procedure has been adopted. Initially, the contact stress (σ) has been assumed to be a function of applied load (P) and femoral head radius (R), as

$$\sigma = k_1 \left(P\right)^{a1} \left(R\right)^{b1} \ . \tag{6.9}$$

Here k_1 is a constant. It may be noted that the applied load is equal to the body weight in Newton multiplied by the activity factor as given in Table 6.2. In this calculation, the

femoral head radius is considered to be in mm and the stress is in MPa. Equation 6.9 could be written as

$$\log(\sigma) = \log(k_1) + a1 \times \log\ (P) + b1 \times \log\ (R) \tag{6.10}$$

Multiplying $\log(P)$ and $\log(R)$ in both sides of equation (6.10) gives the following equations.

$$\log(P) \times \log(\sigma) = \log(k_1) \times \log(P) + a1 \times \left(\log\ (P)\right)^2 + b1 \times \log(P) \times \log(R) \tag{6.11}$$

$$\log(R) \times \log(\sigma) = \log\ (k_1) \times \log\ (R) + a1 \times \log(P) \times \log\ (R) + b1 \times \left(\log(R)\right)^2 \tag{6.12}$$

Now taking *n* sets of data available relating the contact stress, applied load and head radius, the above three equations can be written as

$$\sum_{i=1}^{n} \log \sigma_i = n \log k_1 + a1 \sum_{i=1}^{n} \log W_i + b1 \sum_{i=1}^{n} \log R_i \tag{6.13}$$

$$\sum_{i=1}^{n} \log P_i \log \sigma_i = \log k_1 \sum_{i=1}^{n} \log P_i + a1 \sum_{i=1}^{n} \left(\log P_i\right)^2 + b1 \sum_{i=1}^{n} \log P_i \log R_i \tag{6.14}$$

$$\sum_{i=1}^{n} \log R_i \log \sigma_i = \log k_1 \sum_{i=1}^{n} \log R_i + a1 \sum_{i=1}^{n} \log R_i \log P_i + b1 \sum_{i=1}^{n} \left(\log_{10}(R_i)\right)^2 \tag{6.15}$$

Using the data given in Table 6.3 and solving the above three equations (6.13-6.15), the following relation between contact stress, body weight and head radius could be obtained for down stair activity,

$$\sigma = 10^{4.1659} \times (P)^{1.0106} \times (R)^{-0.7101} \text{ MPa} \tag{6.16}$$

Following similar procedure adopted just described (replacing σ by S_L in equations 6.9), a relation for the sliding distance in terms of applied load (P) and femoral head radius (R) has been obtained using the data given in Table 6.4. This relation is given by

$$S_L = 10^{-0.7863} \times (P)^{1.0123} \times (R)^{-3.6490} \quad \text{mm} \tag{6.17}$$

Now using equations (6.16) and (6.17), in equation (6.2), the following expression for wear volume for down stair activity could be obtained.

$$V = 0.0002 \times A \times (R_a)^{2.03} \times (P)^{2.0229} \times (R)^{-4.3591} \tag{6.18}$$

Here P is the applied load, R_a is the roughness and R is the femoral head radius.

In terms of body weight, the above equation can be written as

$$V = 0.0014 \times A \times (R_a)^{2.03} \times (W)^{2.0229} \times (R)^{-4.3591} \tag{6.19}$$

To find the maximum wear volume, the maximum contact area, which is $A = 2\pi R^2$ should be used. So equation (6.19) can be written as

$$V = 0.0088 \times (R_a)^{2.03} \times (W)^{2.0229} \times (R)^{-2.3591} \quad . \tag{6.20}$$

Equations (6.20) can be used to determine the wear volume in the case of down stair activity in terms of R_a, W and R.

To find the expressions for the empirical relation for other activities, FEA analysis has been carried out. Fig 6.11 shows the contact stress distribution as a function of body weight for nine different activities for a femoral head radius of 16mm and it could be observed that the maximum contact stress occurs in down stair activity and minimum contact stress occurs in knee bend activity. Fig 6.12 shows the sliding distance distribution as a function of body weight for different activities for 16 mm femoral head radius and here also it could be observed that the maximum sliding distance occurs in down stair activity and the minimum-sliding distance occurs in knee bend activity.

Following the procedure similar to the down stair activity, using the data generated for contact stress (Fig 6.11) and sliding distance (Fig 6.12) from FEA, empirical relation for

wear volume is developed for all the nine different daily activities, viz., down stairs climbing, up stair climbing, fast walking, slow walking, normal walking, standing on 2-1-2 legs, standing up, sitting down, and knee bend postures.

The relation for different activities is given by

$$V = K \times (R_a)^{2.03} \times (W)^{2.0229} \times (R)^{-2.3591} \quad (6.21)$$

The constant K for different activities is given in Table 6.15.

Fig 6.13 shows the comparison of wear volume obtained using the contact stress (Fig 6.11) and sliding distances (Fig 6.12) obtained from FEA in equation (6.8) and from the developed empirical relation (6.21). From fig 6.13 it could be observed that the wear volume is almost same in both the cases and the maximum error will be around 5% for static analysis. Minimum wear is found during knee bend activity and maximum during down stairs climbing. The maximum wear volume is found to 7 mm^3/year, which is in well agreement with published clinical valves of wear (Maxian *et al* [126]). Hence, the developed empirical relation could be used to find the wear volume for different patients knowing their weight and daily activity.

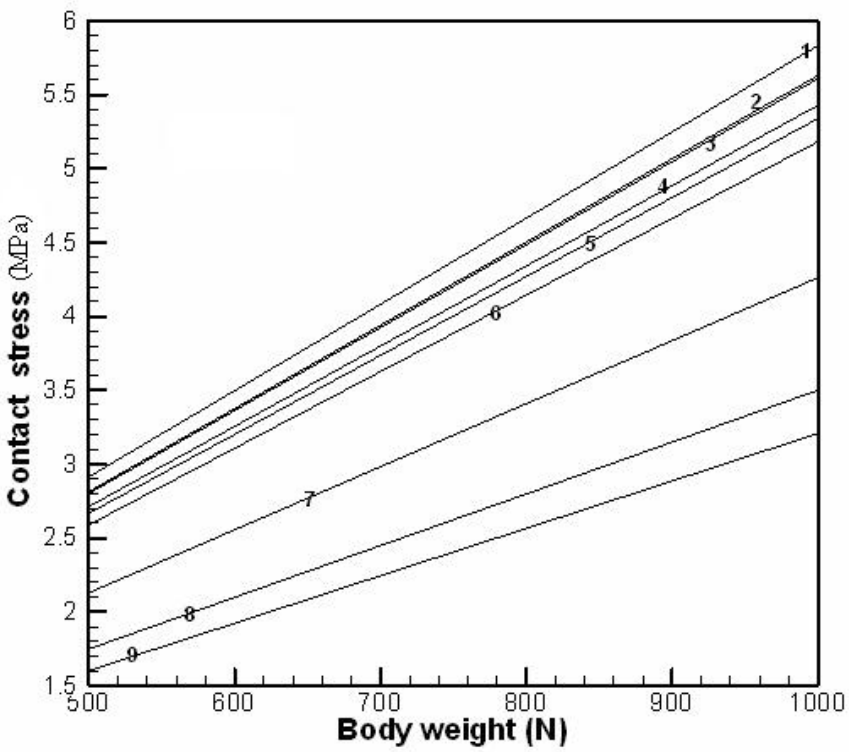

Fig 6.11: Variation of contact stress with body weight for 9 different activities for *R*=16mm. Activities 1. Down stairs, 2 up stair, 3. Fast walking, 4. Slow walking, 5. Normal walking, 6. Standing on 2-1-2 legs, 7. Standing up, 8. Sitting down, 9. Knee bend.

Table 6. 13: Contact stress obtained from the FE analysis in down stairs activity for different body weight and femoral head radius.

Femoral head radius (mm)	Contact stress (MPa)					
	BW 500 N	BW 600 N	BW 700 N	BW 800 N	BW 900 N	BW 1000 N
15	2.987	3.585	4.183	4.782	5.381	5.98
15.1	2.988	3.586	4.185	4.784	5.383	5.982
15.2	2.991	3.59	4.189	4.788	5.388	5.987
15.3	2.967	3.562	4.156	4.751	5.346	5.941
15.4	2.942	3.53	4.12	4.709	5.299	5.888
15.5	2.932	3,519	4.106	4.693	5.28	5.868
15.6	2.927	3.514	4.1	4.686	5.273	5.86
15.7	2.914	3.498	4.081	4.655	5.249	5.833
15.8	2.921	3.506	4.091	4.676	5.26	5.846
15.9	2.915	3.499	4.083	4.667	5.251	5.835
16	2.914	3.497	4.081	4.664	5.248	5.832

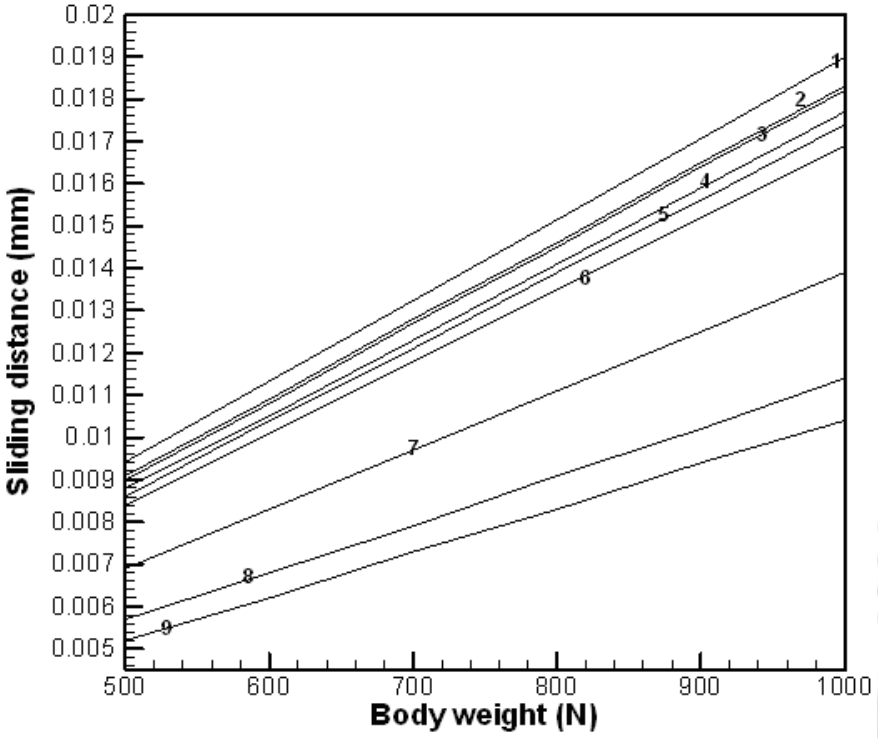

Fig 6.12: Variation of sliding distance with body weight in 9 different activities for a femoral head radius of 16mm. Activities 1. Down stairs, 2 up stair, 3. Fast walking, 4. Slow walking, 5. Normal walking, 6. Standing on 2-1-2 legs, 7. Standing up, 8. Sitting down, 9. Knee bend.

Table 6.14 Sliding distance obtained from the FE analysis in down stair activity for different body weight and femoral head radius

Femoral head radius (mm)	Sliding distance (mm)					
	BW 500 N	BW 600 N	BW 700 N	BW 800 N	BW 900 N	BW 1000 N
15	0.011822	0.014211	0.016609	0.019024	0.02145	0.023888
15.1	0.011632	0.013984	0.016344	0.018528	0.020891	0.023265
15.2	0.011334	0.013465	0.015696	0.017964	0.020242	0.022239
15.3	0.011093	0.013341	0.015596	0.017689	0.019925	0.022165
15.4	0.010796	0.012978	0.015167	0.017365	0.01957	0.02178
15.5	0.010594	0.012733	0.014880	0.016994	0.01915	0.021312
15.6	0.010295	0.012331	0.014405	0.016481	0.018566	0.020659
15.7	0.010059	0.012091	0.014128	0.016174	0.018227	0.02029
15.8	0.009814	0.011799	0.013791	0.015789	0.017804	0.0198211
15.9	0.009646	0.011597	0.013555	0.015521	0.017494	0.019474
16	0.009424	0.01133	0.013236	0.015148	0.017064	0.0189885

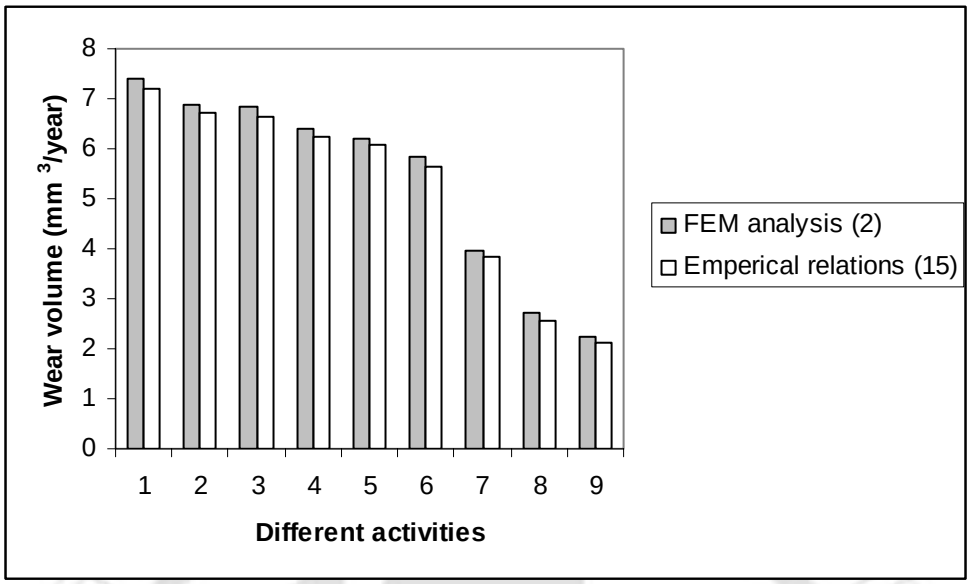

Fig 6.13: Comparison of wear volume with Fem analysis and the empirical relations for different activities for a body weight of 1000 N, femoral head radius 16mm and roughness 0.7µm. Activities 1. Down stairs, 2 up stair, 3. Fast walking, 4. Slow walking, 5. Normal walking, 6. Standing on 2-1-2 legs, 7. Standing up, 8. Sitting down, 9. Knee bend.

Table 6.15: K values for different activities

Activity	K
Down stairs	0.0088
Up stairs	0.0082
Fast walking	0.0081
Slow waking	0.0076
Normal walking	0.0074
Standing on 2-1-2 legs	0.0069
Standing up	0.0047
Sitting down	0.0031
Knee bend	0.0026

6.5. Summary

Three dimensional finite element analyses have been done for contact stress analysis at the interface of acetabular cup and femoral head of an artificial hip prosthesis. Contact stresses and sliding distances obtained from the finite element analyses have been used for

evaluation of wear rate using modified Archard's law. In this work, empirical relations have been proposed through which wear rate can be determined as a function of body weight, femoral head radius and roughness which could be used for assessing wear at the interface of acetabular cup and the femoral head in an artificial hip prosthesis. These relations are developed for nine different daily activities viz., down stairs climbing, up stair climbing, fast walking, slow walking, normal walking, standing on 2-1-2 legs, standing up, sitting down, and knee bend postures. From the present study it has also been observed that the contact stress and wear volume are maximum in the down stair activity and is minimum in the case of knee bend activity. The obtained results are in good agreement with published clinical finding. The empirical relations will find industrial application in the design of hip prosthesis.

CHAPTER 7

CONCLUSIONS AND SCOPE FOR FUTURE WORK

7.1 General Conclusions

Three dimensional finite element models have been developed for failure analysis of hip prosthesis. Failure of the stem due to stress induced in fatigue loading has been analyzed and failure of the acetabular cup due to gradual wear at the interface of the cup and the spherical head has also been analyzed. Two approaches of analysis viz. equivalent static loading analysis as well as complete dynamic analysis have been carried out. In order to understand the implications of different daily activities on the life of hip prosthesis, nine different most commonly used activities such as fast walking, slow walking, normal walking, upstairs climbing, downstairs climbing, standing on 2-1-2 legs, knee bend, standing up and sitting down have been considered in the analysis.

Influences of stem shapes on the performance of prosthesis have also been studied in details in the present work. Importance of choosing a prosthesis material has been studied by considering different prosthesis materials such as UHMWPE, Ti6Al4V and CoCr alloy in the present analysis. In evaluating fatigue life of prosthesis, using residual strength degradation model, a method has been suggested for determination of fatigue constants for materials in absence of experimental data. This method has been successfully used to determine the constants for Ti6Al4V, CoCr alloy and UHMWPE. Fatigue life curves have been generated for prosthesis under different activities, for different types of patients which will be immensely useful for orthopaedic surgeons. A comparative analysis of the results has also been done to study the effect of taking a simplified model and a more realistic model in the finite element analysis. Finite element method in conjunction with modified Archard's law has been used to perform detailed contact stress analysis and estimation of wear of the acetabular cup. Based on the finite element results, empirical relations have been proposed which will be useful for assessing the possible gradual wear and wear volume with time. Knowledge of wear volume of prosthesis for a patient undergoing total hip replacement is of immense importance from

the patient's safety point of view, and the empirical relations developed will find important applications in this regard.

7.2 Specific conclusions

Based on the finite element analysis for failure analysis of the hip prosthesis, the following important conclusions have been drawn.

1. Initial stress analysis results show that among the possible prosthesis materials UHMWPE is more effective in avoiding stress shielding compared to Ti6Al4V and CoCr alloy.
2. From the strength point of view, UHMWPE stands much weaker compared to Ti6Al4V and CoCr alloy to be used as a stem material.
3. Among the three possible stem shapes, it was observed that stepped stem lead to very high stress concentration. Therefore it is not suitable for use even though it leads to better fit inside the femur.
4. Stress induced in straight and conical stems are observed to much less than in stepped stem but conical stem is preferred because of its better fit into the femur.
5. Location of maximum stress depends on the shape as well as stiffness of the stem. For a given stem shape, as the stiffness of the stem decreases, the location of the maximum stress moves towards the proximal end.
6. Among CoCr alloy and Ti6Al4V, Ti6Al4V has been observed to be a better prosthesis material in terms of fatigue life for the patients studied in the present work under different activities.
7. Activities have been observed to have critical importance in deciding the life of prosthesis, and which among the daily activities is most critical depends upon the condition of the patient.
8. It has been observed that for most of the other patients standing 2-1-2 is the critical activity.
9. Present study shows that considering a simplified finite element model (without cancellous bone, abductor muscle force and greater trochanter force) leads to estimating longer fatigue life compared to that of considering more realistic finite element model.

10. Even though many earlier works have been reported in estimating fatigue life using equivalent static loading, it has been observed from the present study that equivalent static loading predicts life which is almost ten times higher compared to that obtained by using actual dynamic loading.
11. It has been observed that Ti6Al4V as prosthesis material leads to more wear of the acetabular cup made of UHMWPE.
12. Wear rate of the acetabular cup increases as the head radius and surface roughness increase.

7.3 Scope for future work

1. Experiments could be conducted for simulating the gait movement and estimating fatigue life and wear of the acetabular cup.
2. Fluid film could be modeled at the cup head interface for more realistic modeling and analysis
3. Cementless prosthesis could be studied for fatigue life and wear analysis.
4. More advanced materials like functionally graded materials could be studied as possible prosthesis materials.
5. Analysis could be done for other activities.

REFERENCES

[1] G. Bergmann, F. Graichen, A. Rohlmann, 1993, Hip joint loading during walking and running, measured in two patients, Journal of Biomechanics, 26, 969-990.

[2] G. Bergmann, H. Kniggendorf, F. Graichen, A. Rohlmann, 1995, Influence of shoes and heel strike on the loading of the hip joint, Journal of Biomechanics, 28, 817-827

[3] G. Bergmann, F. Graichen, A. Rohlmann, 1997, Hip joint forces during load carrying, Clinical Orthopaedics and related Research, 335, 190-201.

[4] G. Bergmann, G. Deuretzbacher, M. Heller, F. Graichen, A. Rohlmann, J. Strauss, G. N. Duda, 2001, Hip contact forces and gait patterns from routine activities, Journal of Biomechanics, 34, 859-871.

[5] G. Bergmann, 2001, HIP98, Free University, Berlin, ISBN 3980784800 [Compact Disc].

[6] G. Bergmann, F. Graichen, A. Rohlmann, 1995, Is stair case walking a risk for the fixation of hip implants?, Journal of Biomechanics, 28,5,535-553.

[7] B. W. Stansfield, A.C. Nicol, J. P. Paul, I. G. Kelly, F. Graichen, G. Bergmann, 2003, Direct Comparison of calculated hip joint contact forces with those measured instrumented implants. An evaluation of a three-dimensional mathematical model of the lower limb, Journal of Biomechanics, 36, 929-936.

[8] B.W. Stansfield and A.C. Nicol, 2002, Hip joint contact forces in normal subjects and subjects with total hip prostheses: walking and stair and ramp negotiation, Clinical Biomechanics, 17, 130-139.

[9] D.E. Hurwitz, K.C. Foucher and T.P. Andriacchi, 2003, A new parametric approach for modeling hip forces during gait, Journal of Biomechanics, 36, 113-119.

[10] A. Vora, J.C. Kudrna, V.S. Harder, B. Mazahery, 2003, Early failure of a proximally cemented, distally uncemented total hip arthroplasty, The Journal of Arthroplasty, 18, 7, 889-896.

[11] C. F. Scifert, T. D. Brown, J. D. Lipman, 1999, Finite element analysis of a novel design approach to resisting total hip dislocation, Clinical Biomechanics, 14, 697-703

References

[12] S. Gross, E. W. Abel, 2001, A finite element analysis of hollow stemmed hip prostheses as a means of reducing stress shielding of the femur, Journal of Biomechanics, 34, 995-1003.

[13] A. Phillips, 2001, Finite element analysis of the acetabulum after impaction grafting, The university of Edinburgh, MS Thesis.

[14] P. Kowalczyk, 2001, Design optimization of cementless femoral hip prosthesis using finite element analysis, ASME Journal of Biomechanical Engineering, 123, 396-402.

[15] P. B. Chang, B. J. Williams, B. B. Kanwaljeet Singh, T. W. Belknap, T. J. Santer, W. Inotz, D. L. Bartel, 2001, Design and analysis of robust total joints replacements: Finite element model experiments with environmental variables, ASME Journal of Biomechanical Engineering, 123, 239-246.

[16] P.B. Chang, B.J. Williams, T. J. Santner, W.I. Notz, and D.L. Bartel, 1999, Robust Optimization of Total Joint Replacements Incorporating Environmental Variables, Journal of Biomechanical Engineering, 121, 3, 304-310.

[17]] S. K. Senapati, S. Pal, 2002, UHMWPE-ALUMINA ceramic composite, an improved prosthesis material for an artificial cemented hip joint, Trends in Biomaterials. Artificial Organs, 16(1), 5-7.

[18] H. Katoozian, D. T. Davy, A. Arshi, U. Saadati, 2001, Material optimization of femoral component of total hip prosthesis using fiber reinforced polymeric composites, Medical Engineering and Physics, 23, 503-509.

[19] H. Katoozian, 1993, Three dimensional design optimization of femoral components of total hip endoprostheses, Ph.D Thesis, Case Western Reserve University.

[20] H. Katoozian, D. T. Davy, 2000, Effects of loading conditions and objective function on three dimensional shape optimization of femoral components of hip endoprostheses, Medical Engineering and Physics, 22,243-251.

[21] D.P. Nicolella, B.H. Thacker, H.Katoozian, D.T. Davy, 2001, Probabilistic risk analysis of a cemented hip implant, ASME Bioengineering conference, 50.

[22] B. Weisse et al., 2003, Improvement of the reliability of ceramic hip joint implants, Journal of Biomechanics, 36, 1633-1639.

[23] P.J. Prendergast, 1997, Review paper - Finite element models in tissue mechanics and orthopaedic implant design, Clinical Biomechanics, 12, No.6, 343-366.

References

[24] J. A. Simoes, A. T. Marques, G. Jeronimidis, 2000, Design of controlled-stiffness composite proximal femoral prosthesis, Composites Science and Technology, 60, 559-567.

[25] J. A. Simoes, A. T. Marques, 2001, Determination of stiffness properties of braided composites for the design of a hip prosthesis, Composites: Part A (32), 655-662.

[26] C. Li, C. Granger, H. D. Schutte Jr., S. B. Biggers Jr., J. M. Kennedy, R. A. Latour Jr., 2002, Progressive failure analysis of laminated composite femoral prostheses for total hip arthroplasty, Biomaterials, 23, 4249-4262.

[27] C. Li, C. Granger, H. D. Schutte Jr., S. B. Biggers Jr., J. M. Kennedy, R. A. Latour Jr., 2003, Failure analysis of composite femoral components for hip arthroplasty, Journal of Rehabilitation Research and Development ,40, 2, 131-146.

[28] Y. Zhou, C. Li, J.J. Mason, 2005, Shape optimization of randomly oriented short fibers for bone cement reinforcements, Material Science and Engineering, A 393, 374-381.

[29] B. Mavčič, B. Pompe, V. Antolič, M. Daniel, A. Iglič and V. Kralj-Iglič, 2002. Mathematical estimation of stress distribution in normal and dysplastic human hips, Journal of Orthopaedic Research, 20, 5, 1025-1030.

[30] H.S. Heida , D.C. Barton, J. Fisher, and T.T. Elmidany, 1996, A method for shape optimization of a hip prosthesis to maximize the fatigue life of the cement, Medical Engineering Physics,18, No:8, 647-654.

[31] A. Werner, Z. Lechniak, K. Skalski, K. Kedzior, 2000, Design and manufacture of anatomical hip joint endoprostheses using CAD/CAM systems, Journal of Materials Processing Technology, 107, 181-186.

[32] J.R. Howell, L.A. Blunt, C. Doyle, R.M. Hooper, A.J.C. Lee, R.S.M. Ling, 2004, In Vivo surface wear mechanisms of femoral components of cemented total hip arthroplasties, The Journal of Arthroplasty, 19, 1, 88-101.

[33] M. Pawlikowski, K. Skalski, M. Haraburda, 2003, Process of hip joint prosthesis design including bone remodeling phenomenon, Computers and Structures, 81, 887-893.

[34] K.E. Tanner, P.E. Reed, W. Bonfield, G.L. Rasmussen, M.A. R. Freeman, 1988, A system for modelling forces on the hip joint in one legged stance, Journal of Biomedical Engineering, 10, 289-290.

References

[35] R. Shirandami, I.I. Esat, 1990, New design of hip prosthesis using carbon fibre reinforced composite, Journal of Biomedical Engineering, 12, 19-22.

[36] G. Selvaduray, 2002, Design Specification and Material Selection of Total Hip Implants, San Jose State University. [http://www.sjsu.edu/].

[37] C.A. Scotchford, M.J. Garle, J. Batchelor, J. Bradley and D. M. Grant, 2003. Use of novel carbon fibre composite material for the femoral stem component of a THR system: in vitro biological assessment, Biomaterials, 24, 4871-4879.

[38] N.J. Hallab, C. Messina, A. Skipor and J.J Jacobs, 2004. Differences in the fretting corrosion of metal-metal and ceramic-metal modular junctions of total hip replacements, Journal of Orthopaedic Research, 250-259.

[39] K.S. Katti, 2004, Biomaterials in total joint replacement, Colloids and Surfaces B: Biointerfaces vol.39, 3, 133-142.

[40] T.P. Schmalzried and J.J. Callaghan, 1999, Current concepts review: Wear in total hip and knee replacements, Journal of Bone and Joint Surgery, 81, 1, 115-136.

[41] Z. Miller, M.B. Fuchs and M. Arcan, 2002. Trabecular bone adaptation with an orthotropic material model, Journal of Biomechanics, 35, 247-256.

[42] J.A. Helsen and H.J. Breme., 1998, Metals as Biomaterials, John Willey& Sons.

[43] S.M. Kurtz, L. Pruit, C.W. Jewett, R.P. Crawford, D.J. Crane and A.A. Edidin, 1998, The yielding, plastic flow, and fracture behaviour of ultra high molecular weight polyethylene used in total joint replacements, Biomaterials, 19, 1989 – 2003.

[44] J.V. Sloten, L. Labey, R.V. Audekercke, G.V.D. Perre, 1998, Materials selection and design for orthopaedic implants with improved long-term performance, Biomaterials, 19, 1455-1459.

[45] V. Waide, L. Cristofolini, J. Stolk, N. Verdonschot, G.J. Boogaard and A. Toni., 2004. Modeling the fibrous tissue layer in cemented hip replacements: experimental and finite element methods, Journal of Biomechanics, 37, 1, 13-26.

[46] S. Zimmerman, W.G. Hawkes, J.I. Hudson, J. Magaziner, J. R. Hebel, T. Towheed, J. Gardner, G. Provenzano and J.E. Kenzora., 2002.Outcomes of surgical management of total hip replacement in patients aged 65 years and older: cemented versus cementless femoral components and lateral or anterolateral versus posterior anatomical approach, Journal of Orthopaedic Research, 20, 2, 182-191.

References

[47]S.K. RoyChowdhury, A. Mishra, B. Pradhan and D. Saha, 2004. Wear characteristic and biocompatibility of some polymer composite acetabular cups, Wear, 256, 1026-1036.

[48] R.N. Kirkwood, E.G. Culham and P.Costigan, 1999. Radiographic and non-invasive determination of the hip joint center location: effect on hip joint moments, Clinical Biomechanics, 14, 227-235.

[49] A.B. Lennon and P.J. Prendergast, 2001. Evaluation of cement stresses in finite element analyses of cemented orthopaedic implants, Journal of Biomechanical engineering, ASME, 123, 623-628.

[50] F. Sibella, M. Galli, M. Romei, A. Montesano and M. Crivellini.2003. Biomechanical analysis of sit-to-stand movement in normal and obese subjects, Clinical Biomechanics, 18, 745-750.

[51] C.M. Styles, S.L. Evans, P.J. Gregson, 1998, Development of fatigue lifetime predictive test methods for hip implants: Part I. Test methodology, Biomaterials, 19, 1057-1065.

[52] B.A.O. McCormack, P.J. Prendergast and D.G. Gallagher, 1996, An experimental study of damage accumulation in cemented hip prostheses, Clinical Biomechanics, 11, 4, 214-219.

[53] B.A.O. McCormack, P.J. Prendergast and B.O. Dwyer, 1999, Fatigue of cemented hip replacements under torsional loads, Fatigue Fracture Engineering Material Structures, 22, 33-40.

[54] R.K. Nalla, J.J. Kruzic, J.H. Kinney, R.O. Ritchie, 2005, Aspects of in vitro fatigue in human cortical bone: time and cycle dependent crack growth, Biomaterials, 26, 2183-2195.

[55] Z. Jin, S. Williams, J. Tipper, E. Ingham, J. Fisher, 2006, Tribology of hip joints from Natural hip joints, cartilage substitution, artificial replacements to cartilage tissue engineering, Journal of Biomechanical Science and Engineering, 1,69-81.

[56] M.J. Mathias, K. Tabeshfar, 2006, Design and development of a new acetabular cup prosthesis, Materials Science and Engineering, C 26, 1428-1433.

[57] J.A. Simoes, A.T. Marques, 2005, Design of a composite hip femoral prosthesis, Materials and Design, 26, 391-401.

References

[58] M.O. Heller, G. Bergmann, G. Deuretzbacher, L. Durselen, M. Pohl, L. Cles, N.P. Hass, G.N. Duda, 2001, Musculo-skeletal loading conditions at the hip during walking and stair climbing, Journal of Biomechanics, 34, 883-893.

[59] J.A.D.O. Simoes, A.T. Marques, 2001, Determination of stiffness properties of braided composites for the design of a hip prosthesis, Composites Part A, 32, 655-662.

[60] D.O. E. Olotu, L. Nokes, H. Rassoulian, J.R. Goddard, 2001, The use of handheld cement sample as a guide to the setting of In Situ cement mantle, The Journal of Arthroplasty, 16, 3, 376-378.

[61] L. Christofoloni, A. Marchetti, A. Cappello, M. Viceconti, 2000, A novel transducer for the measurement of cement-prosthesis interface forces in cemented orthopaedic devices, Medical Engineering and Physics, 22, 493-501.

[62] L. Cristofoloni, P. Erani, A.S. Teutonico, F. Traina, M. Viceconti, A. Toni, 2007, Partially cemented AncaDualFit hip stems do not fail in simulated active patients, Clinical Biomechanics, 22, 191-202.

[63] A.B. Lennon, B.A.O. McCormack, P.J. Prendergast, 2003, The relationship between cement fatigue damage and implant surface finish in proximal femoral prostheses, Medical Engineering and Physics, 25, 833-841.

[64] J.M. Garcia, M. Doblare, J. Cegonino, 2002, Bone remodeling simulation: a tool for implant design, Computational Materials Science, 25, 100-114.

[65] J.N. Yang and M.D. Liu., 1977, Residual strength degradation model and theory of periodic proof tests for graphite/epoxy laminates, Journal of Composite Materials, 11, 176-203.

[66] J.N. Yang., 1978, Fatigue and residual strength degradation for graphite/epoxy composites under Tension-Compression cyclic loadings, Journal of Composite Materials, 12, 19-39.

[67] N.H. Tai, C.C.M. Ma and S.H. Wu, 1995, Fatigue behaviour of carbon fibre/PEEK laminate composites, Composites, 26(8), 551-559.

[68] A.G.D. Valle, B. Becksac, J. Anderson, T. Wright, B. Netsor, P.M. Pellicci, E.A. Salvati, 2005, Late fatigue fracture of a modern cemented forged cobalt chrome stem for total hip arthroplasty, The Journal of Arthroplasty, 20, 8, 1084-1088.

References

[69] R.D. Santis, L. Ambrosio, L. Nicolais, 2000, Polymer-based composite hip prostheses, Journal of Inorganic Biochemistry, 79, 97-102.

[70] M.P. Gispert, A.P. Serro, R. Colaco and B. Saramago, 2006, Friction and wear mechanisms in hip prosthesis: Comparison of joint materials behavior in several lubricants, Wear, 260, 149-158.

[71] V. Saikko, T. Ahlroos, O. Calonius, and J. Keranen, 2001, Wear simulation of total hip prostheses with polyethylene against CoCr alumina and diamond – like carbon, Biomaterials, 22, 1507-1514.

[72] C.M. Wall, D.C. Eberle, M.B. Treuhaft and J.H. Arps, 2005, Technique for high-sensitivity "in vitro" wear measurement of UHMWPE hip joint liners using radioactive tracer technology, Wear, 259, 964-971.

[73] J.S.S. Wu, J.P. Hung, C.S. Shu and J.H. Chen, 2003, The computer simulation of wear behaviour appearing in total hip prosthesis, Computer methods and programs in biomedicine, 70, 81-91.

[74] E.P.J. Watters, P.L. Spedding, J. Grimshaw, J.M. Duffy and R.L. Spedding, 2005, Wear of artificial hip joint material, Chemical Engineering Journal, 112, 137 – 144.

[75] H.J. Cho, W.J. Wei, H.C. Kao and C.K. Cheng, 2004, Wear behaviour of UHMWPE sliding on artificial hip arthroplasty materials, Materials chemistry and physics, 88, 9-16.

[76] P. Podra and S. Andersson, 1999, Simulating sliding wear with finite element method, Tribology International, 32, 71-81.

[77] E. Oral, S.D. Christensen, A.S. Malhi, K.K. Wannomae and O.K. Muratoglu, 2006, Wear resistance and mechanical properties of highly cross – linked Ultrahigh – molecular weight polyethylene doped with Vitamin E, The Journal of Arthroplasty, 21, 580-591.

[78] N. Borlin, S.M. Rohrl and C.R. Bragdon, 2006, RSA Wear measurements with or without markers in total hip arthroplasty, Journal of Biomechanics, 39, 1641-1650.

[79] J. Geringer, B. Forest and P. Combrade, 2006, Wear analysis of materials used as orthopaedic implants, Wear, 261, 971-979.

[80] M.A.L. H. Rodriguez, R.D.M. Solis, A.J.P. Unzueta, D.I.M. Delgado, M.C. Sifuentes, 2005, Wear of cast metal-metal pairs for total replacement hip prostheses, Wear, 259, 958-963.

References

[81] A. Chanda, A.K. Mukhopadhyay, D. Basu, S. Chatterjee, 1997, Wear and friction behaviour of UHMWPE-Alumina combination for total hip replacement, Ceramics International, 23, 437-447.

[82]R. Huiskes and E.Y.S. Chao, 1983, A survey of finite element analysis in orthopaedic biomechanics: the first decade, Journal of Biomechanics, 16, 385-409.

[83] W.A.M. Brekelmans, H.W. Poort and T.J.J.H Slooff, 1972, A new method to analyse the mechanical behaviour of skeletal parts, Acta Orthop Scand, 43, 301-317

[84] H. F. El-Sheikh, B. J. MacDonald, M. S. J. Hashmi, 2003, Finite Element simulation of the hip joint during stumbling: a comparison between static and dynamic loading, Journal of Materials Processing Technology 143-144, 20, 249-255.

[85] R. Varanasi, A. Rajadurai, 2002, Fracture and stress analysis of prosthetic hip joint using finite element method, National Symposium of Research Scholars, IIT Madras.

[86] P.T. Scannell, P.J. Prendergast, 2005, Simulation of changes in bone around hip replacement implants, The Engineers Journal, 59, 372-377.

[87] S. Gross, E.W. Abel, 2001, A finite element analysis of hollow stemmed hip prostheses as a means of reducing stress shielding of the femur, Journal of Biomechanics, 34, 995-1003.

[88] C.L. Peters, K.N. Bachus, M.A. Craig, T.O. Higginbotham, 2001, The effect of femoral prosthesis design on cement strain in cemented total hip arthroplasty, The Journal of Arthroplasty, 16, 2, 216-224.

[89] M.G. Joshi, S.G. Advani, F. Miller, M.H. Santare, 2000, Analysis of a femoral hip prosthesis designed to reduce stress shielding, Journal of Biomechanics, 33, 1655-1662.

[90] R. Sakai, M. Itoman, K. Mabuchi, 2006, Assessments of different kinds of stems by experiments and FEM analysis: Appropriate stress distribution on a hip prosthesis, Clinical Biomechanics, 21, 826-833.

[91] M.A. Perez, J.M. Garcia-Aznar, M. Doblare, B. Seral, F. Seral, 2006, A comparative FEA of the debonding process in different concepts of cemented hip implants, Medical Engineering and Physics, 28, 525-533.

[92] C.C. Hu, J.J. Liau, C.Y. Lung, C.H. Huang, C.K. Cheng, 2001, A two dimensional finite element model for frictional heating analysis of total hip prosthesis, Materials Science and Engineering, C17, 11-18.

References

[93] M. Baleani, M. Viceconti, R. Muccini, M. Ansaloni, 2000, Endurance verification of custom-made hip prostheses, International Journal of Fatigue, 22, 865-871.

[94] Y.S. Yoon, G.H. Jang, Y.Y. Kim, 2004, Shape optimal design of the stem of a cemented hip prosthesis to minimize stress concentration in the cement layer, Journal of Biomechanics, 22, 11-12, 1279-1284.

[95] Y. Watanabe, N. Shiba, S. Matsuo, F. Higuchi, Y. Tagawa, A. Inoue, 2000, Biomechanical study of the resurfacing hip arthroplasty Finite element analysis of the femoral component, The Journal of Arthroplasty, 15, 4, 505-511.

[96] C. Zannoni, M. Viceconti, L. Pierotti, A. Cappello, 1998, Analysis of titanium induced CT artifacts in the development of biomechanical finite element models, Medical Engineering and Physics, 20, 653-659.

[97] K.J. Mathias, J.C. Leahy, A. Heaton, W.F. Deans, D.W.L. Hukins, 1998, Hip joint prosthesis design: effect of stem introducers, Medical Engineering & Physics, 20, 620-624.

[98] M. Taylor, K.E. Tanner, M.A.R. Freeman, A.L. Yettram, 1995, Cancellous bone stresses surrounding the femoral component of a hip prosthesis: an elastic-plastic finite element analysis, Medical Engineering Physics, 17, 7, 544-550.

[99] T.P. Harrigan, 1991, Analysis of the fixation of total hip femoral components using ADINA, Computers and Structures, 40, 2, 463-468.

[100] P.J. Prendergast, D. Taylor, 1990, Stress analysis of the proximo-medial femur after total hip replacement, Journal of Biomedical Engineering, 12, 379-382.

[101] B.P. McNamara, L. Cristofolini, A. Toni, D. Taylor, 1997, Relationship between bone-prosthesis bonding and load transfer in total hip reconstruction, Journal of Biomechanics, 30, 6, 621-630.

[102] P.J. Prendergast, J. Monaghan, D. Taylor, 1989, Materials selection in the artificial hip joint using finite element stress analysis, Clinical Materials, 4, 361-376.

[103] D. Siegele, R. Schäfer, U. Soltész and J. M. Drouin.1998, Stress analyses of ceramic hip joint heads under different loading conditions, Fraunhofer-Institut fhr Werkstoff-mechanik, W'hlerstra8e, Journal of Biomechanics,31, 1,164.

References

[104] J. Hertzler, M.A. Miller and K.A. Mann, 2002. Fatigue crack growth rate does not depend on mantle thickness: an idealized cemented stem construct under torsional loading, Journal of Orthopaedic Research, 20, 676-682.

[105] D.G. Kim, M.A. Miller, K.A. Mann, 2004, A fatigue damage model for the cement-bone interface, Journal of Biomechanics, 37 [10], 1505-1512.

[106] O. Kayabasi, F. Erzincanli, 2006, Finite element modeling and analysis of a new cemented hip prosthesis, Advances in Engineering Software, 37, 477-483.

[107] A.Z. Senalp, O. Kayabasi, H. Kurtaran, 2007, Static, Dynamic and Fatigue behaviour of newly designed stem shapes for hip prosthesis using finite element analysis, Materials and Design, 28, 1577-1583.

[108] P. Colombi, 2002, Fatigue analysis of cemented hip prosthesis: model definition and damage evolution algorithms, International Journal of Fatigue, 24, 8, 895-901.

[109] P. Colombi, 2002, Fatigue analysis of cemented hip prosthesis: damage accumulation scenario and sensitivity analysis, International Journal of Fatigue, 24, 7, 739-746.

[110] M.T. Raimondi and R. Pietrabissa, 1999, Modelling evaluation of the testing condition influence on the maximum stress induced in a hip prosthesis during ISO 7206 fatigue testing, Medical Engineering and Physics, 21, 353-359.

[111] J.P. Hung, J.H. Chen, H.L. Chiang, J.S.S. Wu, 2004, Computer simulation on fatigue behavior of cemented hip prostheses: a physiological model, Computer Methods and Programs in Biomedicine, 76, 103-113.

[112] C.L. Tai, C.H. Shih, W.P. Chen, S.S. Lee, Y.L. Liu, P.H. Hsieh, W.J. Chen, 2003, Finite element analysis of the cervico-trochanteric stemless femoral prosthesis, Clinical Biomechanics, 18, S53-S58.

[113] T.P. Culleton, P.J. Prendergast, D. Taylor, 1993, Fatigue failure in the cement mantle of an artificial hip joint, Clinical Materials, 12, 95-102.

[114] S. H. Teoh, W. H. Chan and R. Thampuran, 2002. An elasto-plastic finite element model for polyethylene wear in total hip arthroplasty, Journal of Biomechanics, 35, 323-330.

References

[115] V. Saikko and O. Calonius, 2002. Slide track analysis of the relative motion between femoral head and acetabular cup in walking and in hip simulators, Journal of Biomechanics, 35, 455-464.

[116] A. Bufford and T. Goswami, 2004. Review of wear mechanisms in hip implants: Paper I – General, Materials and Design 25, 385-393.

[117] M. Slonaker and T. Goswami, 2004. Review of wear mechanisms in hip implants: Paper II – ceramics IG004712, Materials and Design 25, 395-405.

[118] S.L. Bevill, G.R. Bevill, J.R. Penmetsa, A.J. Petrella, P.J. Rullkoetter, 2005, Finite element simulation of early creep and wear in total hip arthroplasty, Journal of Biomechanics, 38, 2365-2374.

[119] D.J. Rapperport, D.R. Carter, and D.J. Schurman, 1985, Contact Finite Element Stress Analysis of the Hip Joint, Journal of Orthopaedic Research,3, 4, 435 – 446.[120] T. Laurian and A. Tudor, 2003, Some aspects regarding the influence of the clearance on the pressure distribution in total hip joint prostheses. ROTRIB'03, National Tribology Conference, 393-397. The annals of university "dunarea de jos" of galati, fascicle viii, Tribology, 2003, i - ROTRIB'03, ISSN 1221-4590

[121] A.L. Galvin, S. Williams, P. Hatto, J Thompson, G. Isaac, M Stone, E. Ingham and J. Fisher, 2005, Comparison of wear of ultra high molecular weight polyethylene acetabular cups against alumina ceramic and chromium nitride coated femoral heads, Wear, 259, 972-976.

[122] O. Calonius, 2002, Tribology of prosthetic joints – Validation of wear simulation methods, Dissertation for the degree of Doctor of Science. Helsinki University of Technology, Finland.

[123] M. Reggiani, A. Tinti, P. Taddei, M. Visentin, S. Stea, M.D. Clerico, and C. Fagnano, 2006, Phase transformation in explanted highly crystalline UHMWPE acetabular cups and debris after in vivo wear, Journal of Molecular Structure,785, 98-105.

[124] T. Goswami and S. Alhassan, 2008, Wear rate model for UHMWPE in total hip and knee arthroplasty, Materials and Design, 29, 289-296.

[125] P.E.S .Jones, J.A. Wharton and R.J.K. Wood, 2005, Micro – abrasion – corrosion of a CoCrMo alloy in simulated artificial hip joint environments, Wear, 259, 898-909.

References

[126]T.A. Maxian, T.D. Brown, D.R. Pedersen and J.J. Callaghan, 1996, A sliding – distance – coupled finite element formulation for polyethylene wear in total hip arthroplasty, Journal of Biomechanics, 5, 687-692.

[127] P. Podra and S. Andersson, 1999, Finite element analysis wear simulation of a conical spinning contact considering surface topography, Wear, 224, 13-21.

[128] P. Podra and S. Andersson, 1997, Wear simulation with the Winkler surface model, Wear, 207, 79-85.

[129] A.L. Ogden, R.H. Mayeux and D.P. Mukherjee, 1997, Wear properties of a ultra high molecular weight polyethylene material, Biomedical Engineering Conference, 1997., Proceedings of the 1997 Sixteenth Southern**,** IEEE, 84-87.

[130] G.K. Sfantos and M.H. Aliabadi, 2006, Total hip arthroplasty wear simulation using the boundary element method, Journal of Biomechanics, 40, 2, 378-389.

[131] T.P. Schmalzried and J.J. Callaghan, 1999, Current concepts review – Wear in total hip and knee replacements, The Journal of Bone and Joint Surgery, 81, 115-136.

[132] P.H. Adegbile, B. Russery, L. Taylor and J. Tong, 2005, Failure of an uncemented prosthesis – a case study, Engineering Failure Analysis, 13, 1, 163-169.

[133] A. Unsworth, 1995, Recent developments in the tribology of artificial joints, Tribology International, 28, 7, 485-495.

[134] P.S.M. Barbour, D.C. Barton, J. Fisher, 1995, The influence of contact stress on the wear of UHMWPE for total replacement hip prostheses, Wear, 181-183, 250-257.

[135] H. Yoshida, A. Faust, J. Wilckens, M. Kitagawa, J. Fetto, Edmund Y.-S. Chao, 2006, Three-dimensional dynamic hip contact area and pressure distribution during activities of daily living, Journal of Biomechanics, 39, 1996-2004.

[136] P.J. Evans and B.J. McGrory, Fractures of the proximal femur, http://www.orthoassociates.com/hipfx.htm

[137] http://www.totaljoints.info/cemented_and_cementless_thr.htm

[138] http://www.hipsandknees.com/hip/

APPENDIX
NEWMARK INTEGRATION SCHEME

Newmark integration scheme [Finite Element Procedures by Bathe, K. J. Prentice-Hall, Englewood Cliffs, 1995] has been used for full transient dynamic solution of the problem, which is based on the assumption of linear variation of acceleration from time '*t*' to '$t+\Delta t$'. Here the following assumptions are used

$$\{\dot{U}\}^{t+\Delta t} = \{\dot{U}\}^{t} + \left[(1-\delta)\{\ddot{U}\}^{t} + \delta\{\ddot{U}\}^{t+\Delta t}\right]\Delta t \qquad \text{(A1)}$$

$$\{U\}^{t+\Delta t} = \{U\}^{t} + \{\dot{U}\}^{t}.\Delta t + \left[\left(\frac{1}{2}-\alpha\right)\{\ddot{U}\}^{t} + \alpha\{\ddot{U}\}^{t+\Delta t}\right]\Delta t^{2} \qquad \text{(A2)}$$

Where α and δ are the parameters that can be determined to obtain the accuracy and stability. When $\delta = \frac{1}{2}$ and $\alpha = \frac{1}{6}$, (1) and (2) corresponds to linear acceleration method. When $\delta = \frac{1}{2}$ and $\alpha = \frac{1}{4}$, it leads to constant average acceleration method which was originality proposed by Newmark as unconditionally stable scheme.

Considering equilibrium of equation at $t+\Delta t$,

$$[M]\{\ddot{U}\}^{t+\Delta t} + [C]\{\dot{U}\}^{t+\Delta t} + [K]\{U\}^{t+\Delta t} = \{F\}^{t+\Delta t} \qquad \text{(A3)}$$

(A2) gives us $\{\ddot{U}\}^{t+\Delta t}$ in terms of $\{U\}^{t+\Delta t}$ and using this in (A1) gives us $\{\dot{U}\}^{t+\Delta t}$ in terms of $\{U\}^{t+\Delta t}$. Using these expressions in (A3) we can solve for $\{U\}^{t+\Delta t}$ and subsequently calculate $\{\dot{U}\}^{t}$ and $\{\ddot{U}\}^{t+\Delta t}$. from (A2) and (A3).

Algorithm:

1. *Form [K], [M], [C]*
2. *Initialize* $\{U\}^{0}, \{\dot{U}\}^{0}$ *and* $\{\ddot{U}\}^{0}$
3. *Select* $\Delta t, \alpha$ *and* δ *and calculate constants*

$\delta \geq 0.5$ *and* $\alpha \geq 0.25(0.5+\delta)^{2}$

$$q_0 = \frac{1}{\alpha \Delta t^{2}};\ q_1 = \frac{\delta}{\alpha.\Delta t};\ q_2 = \frac{1}{\alpha.\Delta t};\ q_3 = \frac{1}{2\alpha} - 1;$$

Appendix

$$q_4 = \frac{\delta}{\alpha} - 1; \quad q_5 = \frac{\Delta t}{2}\left(\frac{\delta}{\alpha} - 2\right); \quad q_6 = \Delta t(1-\delta); \quad q_7 = \delta.\Delta t;$$

4. *Form effective stiffness matrix* $\left[\hat{K}\right]$ *as*

$$\left[\hat{K}\right] = [K] + q_0[M] + q_1[C]$$

5. *Triangularize* $\left[\hat{K}\right]$ *as* $\left[\hat{K}\right] = LDL^T$

7. *Calculate effective load at* $t + \Delta t$ *as*

$$\left\{\hat{F}\right\}^{t+\Delta t} = \{F\}^{t+\Delta t} + [M]\left(q_0\{U\}^t + q_2\{\dot{U}\}^t + q_3\{\ddot{U}\}^t\right) + [C]\left(q_1\{U\}^t + \{\dot{U}\}^t + q_5\{\ddot{U}\}^t\right)$$

1. *Solve for displacement at* $t + \Delta t$

$$LDL\{U\}^{t+\Delta t} = \left\{\hat{F}\right\}^{t+\Delta t}$$

2. *Calculate acceleration and velocity at* $t + \Delta t$ *as*

$$\{\dot{U}\}^{t+\Delta t} = q_0\left(\{U\}^{t+\Delta t} - \{U\}^t\right) - q_2\{\dot{U}\}^t - q_3\{\ddot{U}\}^t$$

$$\{\dot{U}\}^{t+\Delta t} = \{\dot{U}\}^t + q_6\{\ddot{U}\}^t + q_7\{\ddot{U}\}^{t+\Delta t}$$

List of publications from this thesis work

1. M. Sivasankar, D. Chakraborty, S. K. Dwivedy, 2004, Finite element analysis of composite hip prosthesis, Proceedings of National Conference on Biomechanics held on 19th-21st November 2004, 30, 214-220.
2. M. Sivasankar, D. Chakraborty, S.K. Dwivedy, 2006, Fatigue analysis of artificial hip joints for different materials, Proceedings of Society for Biomaterials and Artificial Organs of India (SBAOI) conference, IIT Delhi, Feb'24-26.
3. M. Sivasankar, D. Chakraborty, S.K. Dwivedy, 2006, Fatigue analysis of artificial hip joints for different materials and activities, Published in recent Advances in Computational Mechanics and Simulations, Vol-II, pp.2043-2048, Proceeding of Second International Congress on Computational Mechanics and Simulations, ICCMS'06, IIT Guwahati, Dec 8-10.
4. M. Sivasankar, T. Benarjee, D. Chakraborty, S.K.Dwivedy, 2006, Dynamic stress and fatigue analysis of artificial hip prosthesis, National Conference on Biomechanics, BESU, West Bengal, held in December, 2006. Also published in Indian Journal of Biomechanics.
5. M.Sivasankar, T.Banarjee, N.Ravikiran, D.Chakraborty, S.K.Dwivedy, 2007, Dynamic stress and fatigue analysis of artificial hip prosthesis, Indian Journal of Biomechanics, 1, 53-58.

.